WHOI-2016-02

Woods Hole Oceanographic Institution

# Microscale, Finescale, and Mesoscale Measurements Made During the 2004 Structured Mixing Project (Micro-Tow 04) Cruise

by

Timothy F. Duda and Cynthia J. Sellers

April 2016

## Technical Report

Funding was provided by the Office of Naval Research through
Contract nos. N00014-03-1-0335 and N00014-14-1-0223.

**WHOI-2016-02**

# Microscale, Finescale, and Mesoscale Measurements Made During the 2004 Structured Mixing Project (Micro-Tow 04) Cruise

by

Timothy F. Duda and Cynthia J. Sellers

Woods Hole Oceanographic Institution
Woods Hole, Massachusetts 02543

April 2016

**Technical Report**

Funding was provided by the Office of Naval Research through
Contract nos. N00014-03-1-0335 and N00014-14-1-0223.



**Approved for Distribution:**

**John Trowbridge, Chair**

Department of Applied Ocean Physics and Engineering

**Microscale, finescale, and mesoscale measurements made during the 2004 Structured Mixing Project (Micro-Tow 04) cruise**

Timothy F. Duda and Cynthia J. Sellers

*Applied Ocean Physics and Engineering Department*
*Woods Hole Oceanographic Institution*
*Woods Hole, MA 02543*

*Abstract*

A physical oceanographic sampling voyage was made with *RV Endeavor* during August 2004 to evaluate diapycnal mixing processes on the continental shelf south of Massachusetts and Rhode Island, USA. The goal of the project was to look for a relationship between intensity of microstructure (thermal variance dissipation rate) and finestructure (background temperature gradient), in so-called doubly-stable water, which would be indicative of a density gradient-dependent diapycnal heat flux. To satisfy the requirement that a large amount of data be collected to constrain the statistically estimated result, a microstructure sensor was towed on a platform behind the ship, providing continuous sampling at the depths of interest. To obtain the necessary finestructure quantities the platform measured temperature, conductivity and depth with a standard pumped Seabird 9plus CTD. Attitude and speed of the platform were recorded to assure proper data quality.

This report shows temperature, salinity, density, and sound speed in twenty-five tow-yo transects obtained using the towed unit. Only statistics and results from microscale data are shown. In waters with stable salt stratification and stable temperature stratification, a previously obtained empirical result of reduced flux at increased density gradient is supported by the data.

The 2004 Cruise Report is included (Appendix).

## 1. Introduction

In order to address a long-term goal of understanding diapycnal mixing processes of outer shelf waters in stratified conditions, a project with two towed finestructure and microstructure measuring systems was undertaken on August 8-14, 2004. Figure 1 shows the operational area and the track lines along which the measurement system was towed.

The objective of the project was to determine whether the net effects of intermittent shear-driven diapycnal mixing events (i.e. turbulent events that cause cross-isopycnal mass flux) are sensitive to the background conditions in a specific way. The hypothesis is that within a field exhibiting a step-like density structure, mixing will be more rapid in layers with weak stratification than in layers with strong stratification (interfaces). Such an effect would cause density-gradient perturbations to grow, analogous to a negative eddy diffusivity being in effect, a process sometimes referred to as the Phillips instability (Phillips, 1972; see also Balmforth *et al*., 1998). Briefly, with buoyancy flux being defined as $F=KN^2(z)$ with $K$ being the Fickian turbulent diffusion coefficient, $N(z)$ being the buoyancy frequency proportional to the density ($\rho$) gradient $N^2(z) = g\rho^{-1}d\rho/dz$, the Phillips instability occurs when $F$ is a decreasing function of $N$ or $N^2$. This can also be stated as $K$ being inversely related to $N$ and falling more steeply than $K(N) \propto N^{-2}$. Some evidence of gradient-dependent $K$ behaving in this way was found in the ONR Coastal Mixing and Optics (CMO) program dye diffusion studies and towed-microscale conductivity measurements (Duda and Rehmann, 2002). We sought to expand on the CMO work by collecting and analyzing more data of better quality than previously available. Obtaining a gradient-dependent or gradient-independent flux result $F(N)$ with small error bars would confirm or reject the likelihood of the Phillips instability, at least in the sampled waters.

The required large set of microscale conductivity data and supporting data was obtained with a towed sensor package (called Micro-Tow, MT) during a seven-day research cruise on *RV Endeavor* during August 2004. A report on the cruise is appended. The towed platform and the onboard data-acquisition electronics were of our own design. Additional data were collected with the Naval Research Laboratory microscale conductivity package affixed to the towed undulating Scanfish platform owned and operated by the University of Rhode Island (the operator of the ship). The MT data are reported here.

Section 2 explains the technical details of the study. Section 3 shows the structure of the front that existed in the work area, and temperature ($T$) and salinity ($S$) characteristics within 25 transects. Variations of the quantities $T$, $S$, $T(S)$, $\rho$ and sound speed ($c$) are shown. Section 4 briefly discussed the scalar dissipation rate. Section 5 shows $K(N)$ results in waters (one-second tow-sample intervals) where both $T(z)$ and $S(z)$ are (independently) gravitational stable, which we refer to as doubly-stable (DS) waters. The computation of $K$ and $F$ is most reliable in DS waters where mixing is caused by shear-driven events, explaining why the analysis was done only for this subset of data.

## 2. Instruments

A measurement platform was towed behind the ship at 4 to 4.5 knots (2.0- 2.25 m/s). It oscillated in depth under control of the winch payout, except during a few short horizontal towing moments. The platform had a Seabird model 9+ CTD aboard, with two separate (redundant) pumped temperature/conductivity cell systems. These measured at 24 Hz and were averaged and

recorded at 12 Hz (double the CMO dye-experiment recording rate). The platform also had two 2-electrode Seabird Electronics model SBE7 microscale conductivity probes sampling at 400 Hz (200 points per meter, usually). These probes were arranged horizontally across the nose of the platform to be at the same depth. Below them was a two-axis electromagnetic current meter sensing the flow speed past the probes and the angle of attack of the platform, for data calibration and quality control purposes. Further discussion of the instruments and their performance is available in a journal article showing the results of earlier work with this system (Rehmann and Duda, 2000).

## 3. Water mass properties

*A. Intrusions*

The data-collection transects (tow paths) (Figure 1) criss-cross a frontal feature related to the shelf/slope water front, where warm and salty (for a given density) Slope Water meets fresher and colder shelf water. Figure 2 shows the salinity in the later portion of tow section T3, with data collected in sections T2 through T8. The locations of the individual sections are shown in figures to follow; their times are given in the Appendix (Cruise Report).

Salty intrusions that are vertically thin can be seen in red in Figure 2. The tow tracks are too sparse to map these intrusions. These intrusions create conditions favorable for double diffusive instabilities, which cause diapycnal mixing through processes that are substantially different from the shear-driven turbulence events that were targeted for study. Above a salty intrusion the thermal structure is destabilizing, and below a salty intrusion the salinity structure is destabilizing. (The situation is reversed for fresh intrusions; for vertically stacked intrusions it may be better to describe the process as interleaving rather than intrusion.) It was hoped that intrusions would diminish in areas away from a relatively narrow and well-formed front, but intrusions were common throughout most of the 50 by 100 km work area.

The wide spacing of the MT towing paths renders mapping of intrusions from MT tows impossible. The Scanfish was deployed periodically to find and map intrusions and their microscale conductivity activity, but that instrument apparently hit a submerged object and was damaged before that work was completed, compromising the success of that part of the project.

*B. Mesoscale*

The meanders of the front form a major mesoscale feature of the area. The presence of many intrusions at many depths makes horizontal mapping of frontal details using objective analysis (Emery and Thomson, 2001) quite challenging. A robust parameter to be used to define the front was found to be depth-averaged salinity $S_z$. The profile depth ranges were slightly variable throughout the exercise, adding some error to this method. However, a fairly smooth $S_z$ was obtained. This was objectively mapped, for frontal illustration only, using simple Kriging and two sets of parameters: (1) a sill value of 0.9 and a correlation scale of 4 km, and (2) a sill value of 0.85 and correlation scale 12 km (Figure 3). The frontal boundary, as defined with this mean-salinity metric, is wavy, as expected, although the detailed shape remains indeterminate given the limited amount of data.

Summary plots for twenty-five towing transects are shown here. Thirty-two figures appear in total. Twenty-five figures show transect data, labeled “Figure 4.n.m”, with n being tow

number (2 through 8, for T2 through T8) and m being transect number in a tow. Seven figures labeled "Figure 4.n.0") show the seven tow tracklines. The figures show, on the left, interpolated temperature, salinity, density anomaly and sound speed in the transects. In the center they show time-mean (transect-mean) values of each of these at each depth (i.e. mean profiles), profiles of minimum and maximum values at each depth are additionally shown. On the right the figures show plots of variables against one another other. The final type of plot that is included is the classic "TS plot" with density contours superimposed, which shows signatures of intrusions as zig-zags between the lower left and the upper right.

## 4. Thermal variance dissipation rate $\chi$

The time series of estimated thermal variance dissipation rate, defined by

$$\chi = 2k_t \left\langle \left(\nabla T'\right)^2 \right\rangle \approx 6k_t \left\langle \left(\partial T'/\partial x\right)^2 \right\rangle$$

with $k_t$ equal to the molecular diffusivity of heat ($1.5 \times 10^{-7}$ m$^2$/s), are plotted in twenty-five figures, one for each transect. These are numbered 5.n.m, where n is tow number and m is transect number in the tow (as with Figure 4). The figures show the timeseries of $\chi$, color coded by stratification type (DS type, salt-finger double-diffusive instability type, and layering double-diffusive instability type), and also show the tow-yo undulations with color-coding of the stratification type. These calculation methods are described in Rehmann and Duda (2000), Section 2b.

## 5. Gradient-dependent flux law testing

To test the gradient-dependent flux hypothesis, the flux $F = KN^2$ is computed as a function of $N$ for each transect with a suitably large data quantity. Figures here will show the exponent $q$ of $K$ fitted to power-law relationship, $K=aN^q$. An exponent $q < -2$ means that $F$ is a decreasing function of $N$. The analysis uses only data from doubly-stable water, salinity increasing with depth and temperature decreasing, so that interference from double-diffusive instability microstructure should be minimized.

Because the instrument profiles slowly in the vertical, short data sections of two seconds length cover a few tens of centimeters vertically and 4.0 to 4.5 m horizontally, allowing estimation of the vertical density gradients needed for the computations. Using processing code MT04 Version 8, flux as a function of density gradient is computed as described below. The methods used are very smilar to those used in Rehmann and Duda (2000) and Duda and Rehmann (2002).

First, gradients $\partial T/\partial p$, $\partial S/\partial p$, $\partial S/\partial T$ and $\partial \rho/\partial p$ are computed in each bin for the 24-member finestructure time series, and quality of each fit is recorded. The density ratio (see for example Schmitt, 1983) and Turner angle (see for example Rehmann and Duda, 2000) are also computed. Next, using the measured speed through the water, the conductivity gradient spectrum in spatial units is computed from the 400-Hz data. The attenuation effects of a hardware 120-Hz cutoff frequency anti-aliasing filter are then corrected for. The thermal variance dissipation rate $\chi$ is then computed using methods of Washburn et al. (1996), with the "low" $\chi$ estimate from the Washburn et al. algorithms selected for use in doubly-stable water based on analysis in that paper.

Next, data are selected to satisfy a low angle of attack criterion (undisturbed flow into the 400-Hz probes, angle less than 20 degrees) and a doubly stable gradient critieron (conditions not suited to double-diffusive instability and resulting flux), and gradients must be unambiguous (good regression fits). The value of |dS/dT| can not exceed 0.12, so that salinity does not dominate the 400-Hz conductivity gradients. Selected 2-sec data intervals are binned according to $N$ value into six groups with equal numbers of points. Mean $N$, mean $\partial T/\partial z$, and mean $\chi$ are computed for each bin. Figure "6.n.m" show individual values of these and means of these in the top two panels.

For each of the six bins for each transect, $K$ is determined from mean $\partial T/\partial z$ and mean $\chi$ using the Osborn Cox model, consistent with the statistical nature of the model. Instantaneous $K_i$ values are also computed for each selected 2-s interval, for illustration only. $K$ and $K_i$ values are shown in Figures "6.n.m". 150-sample bootstrap $K$ means (blue dots) are also shown, with 95% confidence intervals. Red $K$ estimates are the arithmetic means, with top and bottom 4 percent of samples trimmed away (usually a point or two for each bin).

Again, note that the situation with unstable salinity contribution is the salt finger double-diffusive instability situation. The situation with unstable temperature contribution is the diffusive layering double-diffusive instability situation. These two situations are not conducive to use of the Osborn-Cox model in this manner, and these data are not analyzed in this report.

The turbulent diffusive flux for each bin is given by $F = KN^2$. For eighteen of the twenty-five transects $K(N)$ is steeper than $N^{-2}$ (or equally steep), so $F$ is a decreasing function of density gradient; agreeing with the prior published results (Rehmann and Duda, 2000; Duda and Rehmann 2002).

Figure 7 shows $K$ versus $N$ computed for all the selected doubly-stable 2-s intervals for Transects 1-25. The same 6-bin method and data selection processes are used. $K$ is proportional to $N^{-2.2}$, so that flux $F$ is proportional to $N^{-1/5}$. The minus 2.2 exponent is a bit less negative than the -2.5 to -3.3 estimates in the Duda and Rehmann (2002) paper, so that $F$ as reported here decreases less rapidly with increasing $N$ than the prior result.

**6. Acoustic mode property anomalies in an intrusion zone.**

A final computation that is presented gives the phase speeds of acoustic waveguide normal modes for Transect 2. Data from this transect show both short-wavelength internal waves and intrusions, and their effects on modal wavelength (phase speed) for 150 and 250 Hz sound are shown. The modal properties are computed using the code "KRAKEN" (Porter, 1991).

The sound speeds in the water are shown in Section 3. The chosen seabed parameters were a slow layer (with two thin transition zones) over a faster-speed basement beginning at 20.1 m beneath the seafloor, justifiable for this area, but not corroborated along this track line, with the upper layer perhaps overly thick. (The constant seabed properties may be improved to fit observations better, but are suitable for evaluating changes in modal properties caused by features in the water.) This is the "Modified Chapman Model for Rhode Island", which is similar to the "Simplified Chapman Model for the SW06 experiment" (Newhall et al., 2007). The water depth was kept at 70.0 m, also to highlight water-column effects on modal properties. Interfaces

between layers (constant-property or constant-gradient) were at 70.1, 90, 90.1 and 200 m depth below the sea surface, with a half-space below. Density was 1900 kg/m$^3$ from 70 to 90.1 m deep, and 2050 kg/m$^3$ below this. Attenuation was 0.1 dB/wavelength down to 200 m, and 1 dB/wavelength below. Sound speed layering was slightly more complex. A top transition layer had linearly increasing sound speed from 1497.5 at 70 m to 1600 m/s at 70.1 m. The next layer had speed 1600 m/s and spanned 70.1 to 90 m. A linear increase was given to the 90.0 to 90.1 m transition layer, from 1600 to 1750 m/s. From 90.1 to 200 m, and into the highly attenuating half-space below 200 m, the speed was 1750 m/s.

Figure 8 shows the sound speed in Transect 2, with contours of high-salinity intrusion that is linked to high temperature and high sound speed at about 20 m depth. Phase speeds of modes 1 to 5 for 250 Hz sound are shown, along with phase speeds of modes 1 to 3 for 150 Hz. The phase speed changes in the intrusion are equal in size to those from three internal waves.

**Acknowledgements**

Nick Witzell is thanked for expert work on this project, as is Ed Hobart, who wrote the topside data-logging and underway data-display software. Prof. Chris Rehmann wrote many of the microstructure and CTD analysis code modules. Acoustic modal computations were made by Dr. Jon Collis, who is thanked. Funding was provided by the Office of Naval Research grant numbers N00014-03-1-0335 and N00014-14-1-0223.

**References**

Balmforth, N. J., S. G. Llewellyn Smith, and W. R. Young, Dynamics of interfaces and layers in a stratified turbulent fluid, *J. Fluid Mech.,* 355, 329-358, 1998.

Duda, T. F., and C. R. Rehmann, Systematic microstructure variability in double-diffusively stable coastal waters of nonuniform density gradient, *J. Geophys. Res.,* 107(C10), 3145, doi:10.1029/2001JC000844, 2002.

Emery, W. J., and R. E. Thomson, *Data Analysis Methods in Physical Oceanography*. 2nd and revised edition, Elsevier, 638 pp., 2001.

Newhall, A. E., T. F. Duda, K. von der Heydt, J. D. Irish, J. N. Kemp. S. A. Lerner, S. P. Liberatore, Y.-T. Lin, J. F. Lynch, A. R. Maffei, A. K. Morozov, A. Shmelev, C. J. Sellers, W. E. Witzell, Acoustic and oceanographic observations and configuration information for the WHOI moorings from the SW06 experiment, Woods Hole Oceanog. Inst. Tech. Rept., WHOI-2007-04, 2007.

Phillips, O. M., Turbulence in a strongly stratified fluid – is it unstable? *Deep-Sea Res., 19,* 79-81, 1972.

Porter, M. B., The KRAKEN Normal Mode Program, SACLANTTECN Memorandum No. SM-245, SACLANT Undersea Research Centre, La Spezia, Italy, 1991.

Rehmann, C. R. and T. F. Duda, Diapycnal diffusivity inferred from scalar microstructure measurements near the New England shelf/slope front, *J. Phys. Oceanogr.,* 30, 1354-1371, 2000.

Schmitt, R. W., The characteristics of salt fingers in a variety of fluid systems, including stellar interiors, liquid metals, oceans, and magmas, *Physics of Fluids,* 26(9), 2373–2377. 1983.

Washburn, L., T. F. Duda and D. C. Jacobs, Interpreting conductivity microstructure: Estimating the temperature variance dissipation rate, *J. Atmos. Oceanic Technol.,* 13, 1166-1188, 1996.

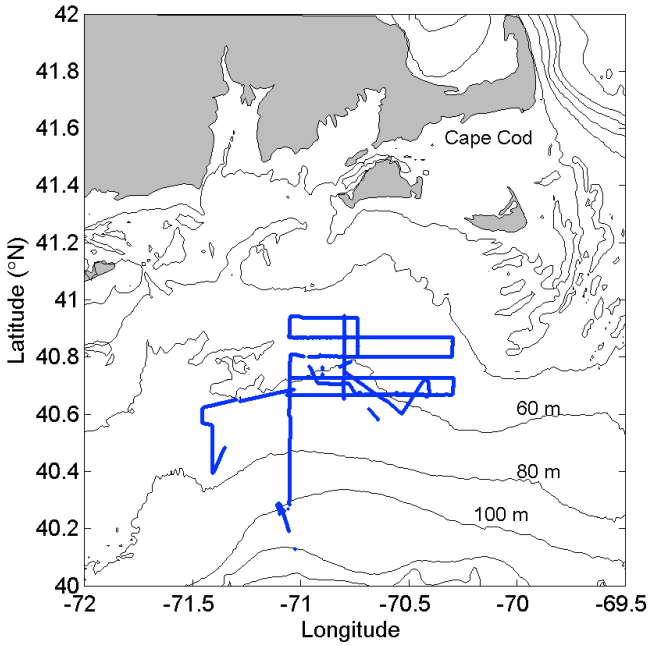


**Figure 1. The operational area is shown. The blue lines show the ship position at times of data collection. The entire track is composed of 8 tows (T1 to T8), each with one to 6 linear legs, referred to as transects. Figures to follow show the individual tows.**

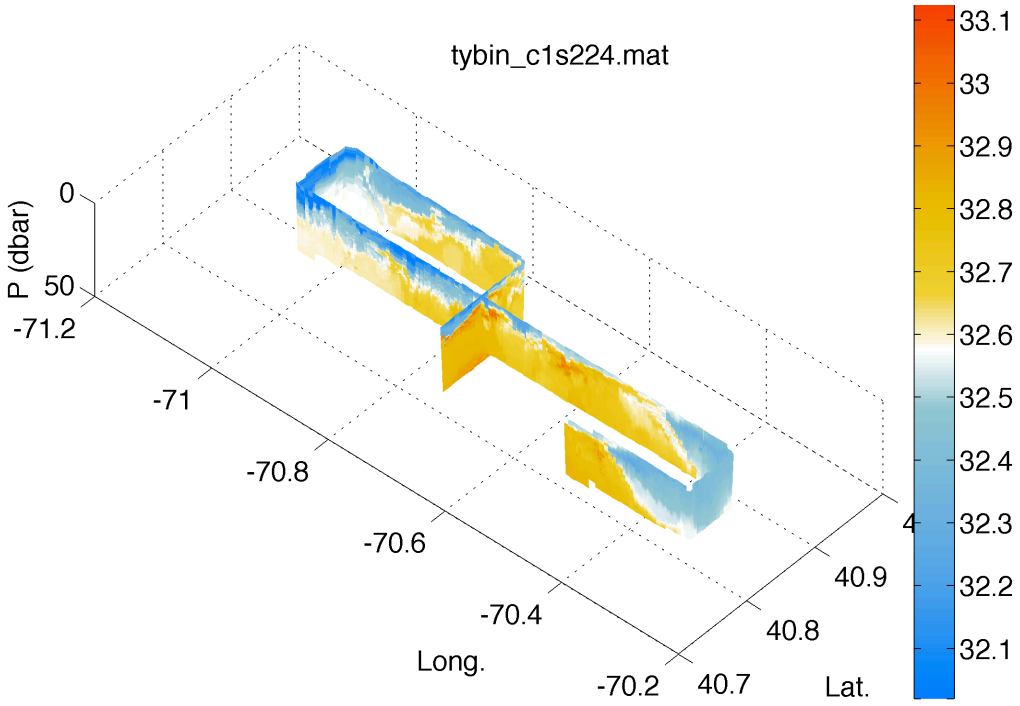


**Figure 2. Salinity in the later portion of tow T3, the northernmost, is shown.**

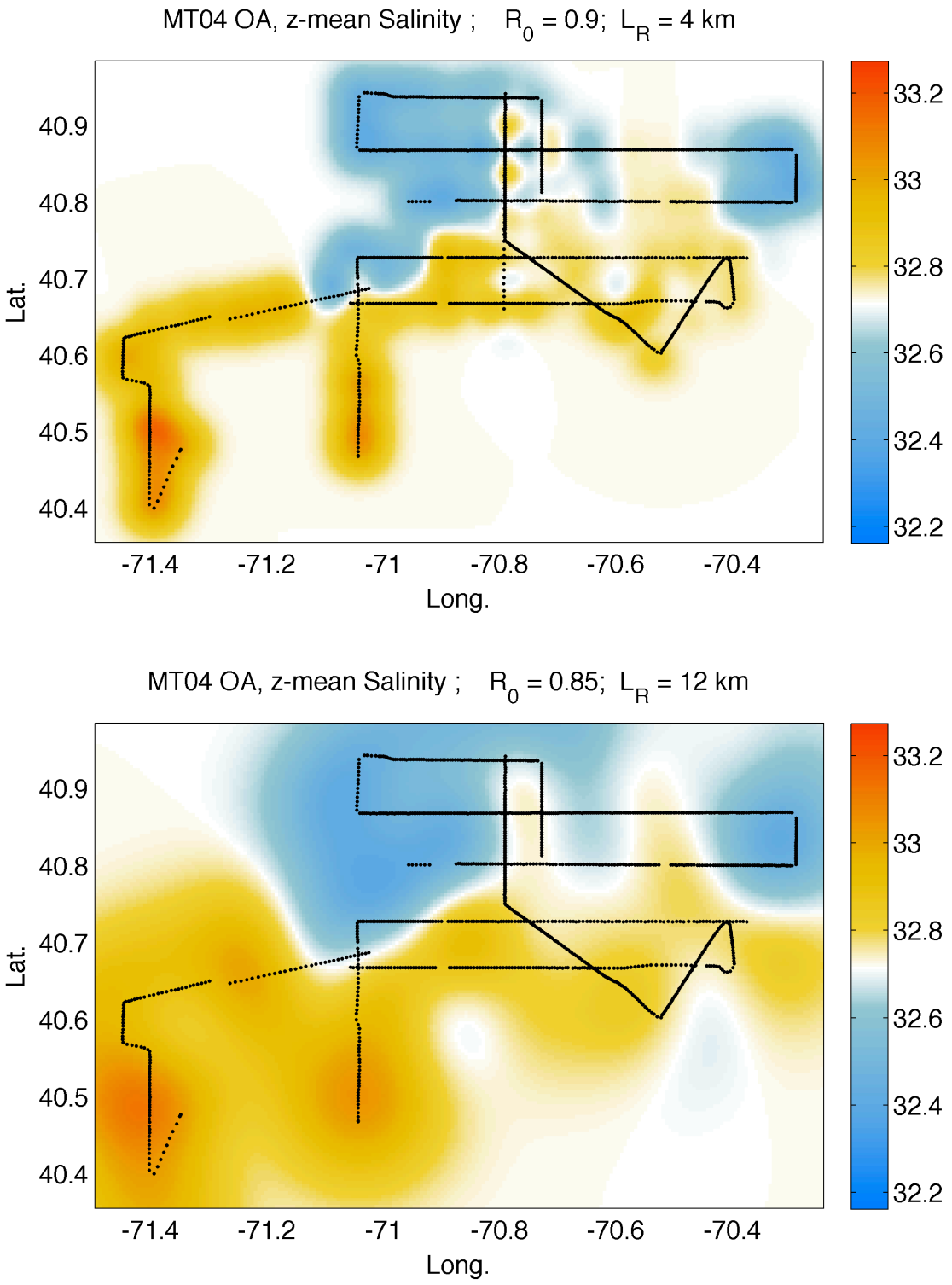


**Figure 3. Objective analysis maps of the depth-mean salinity showing the frontal structure.**

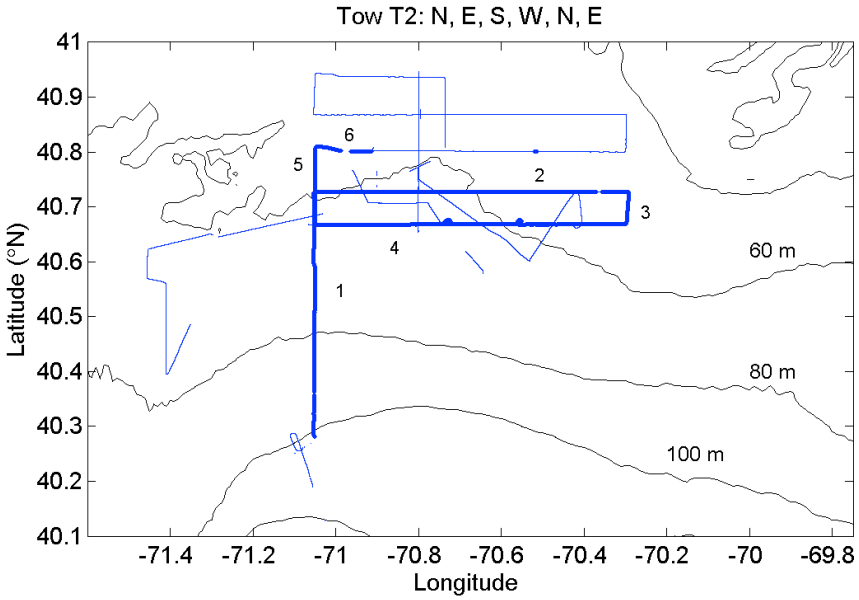


**Figure 4.2.0 The track of T2, which has six linear legs progressing northward, eastward, southward, etc. as listed in the title.**

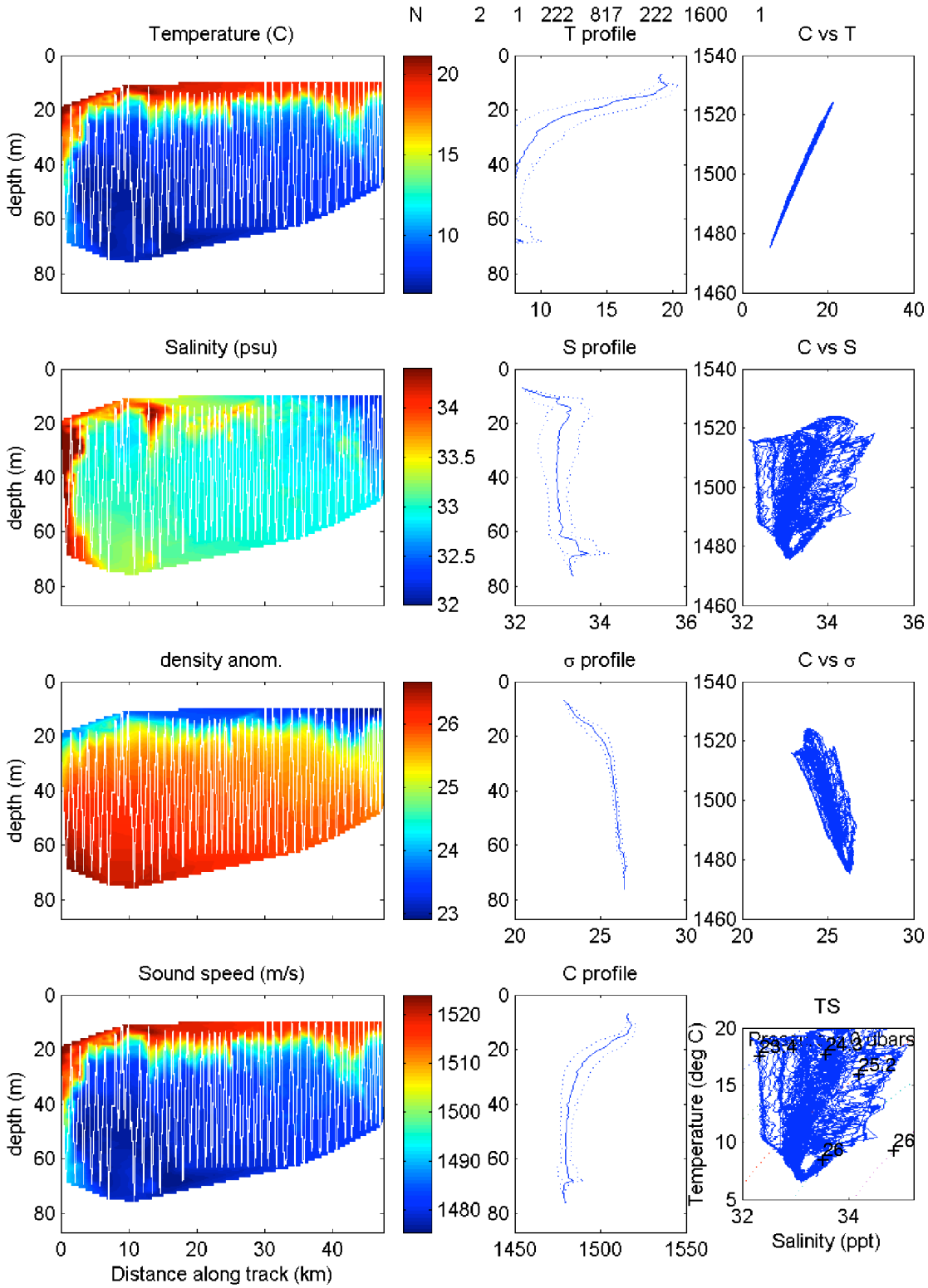


**Figure 4.2.1. T2-leg 1 (Transect 1). On the left are transect data with sensor trajectories in white. The central panels are the mean profiles (lines) and the upper and lower extremes of the data at each depth (dots lines). At the right are sound speed (*C* here) versus *T, S* and density, and TS diagram. Top text gives direction, tow, leg, start/end day hr min, transect.**

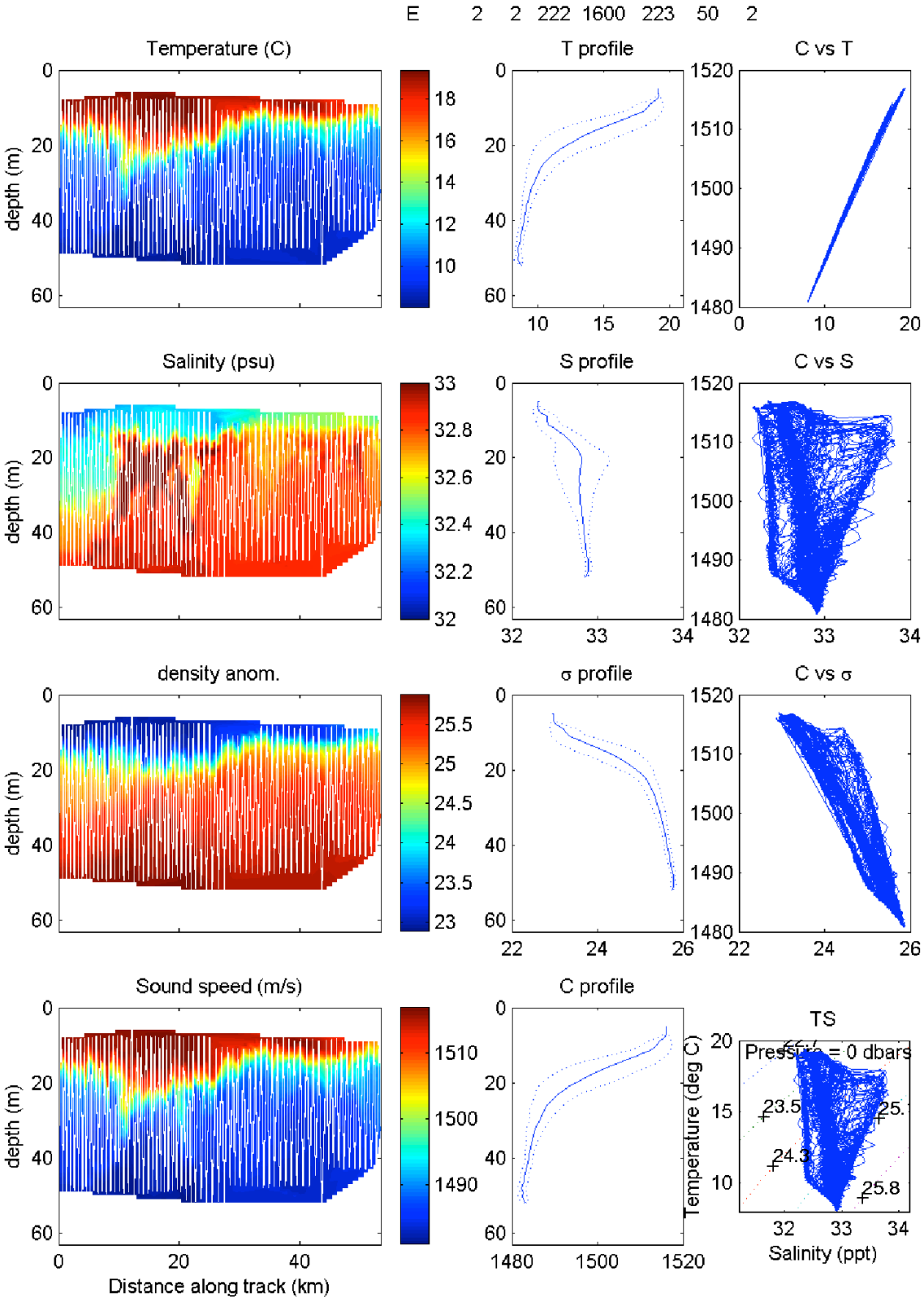


**Figure 4.2.2. T2-leg 2 (Transect 2).**

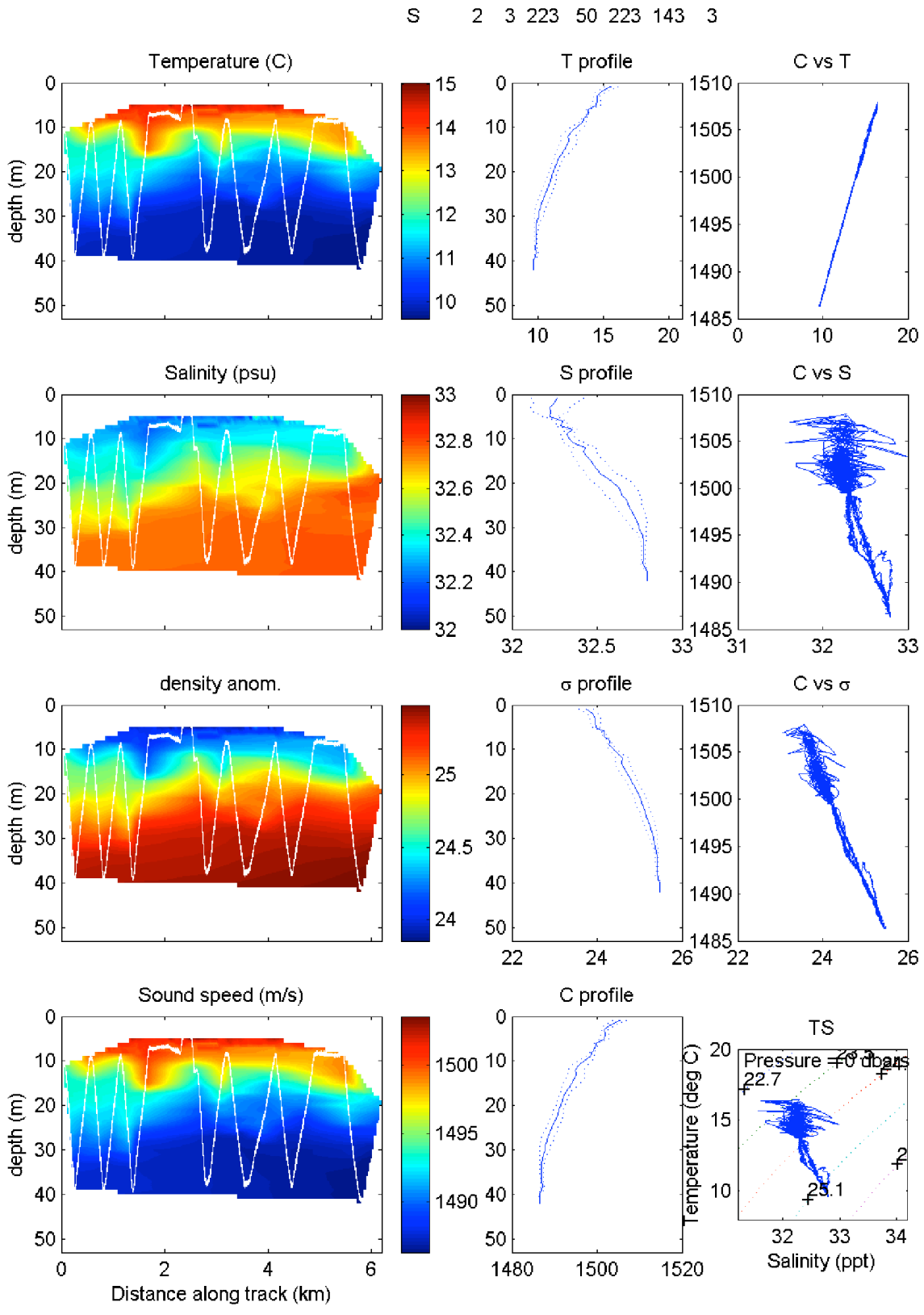


**Figure 4.2.3. T2-leg 3 (Transect 3).**

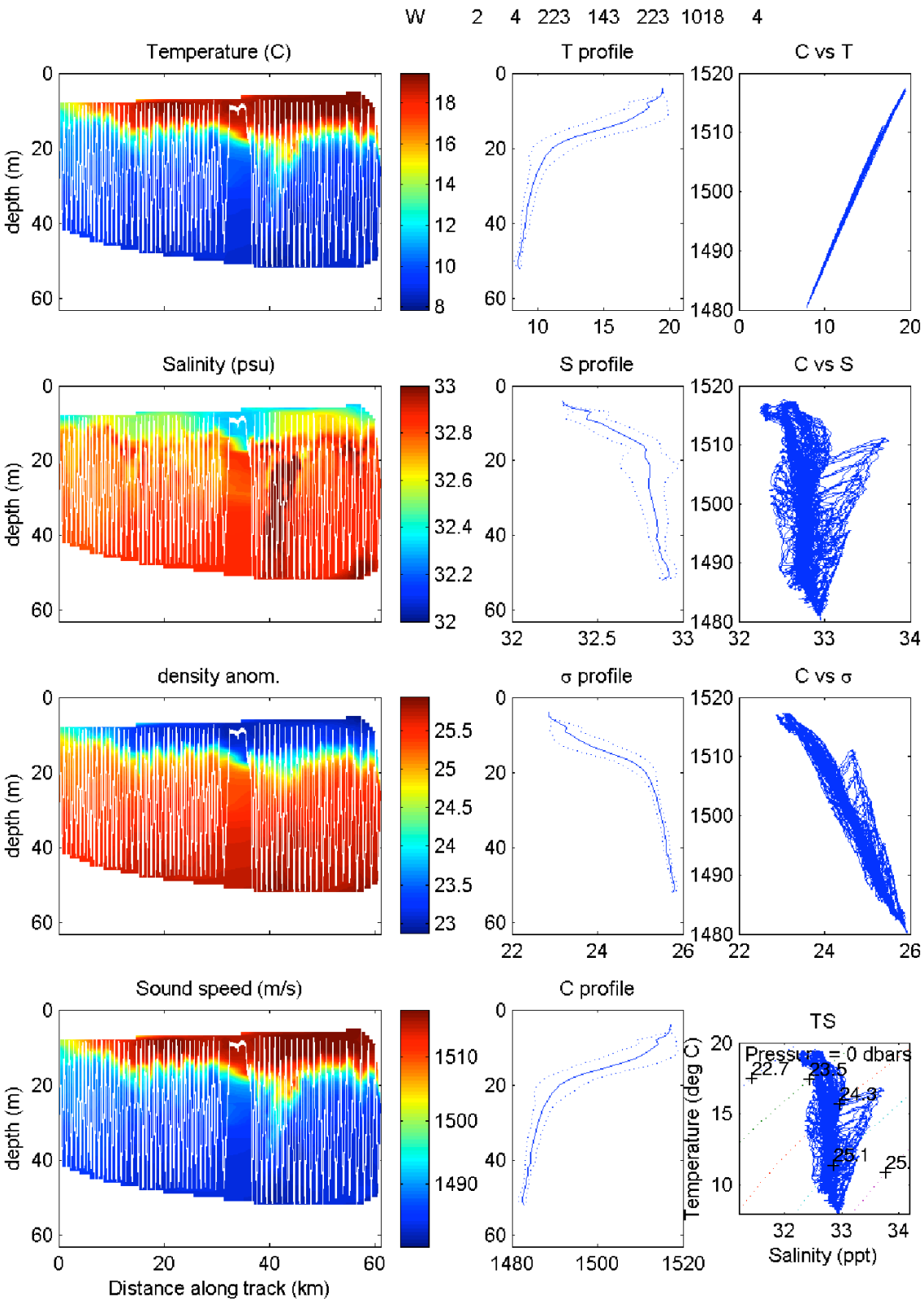


**Figure 4.2.4. T2-leg 4 (Transect 4.)**

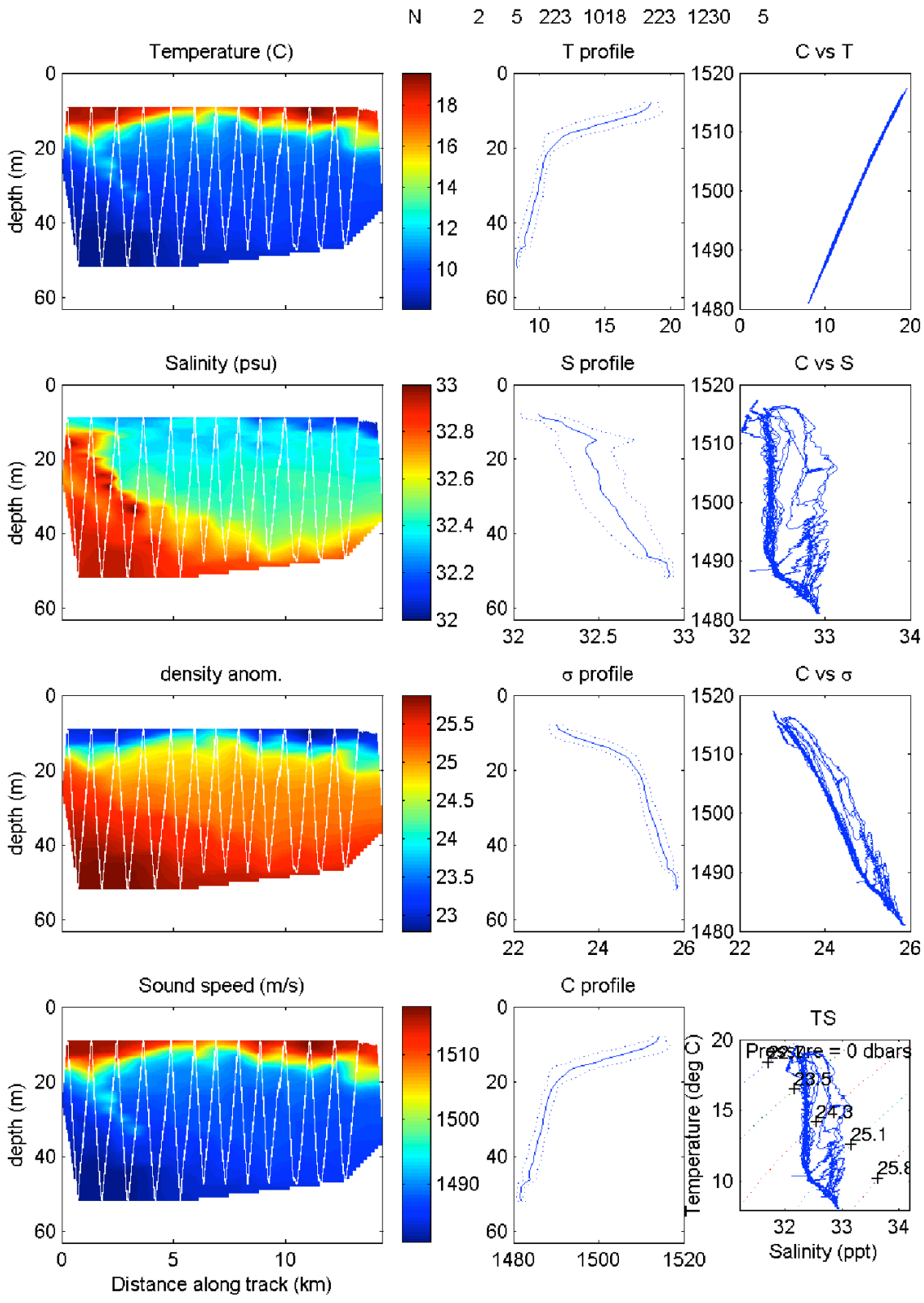


**Figure 4.2.5. T2-leg 5 (Transect 5).**

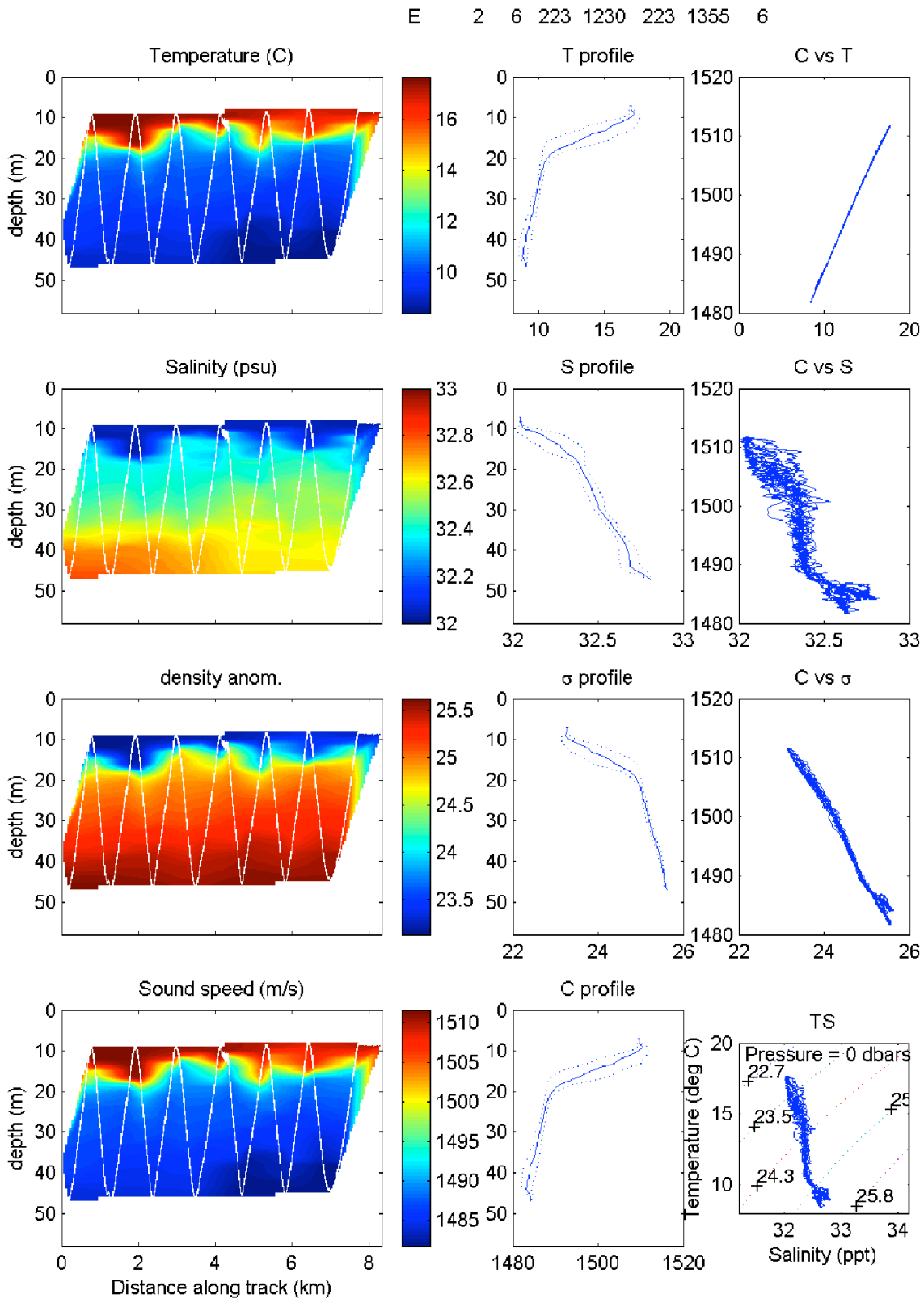


**Figure 4.2.6. T2-leg 6 (Transect 6).**

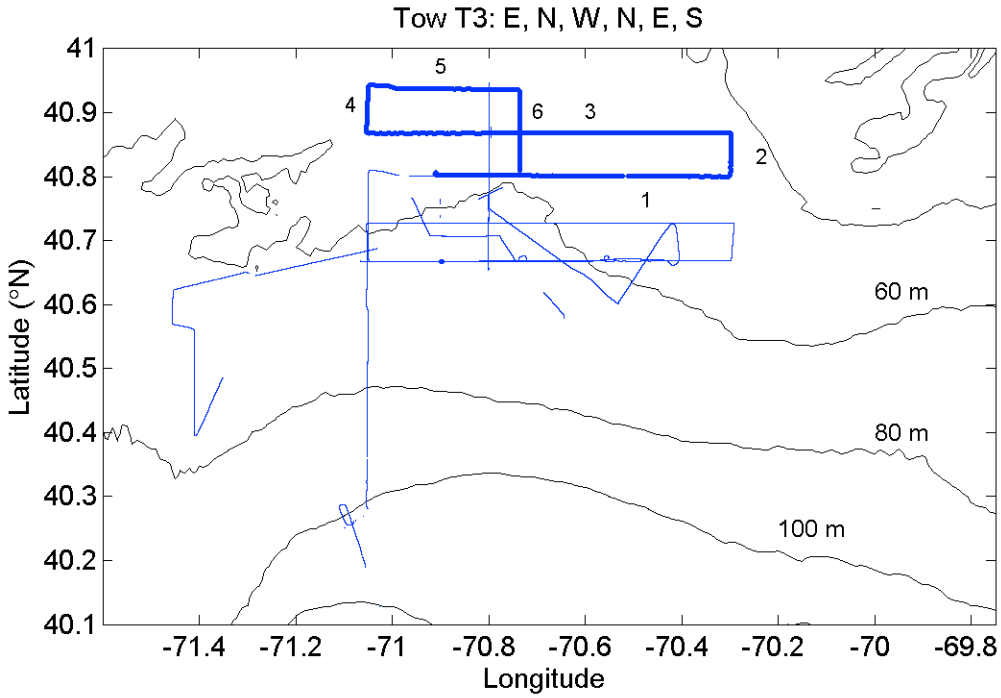


**Figure 4.3.0. T3 legs 1 through 6 are shown.**

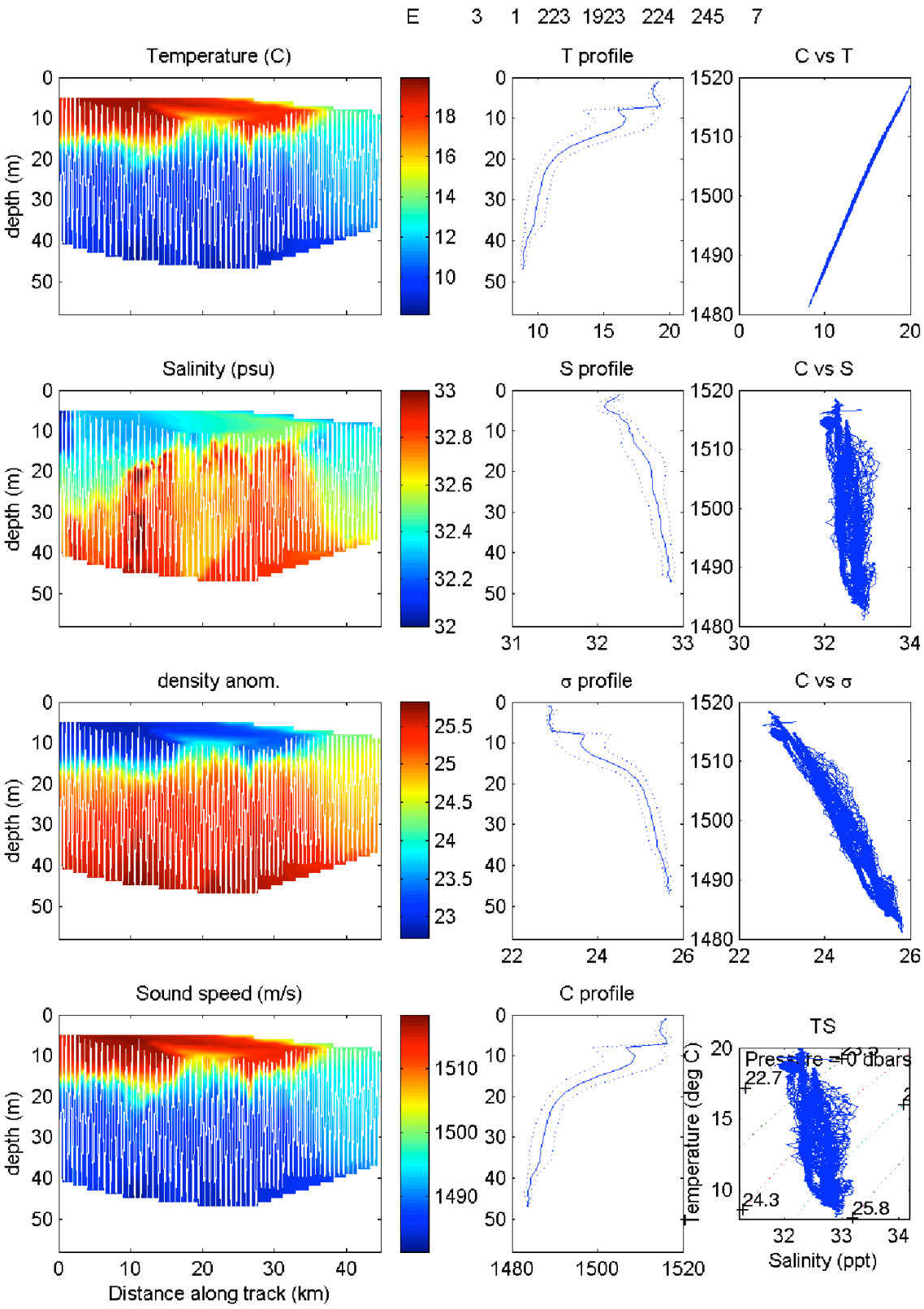


**Figure 4.3.1. T3-leg 1 (Transect 7).**

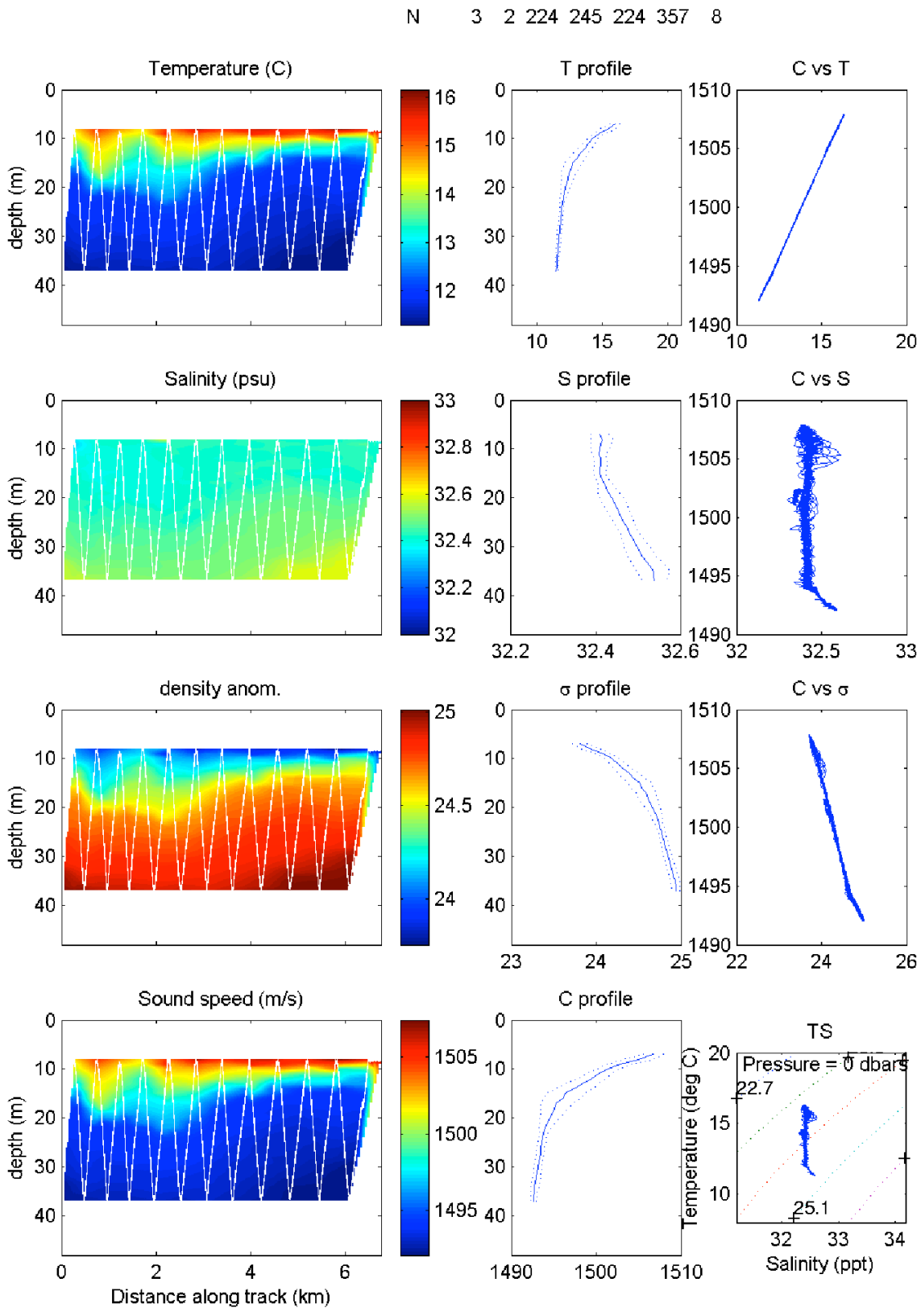


**Figure 4.3.2. T3-leg 2. (Transect 8).**

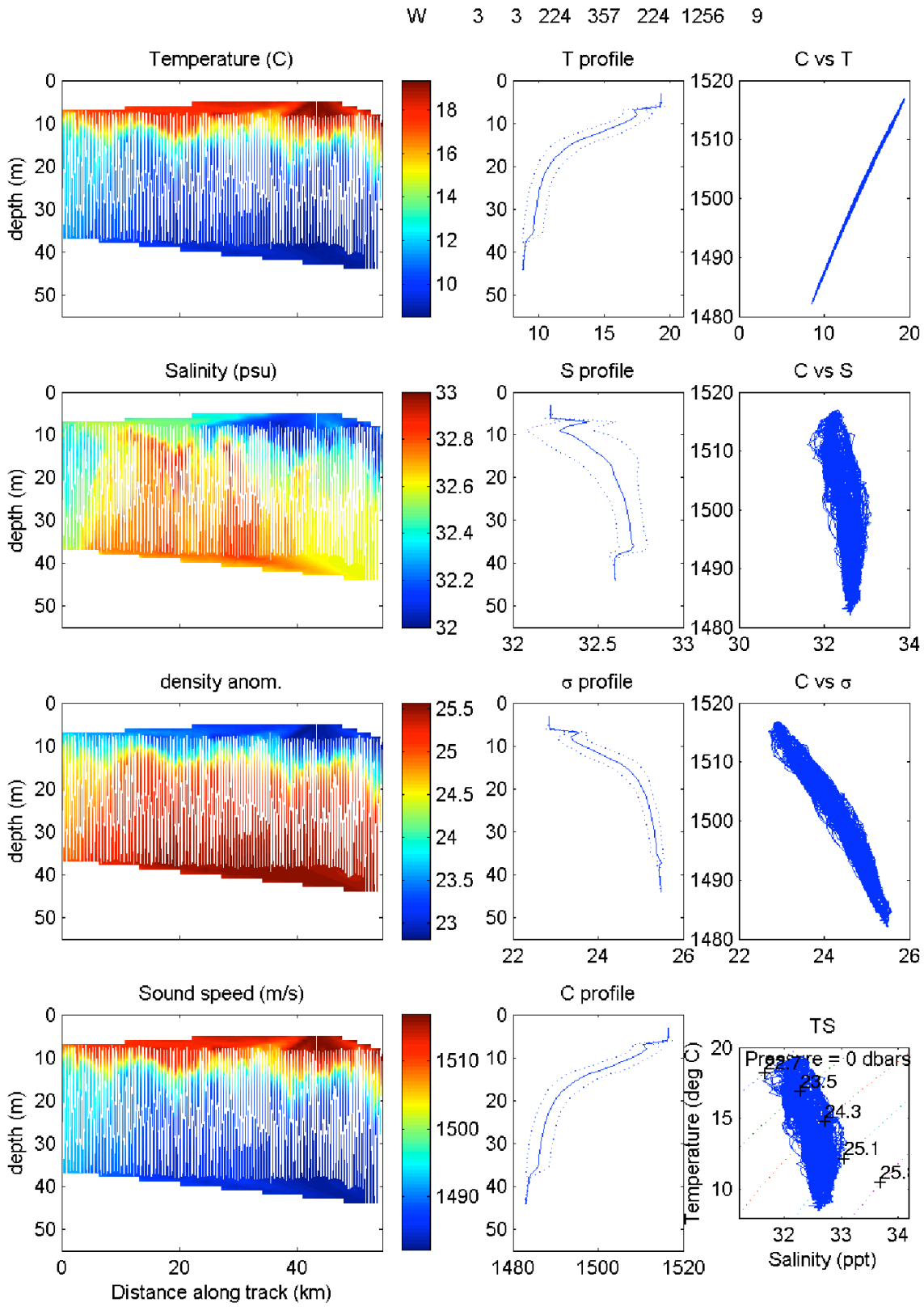


**Figure 4.3.3. T3-leg 3 (Transect 9).**

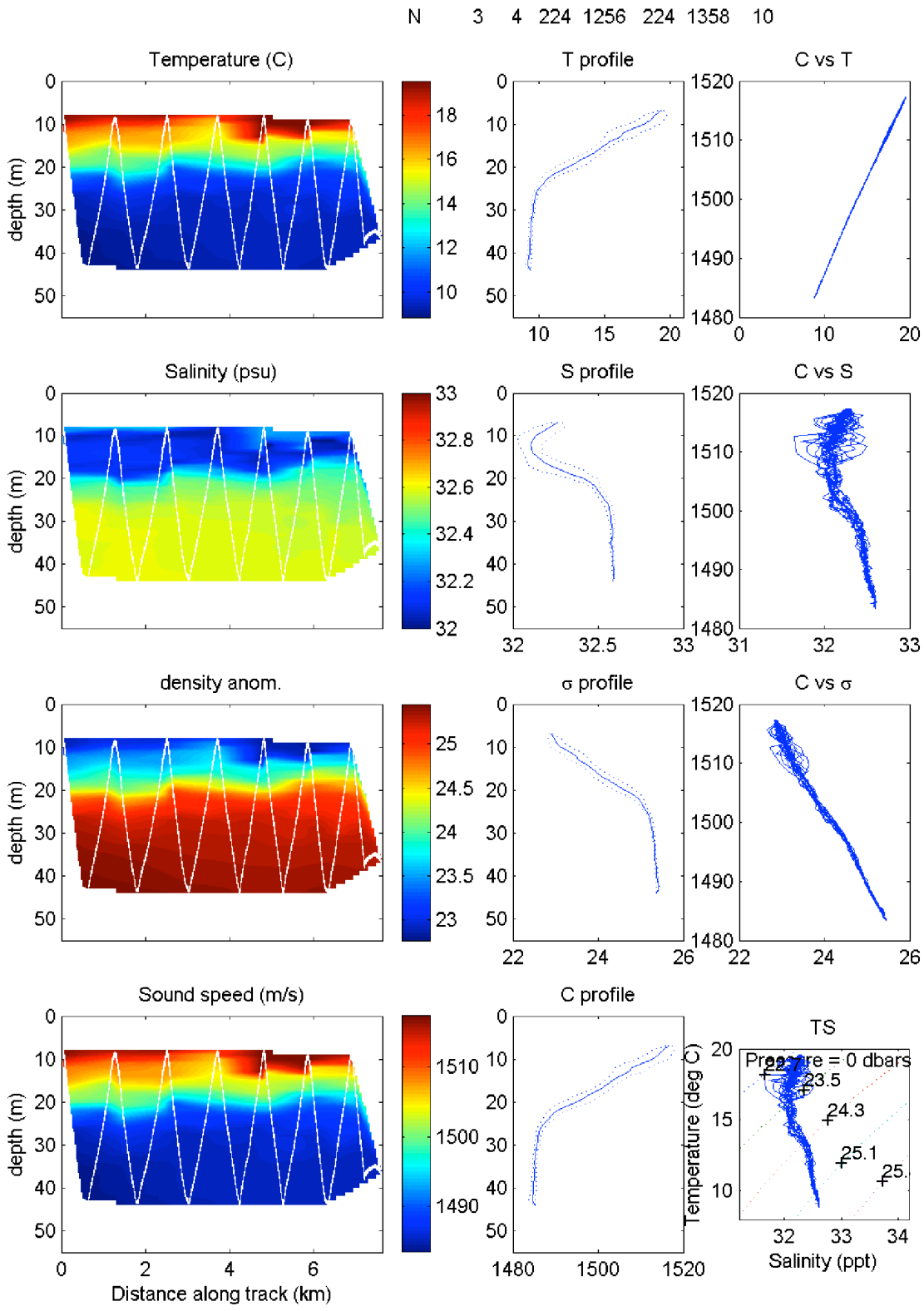


**Figure 4.3.4 T3-leg 4 (Transect 10).**

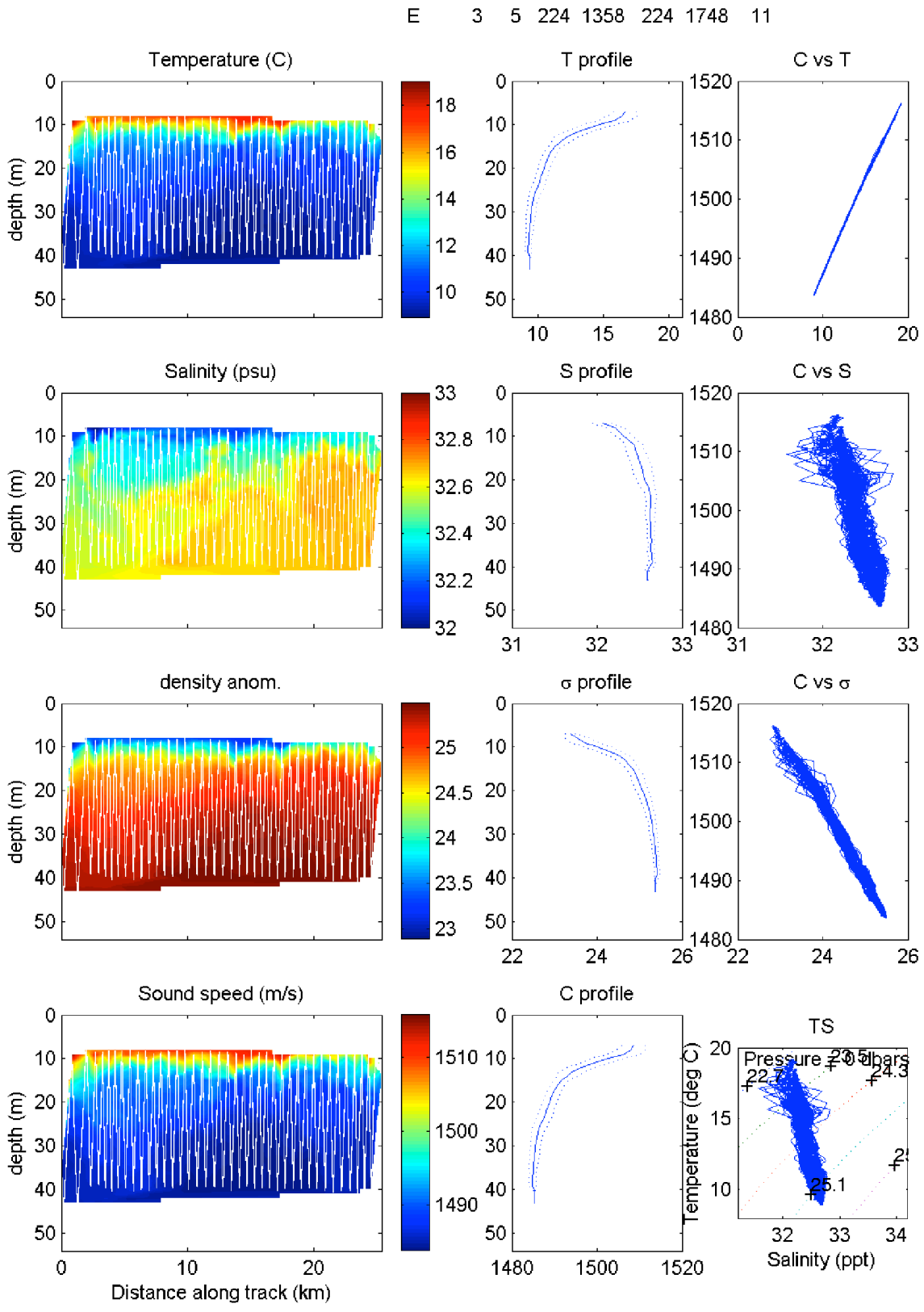


**Figure 4.3.5. T4-leg 5 (Transect 11).**

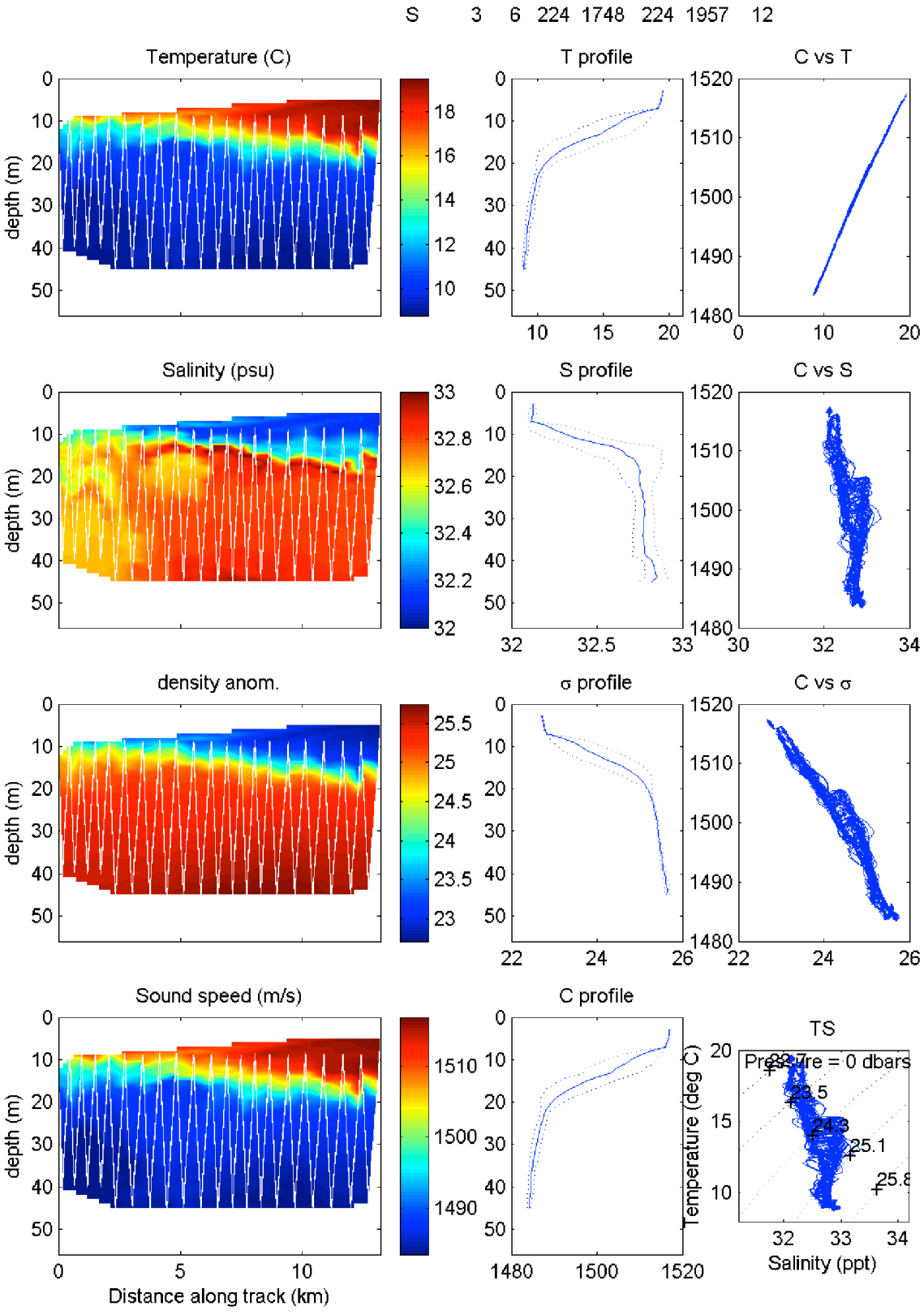


**Figure 4.3.6. T3-leg 6 T(ransect 12).**

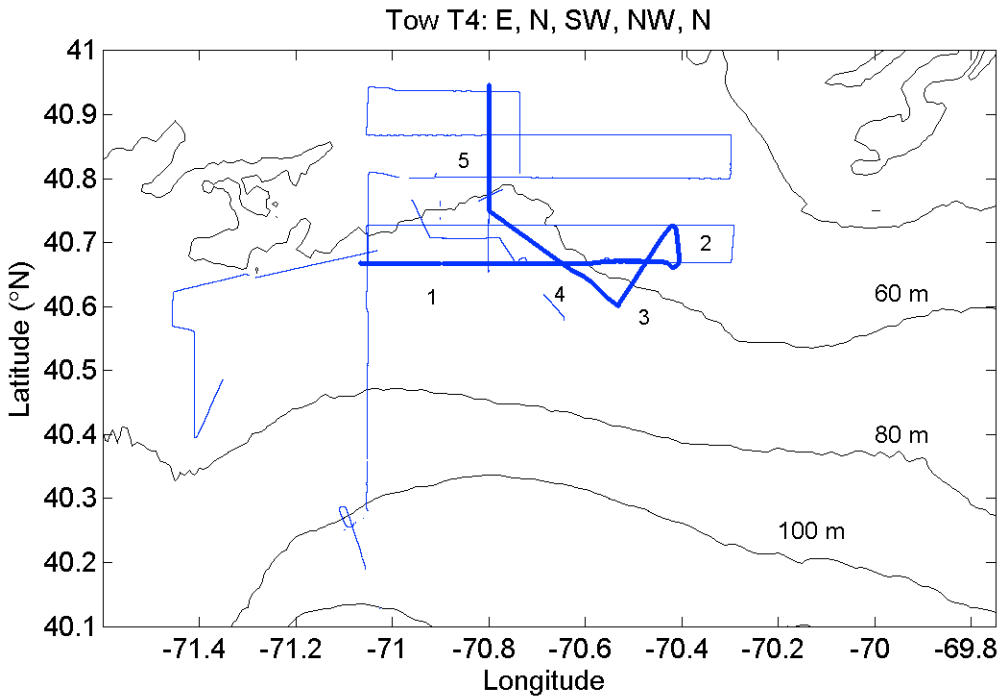


**Figure 4.4.0. The five T4 transects are shown.**

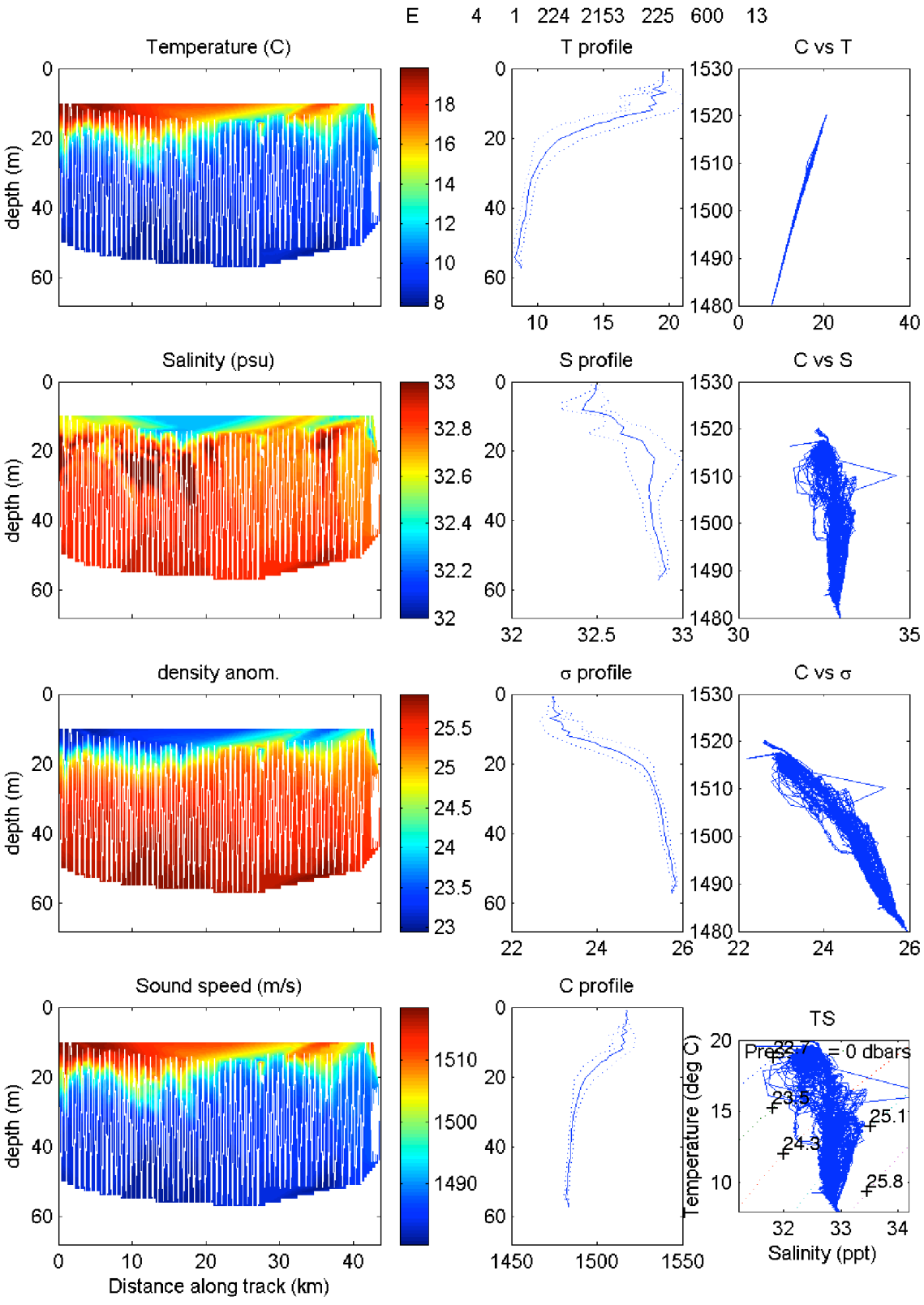


**Figure 4.4.1. T4-leg 1 (Transect 13).**

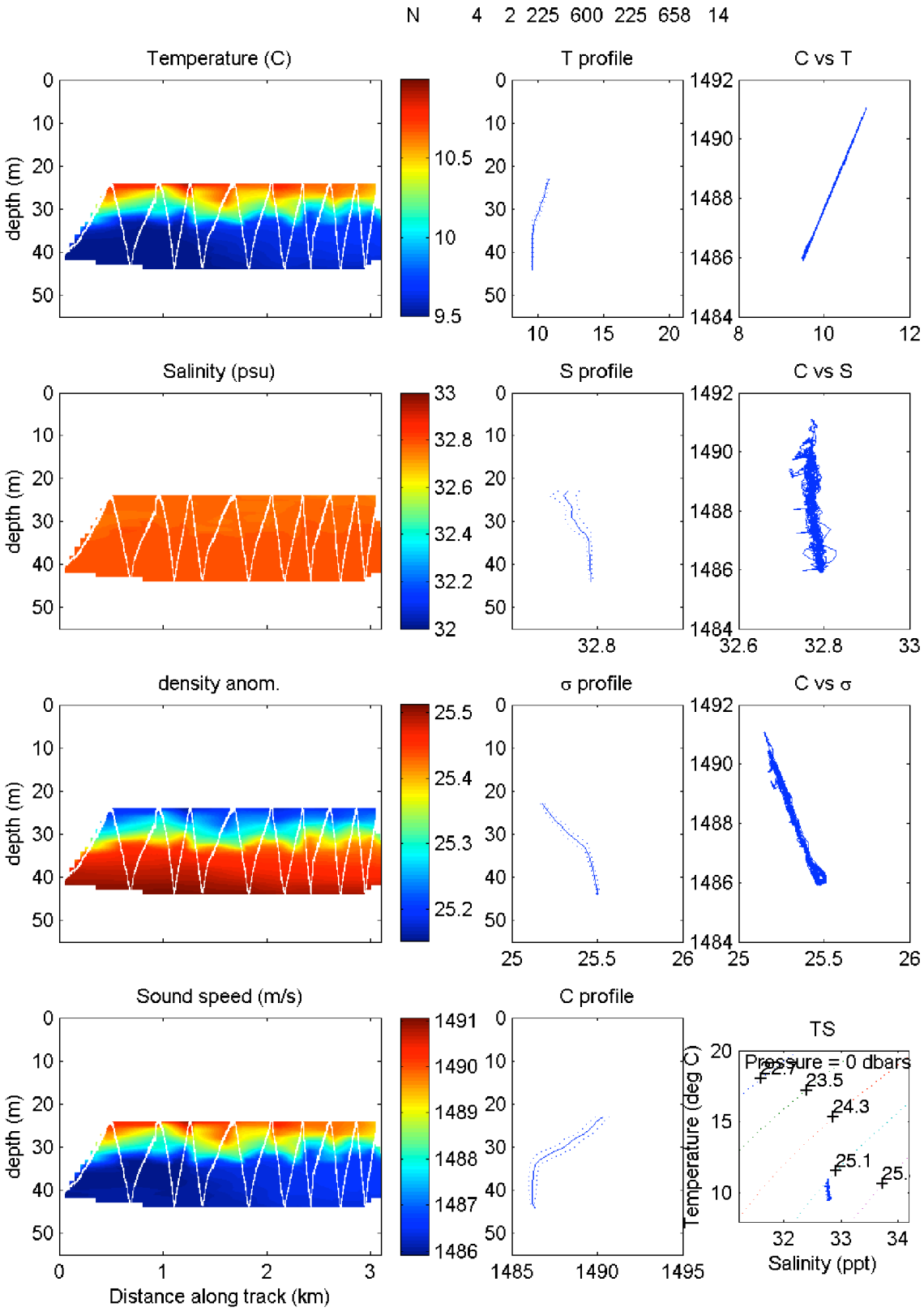


**Figure 4.4.2. T4-leg 2 (Transect 14).**

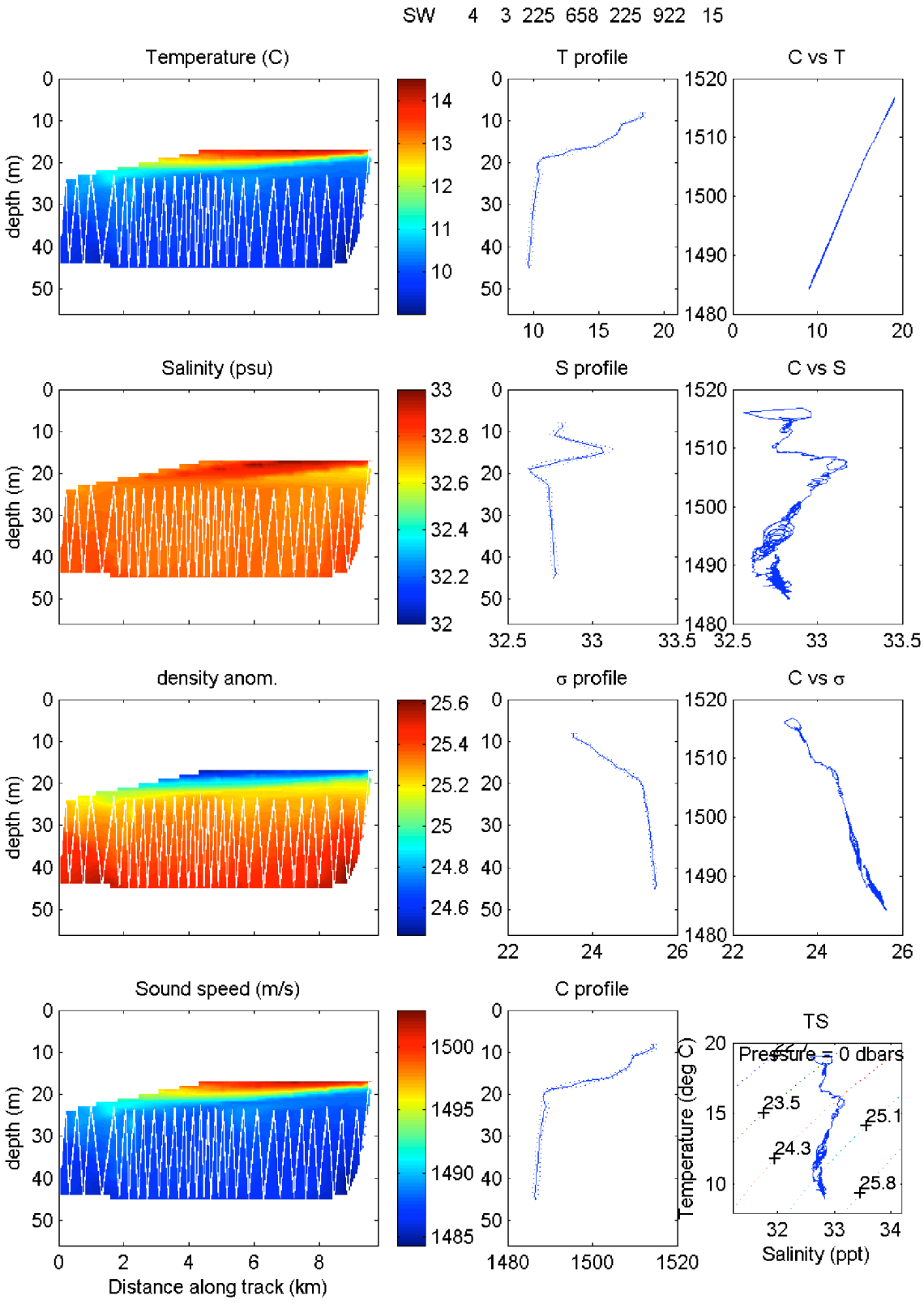


**Figure 4.4.3. T4-leg 3 (Transect 15).**

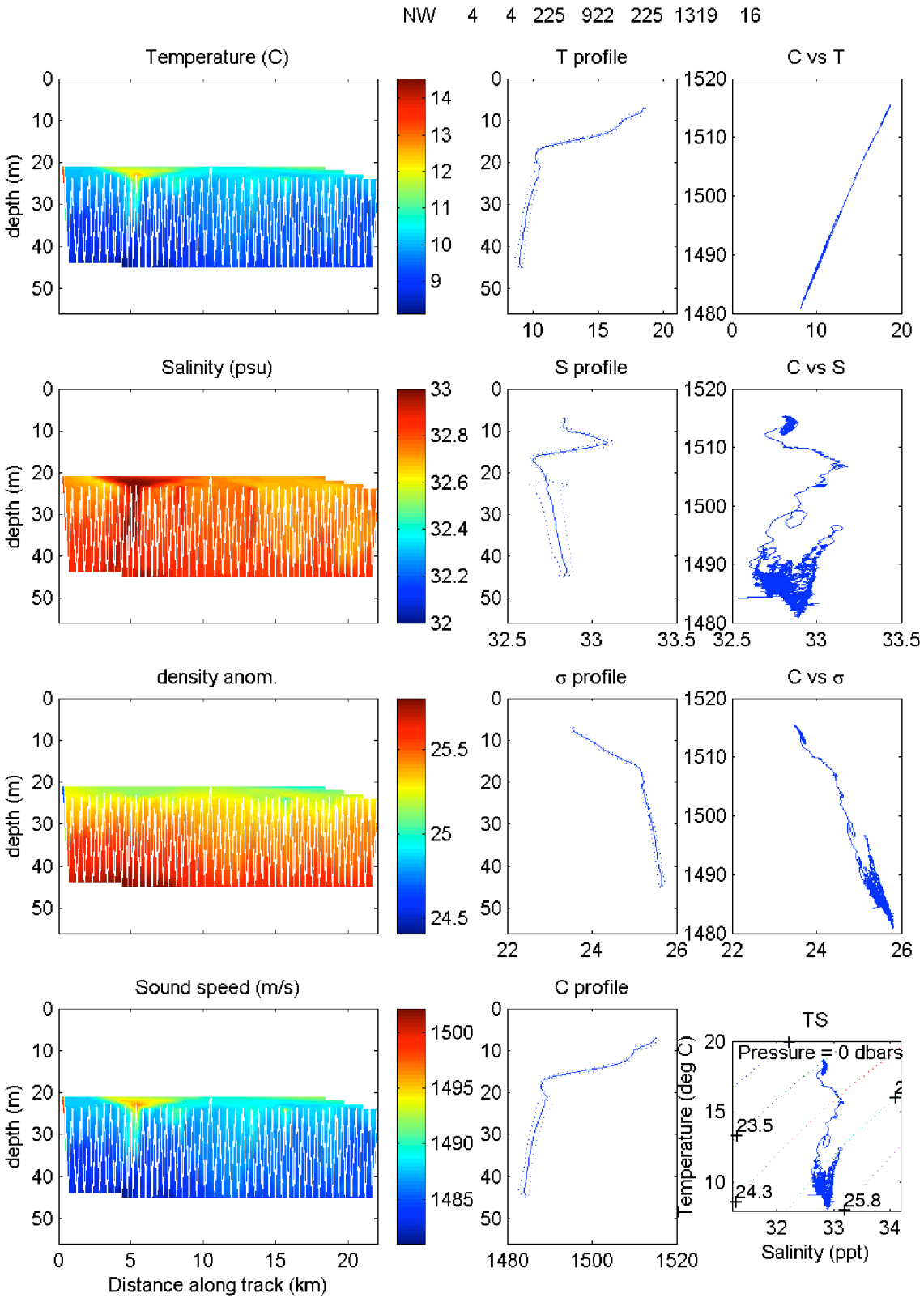


**Figure 4.4.4. T4-leg 4 (Transect 16).**

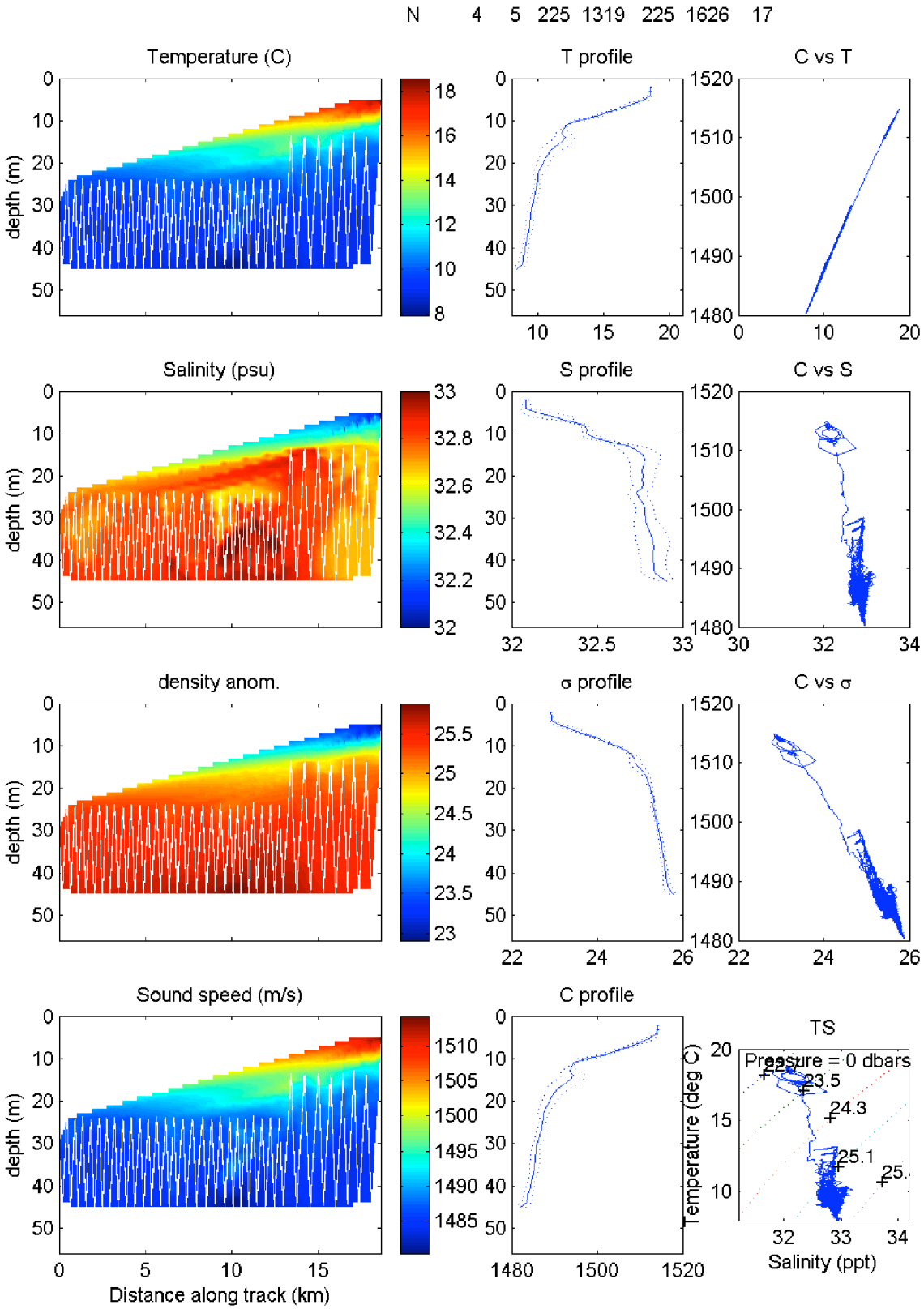


**Figure 4.4.5. T4-leg 5 (Transect 17).**

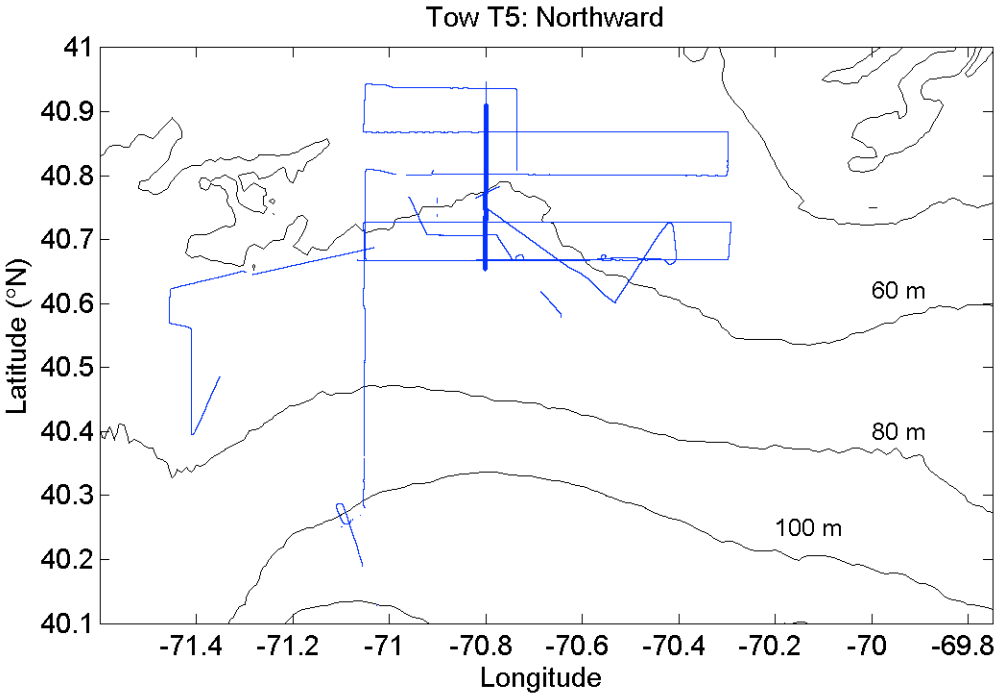


**Figure 4.5.0. The single leg of T5.**

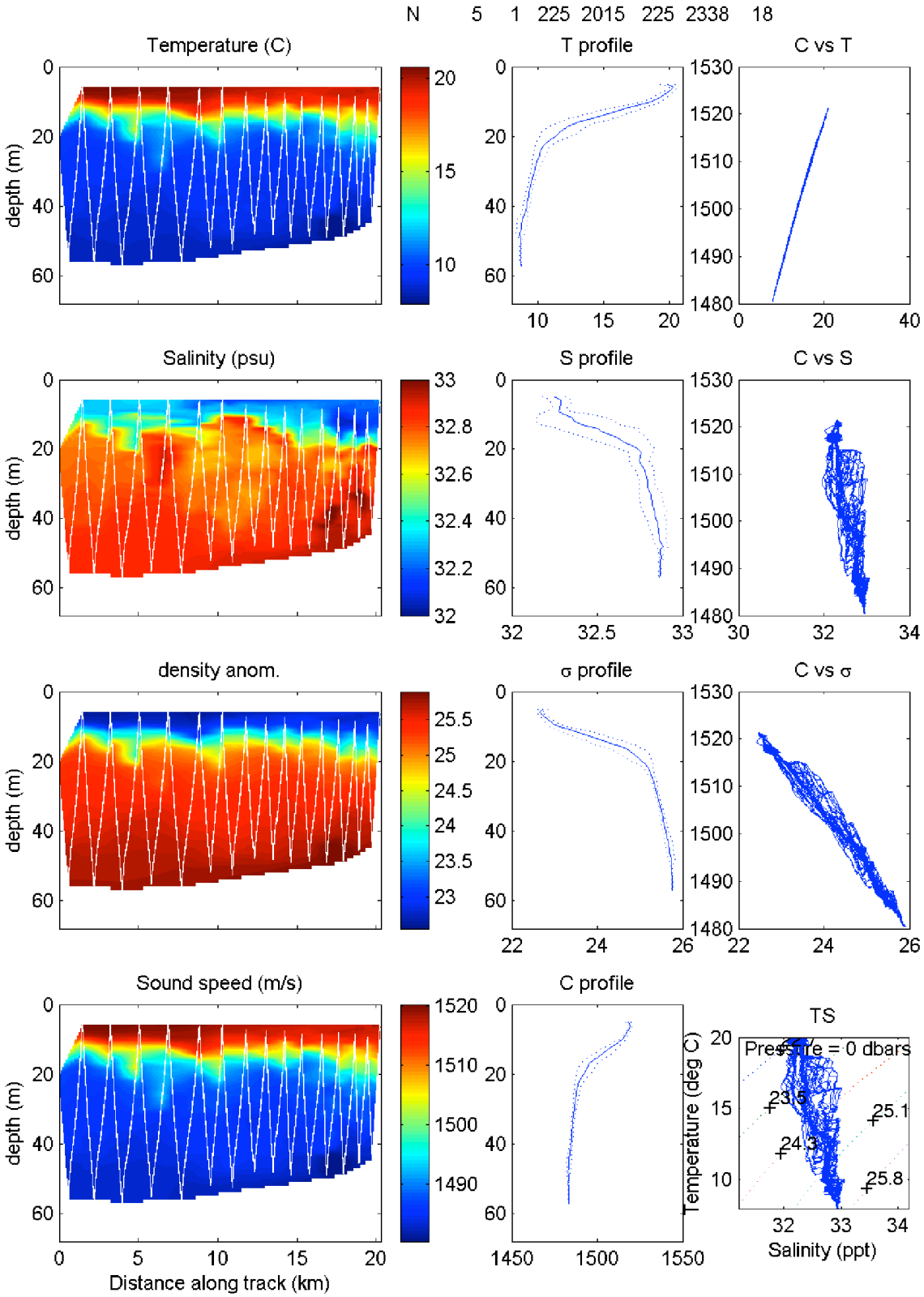


**Figure 4.5.1. T5-leg 1 (Transect 18).**

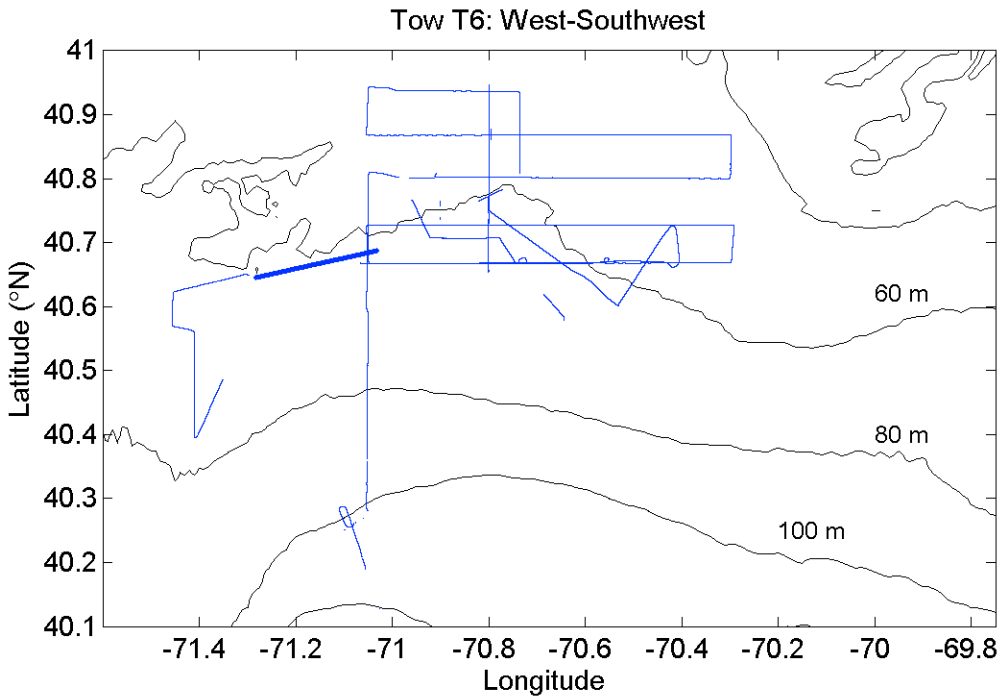


**Figure 4.6.0. The single leg of T6.**

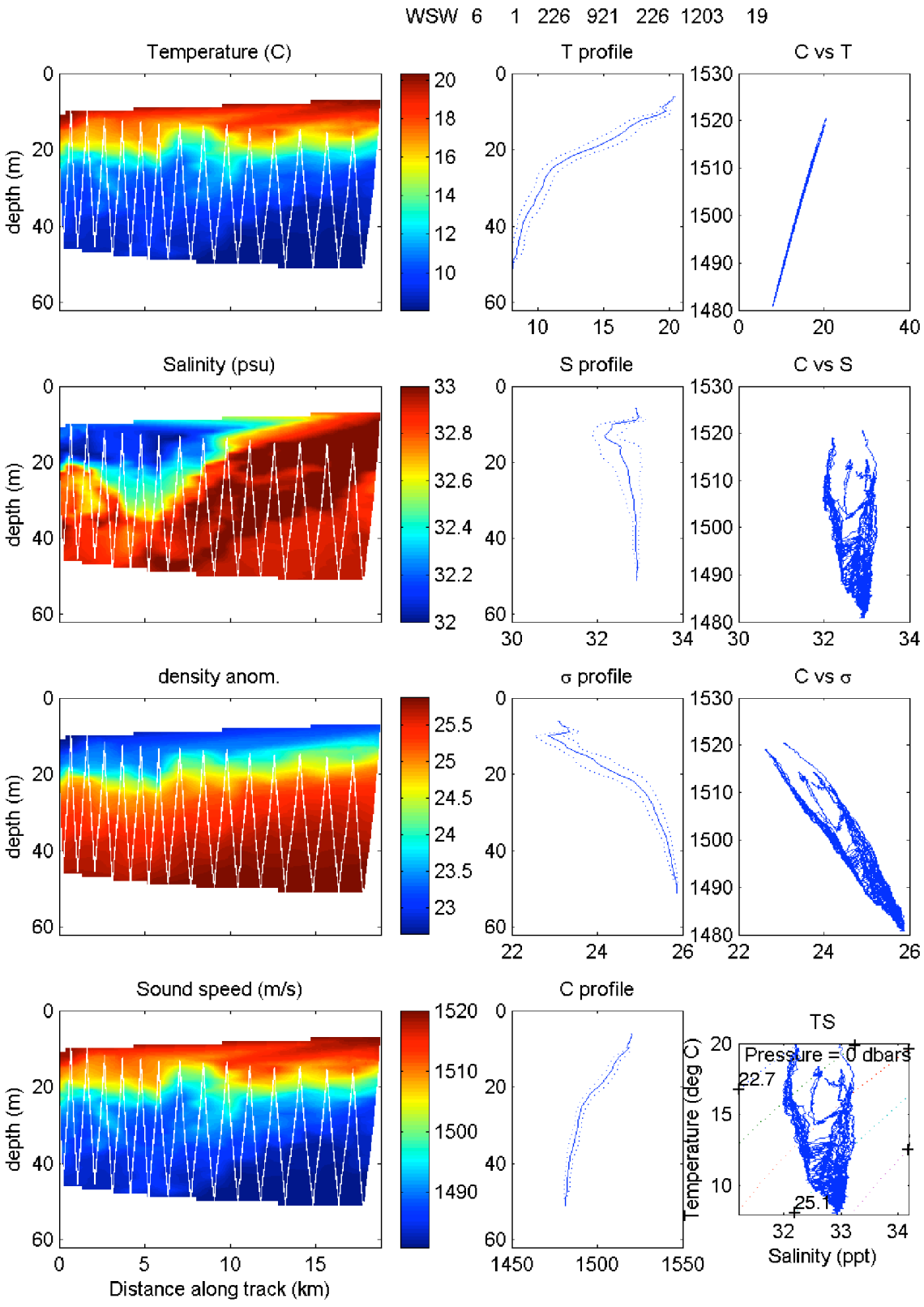


**Figure 4.6.1. T6-leg 1 (Transect 19).**

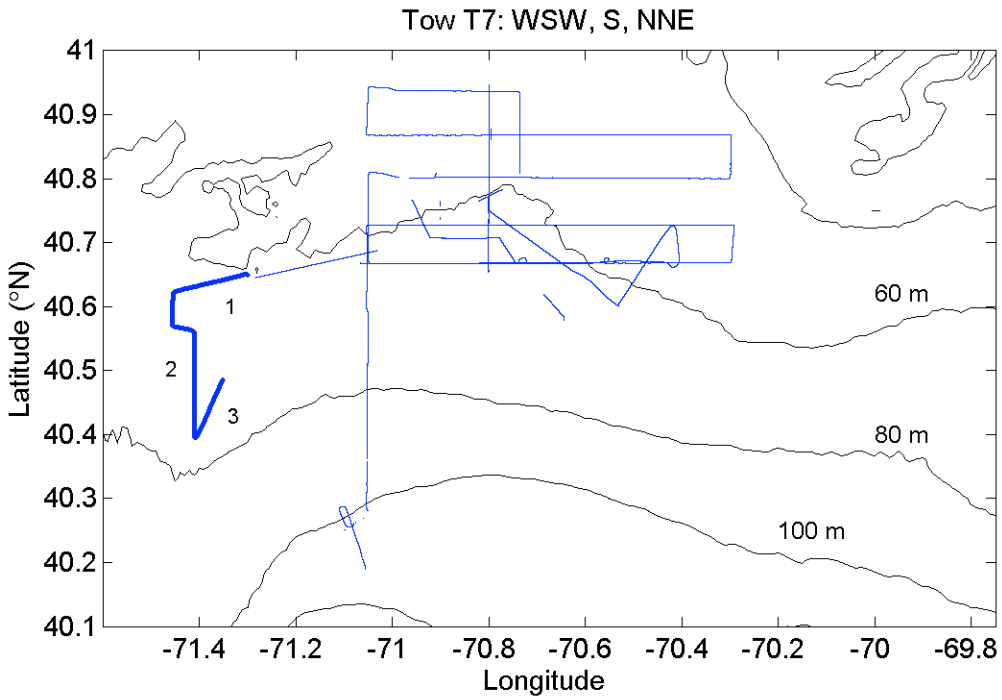


**Figure 4.7.0. T7 legs are shown.**

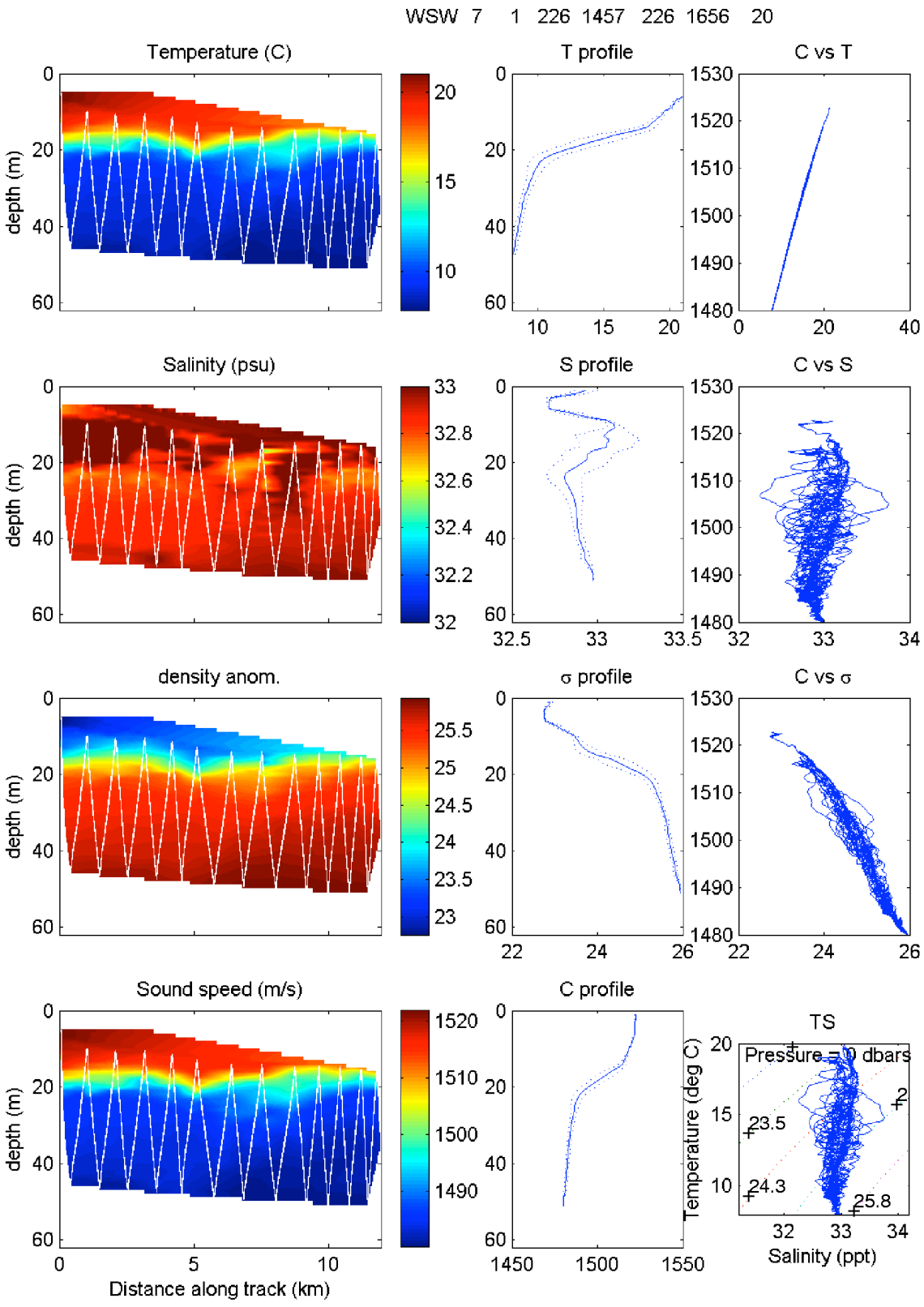


**Figure 4.7.1. T7-leg 1 (Transect 20).**

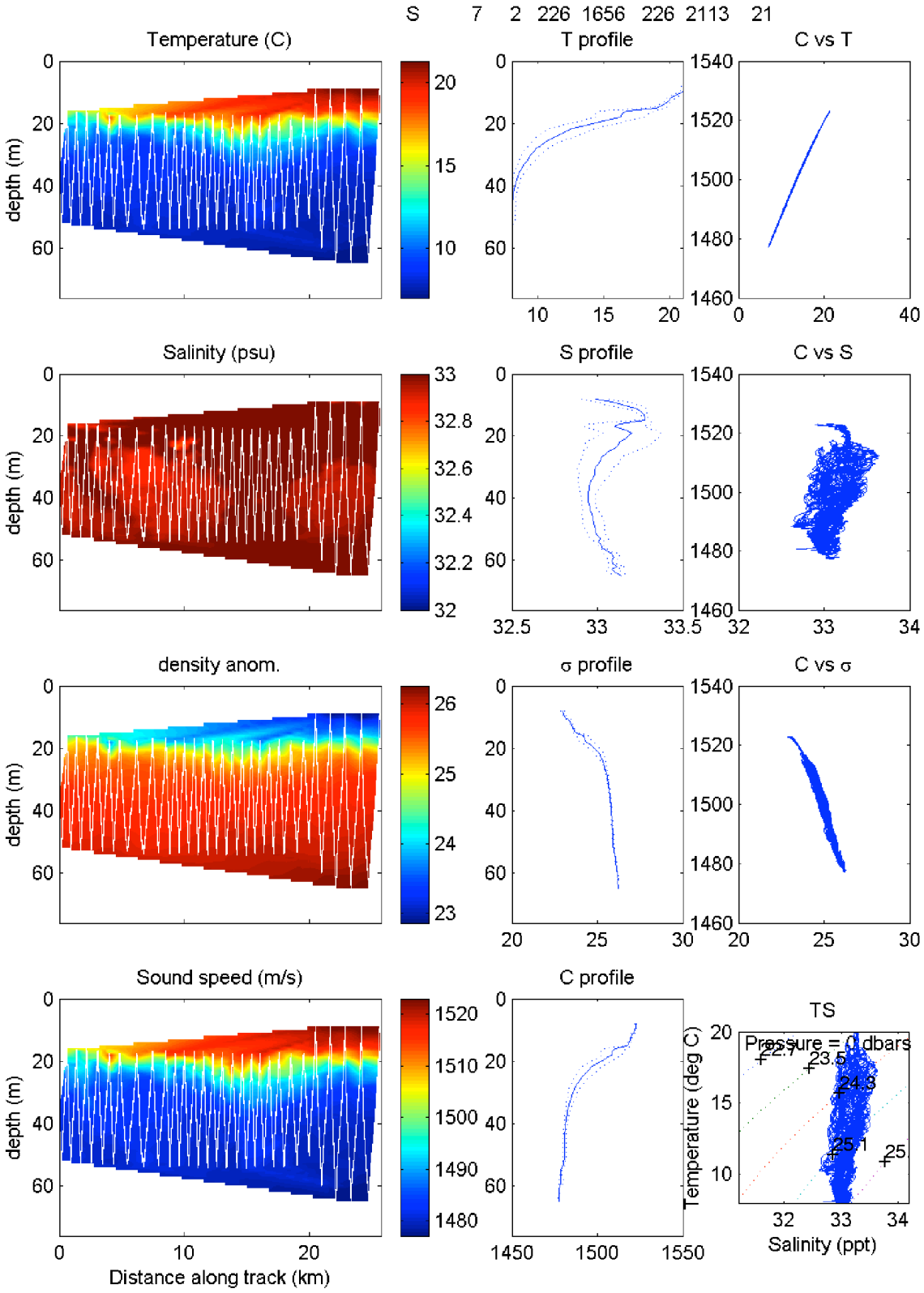


**Figure 4.7.2. T7-leg 2 (Transect 21).**

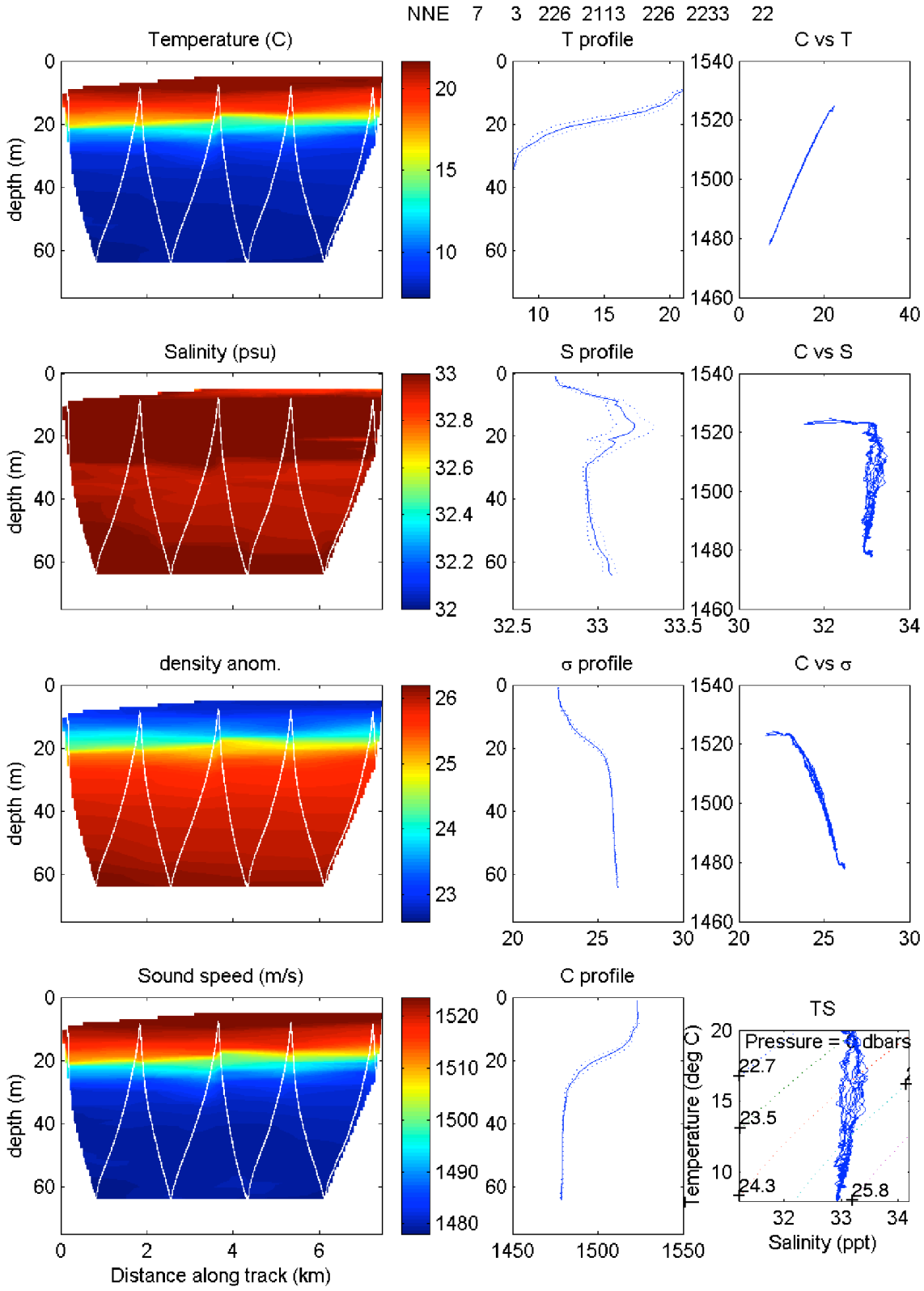


**Figure 4.7.3. T7-leg 3 (Transect 22).**

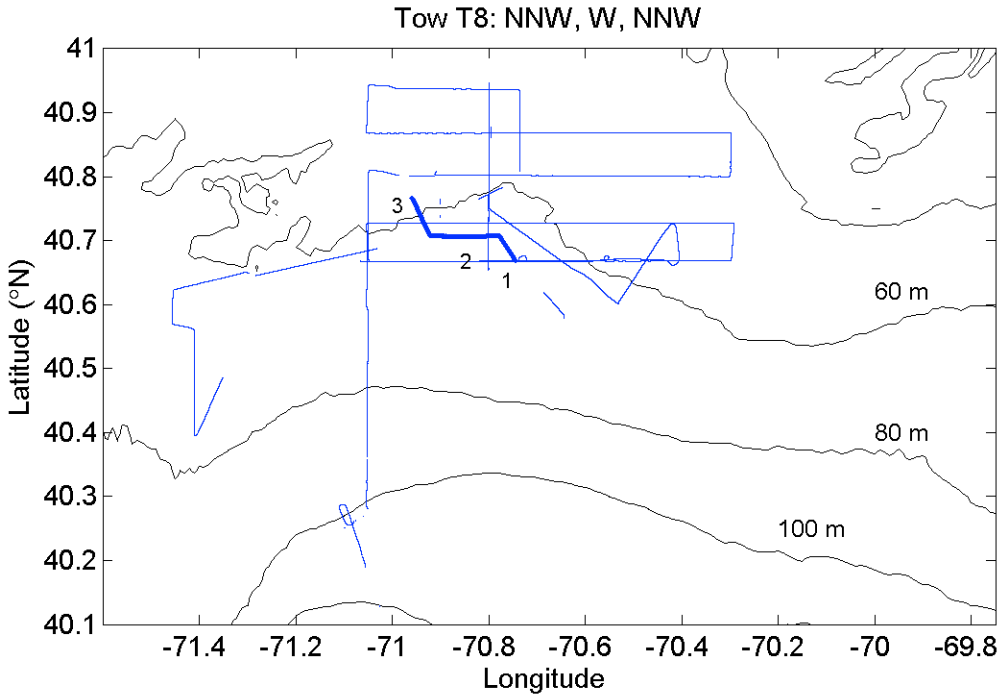


**Figure 4.8.0. T8 is shown.**

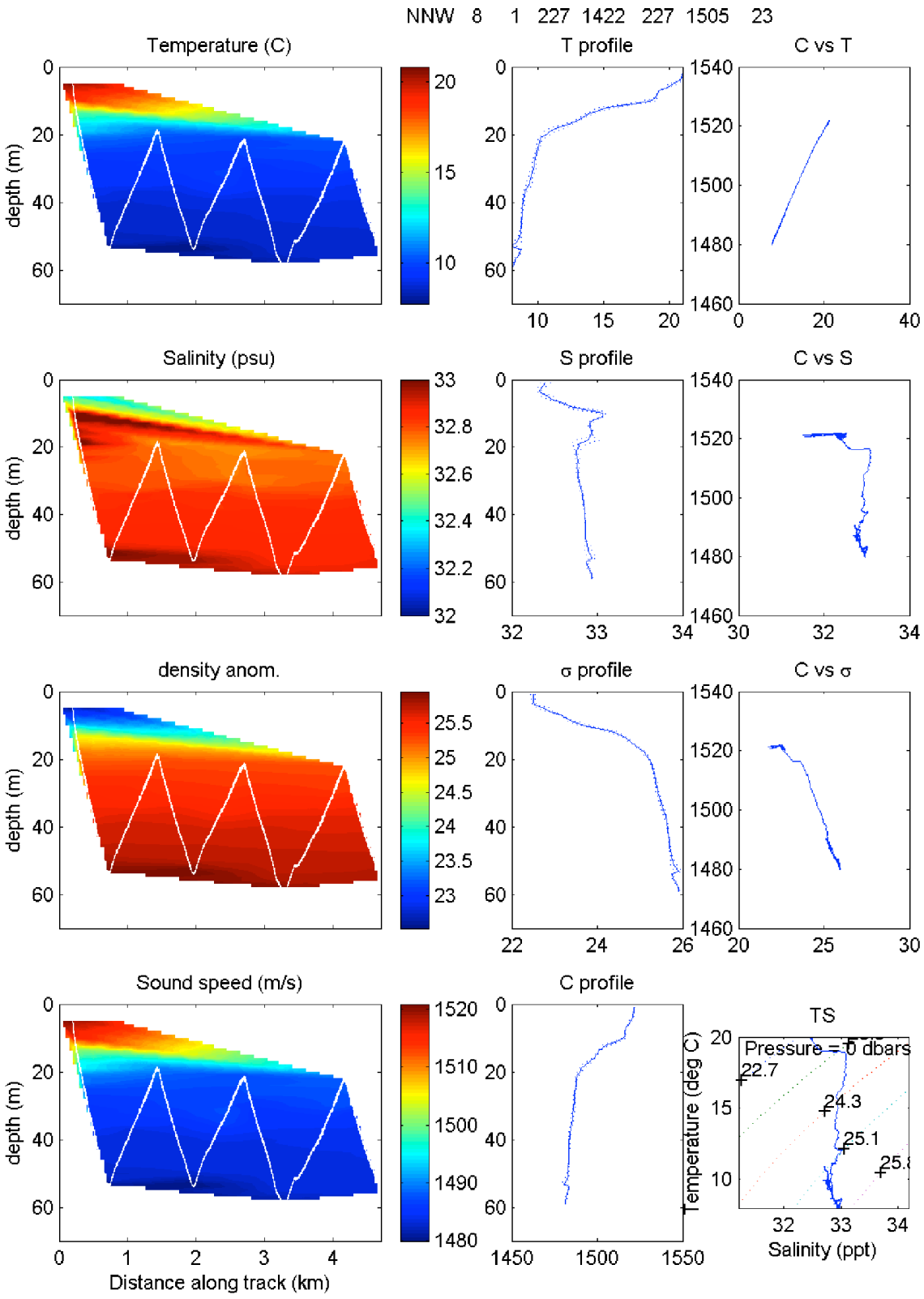


**Figure 4.8.1. T8-leg 1 (Transect 23).**

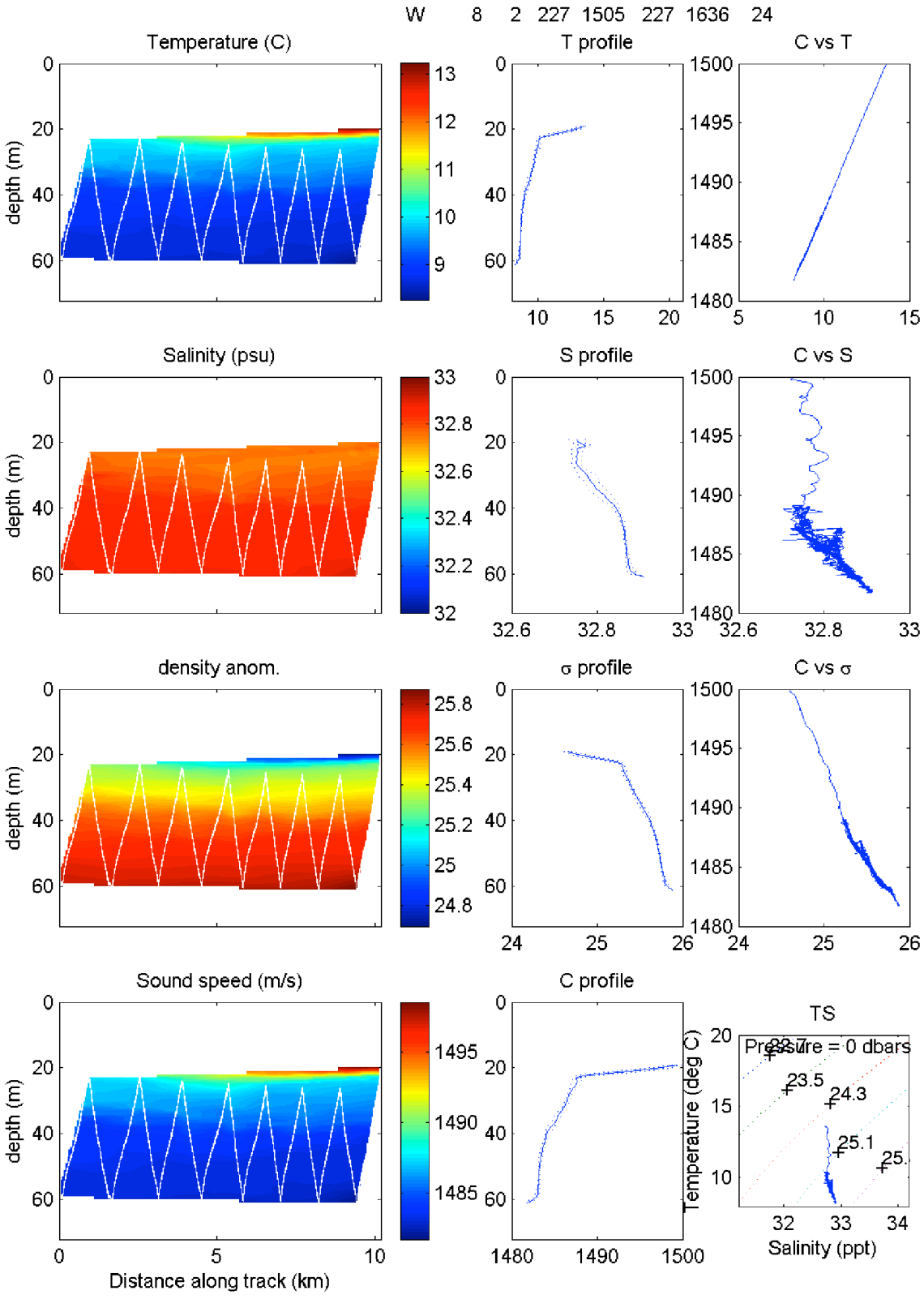


**Figure 4.8.2. T8-leg 2 (Transect 24).**

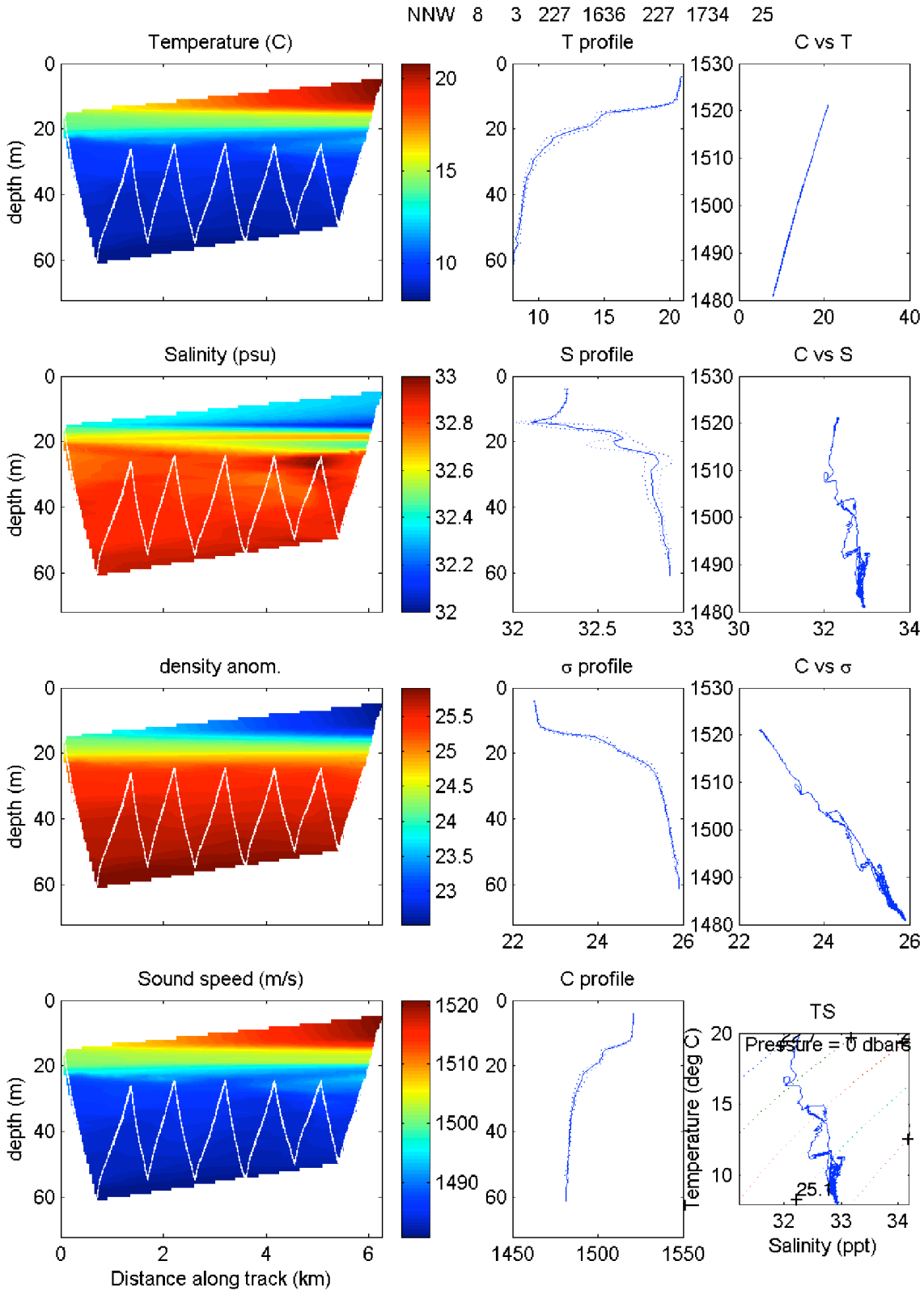


**Figure 4.8.3. T8-leg 3 (Transect 25).**

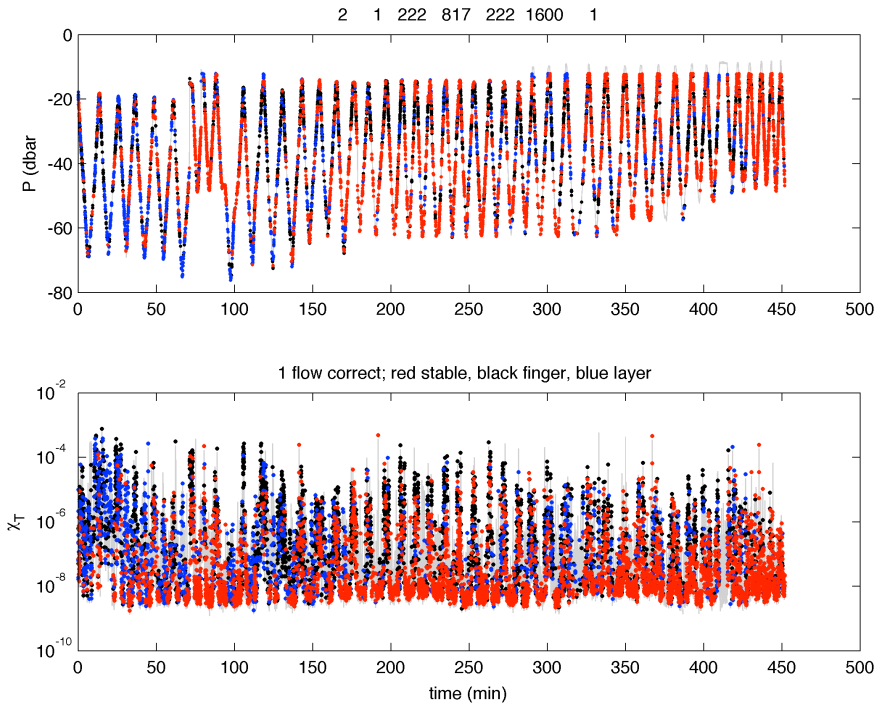


**Figure 5.2.1. T2-leg 1 (Transect 1). (top) The dots along the tow path indicate salt-finger favorable conditions in black, double-diffusive layering instability favorable conditions in blue, and doubly stable stratification in red. (bottom) Thermal variance dissipation rate is shown versus time, with the colors indicate stratification as above.**

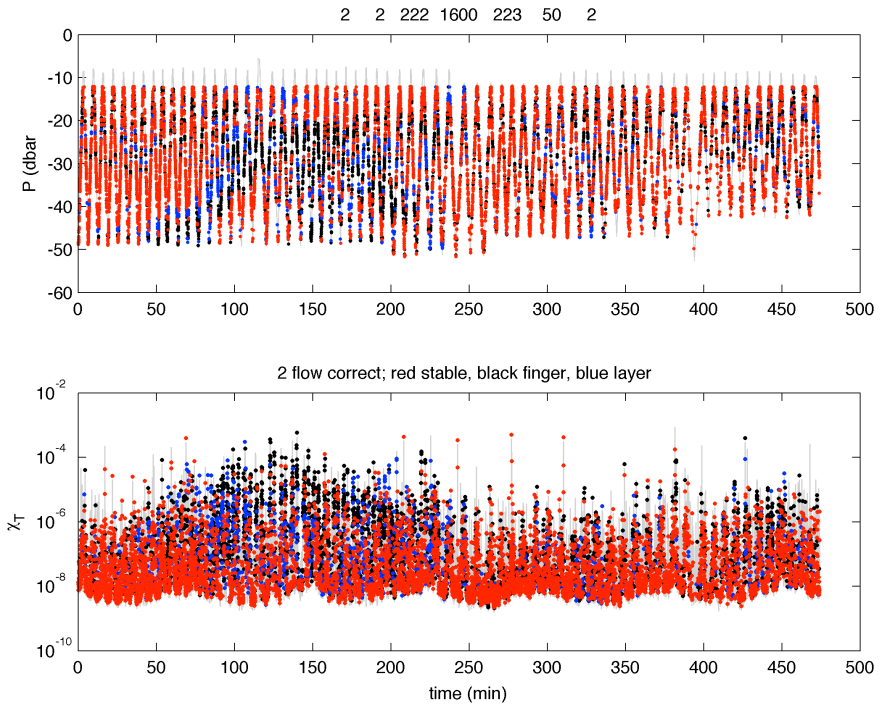


**Figure 5.2.2. T2-leg 2 (Transect 2).**

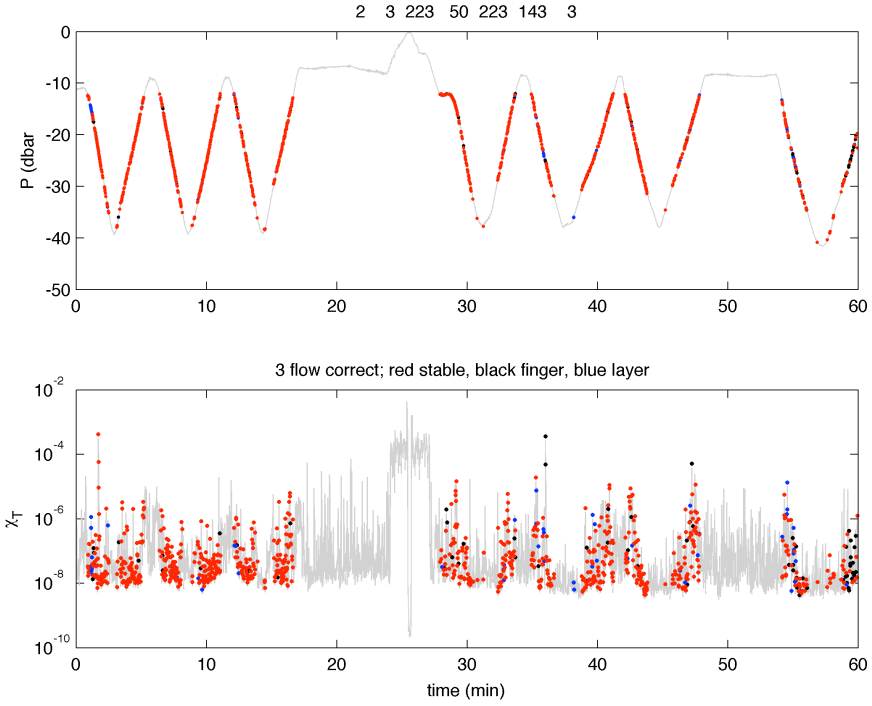


**Figure 5.2.3. T2-leg 3 (Transect 3).**

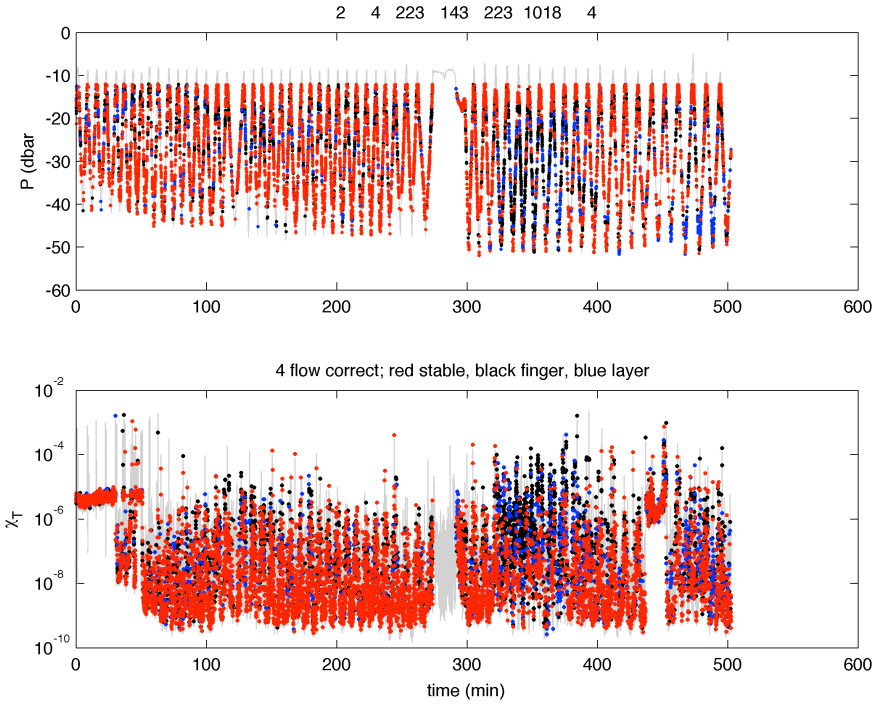


**Figure 5.2.4. T2-leg 4 (Transect 4).**

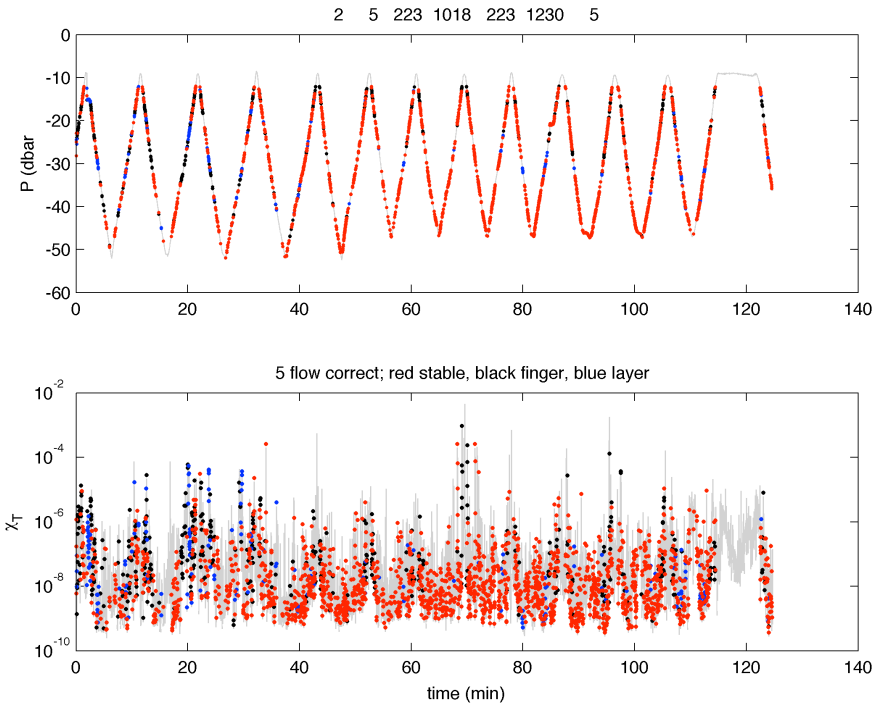


**Figure 5.2.5. T2-leg 5 (Transect 5).**

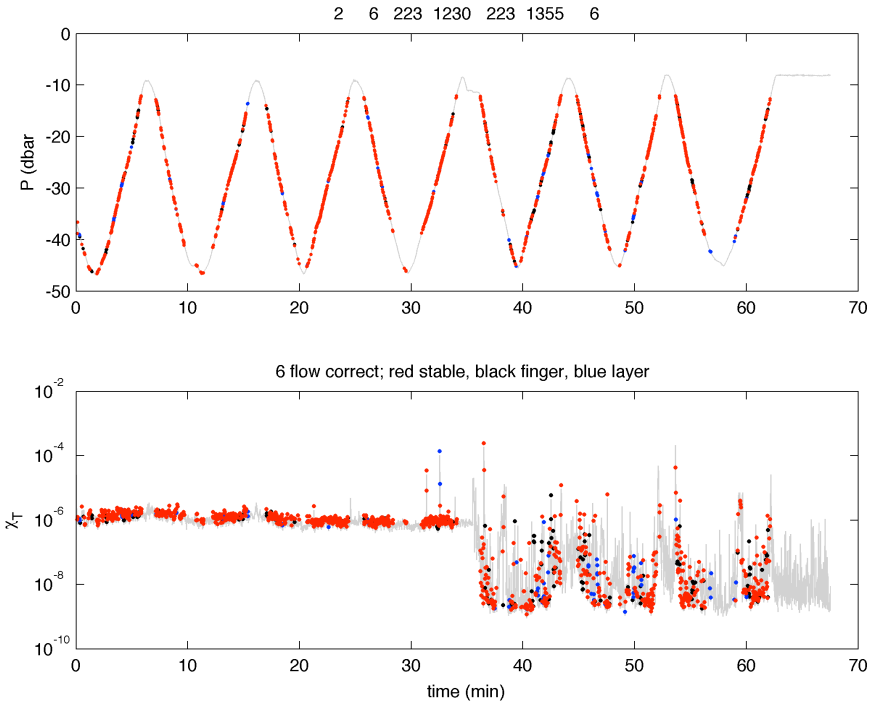


**Figure 5.2.6. T2-leg 6 (Transect 6).**

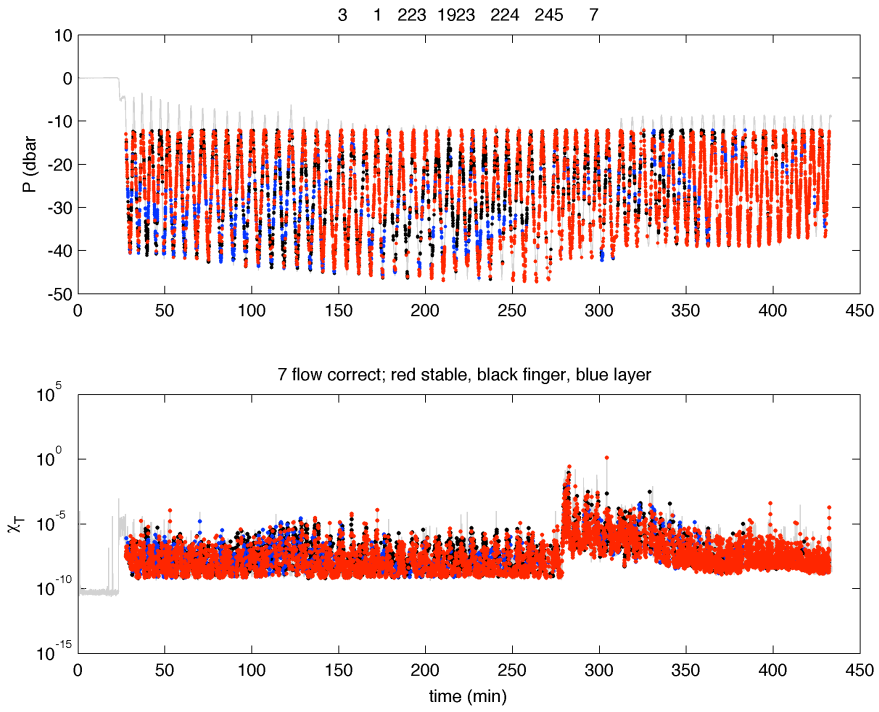


**Figure 5.3.1. T3-leg 1 (Transect 7).**

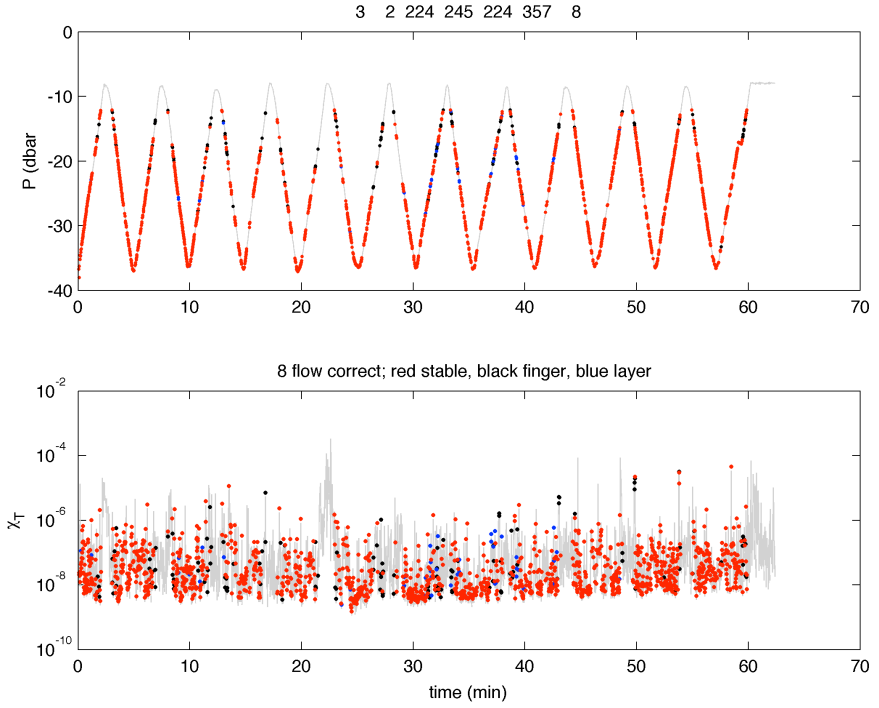


**Figure 5.3.2. T3-leg 2 (Transect 8).**

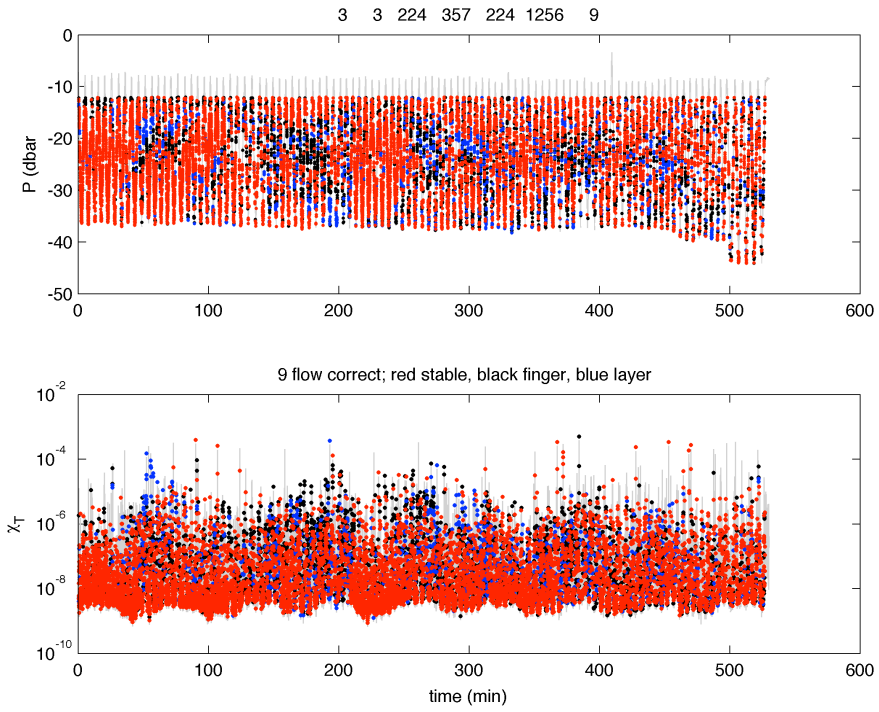


**Figure 5.3.3. T3-leg 3 (Transect 9).**

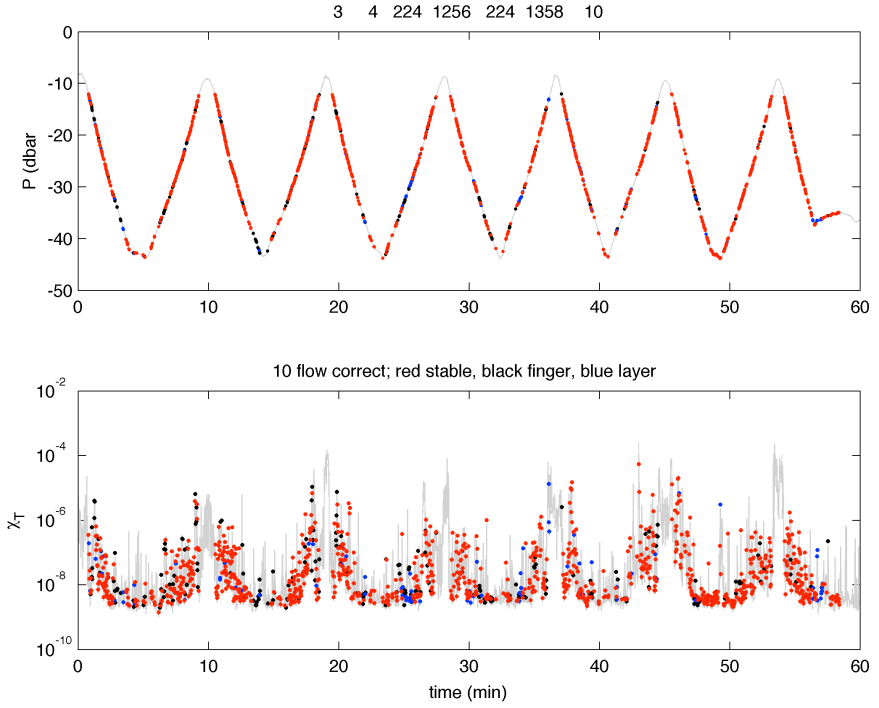


**Figure 5.3.4. T3-leg 4 (Transect 10).**

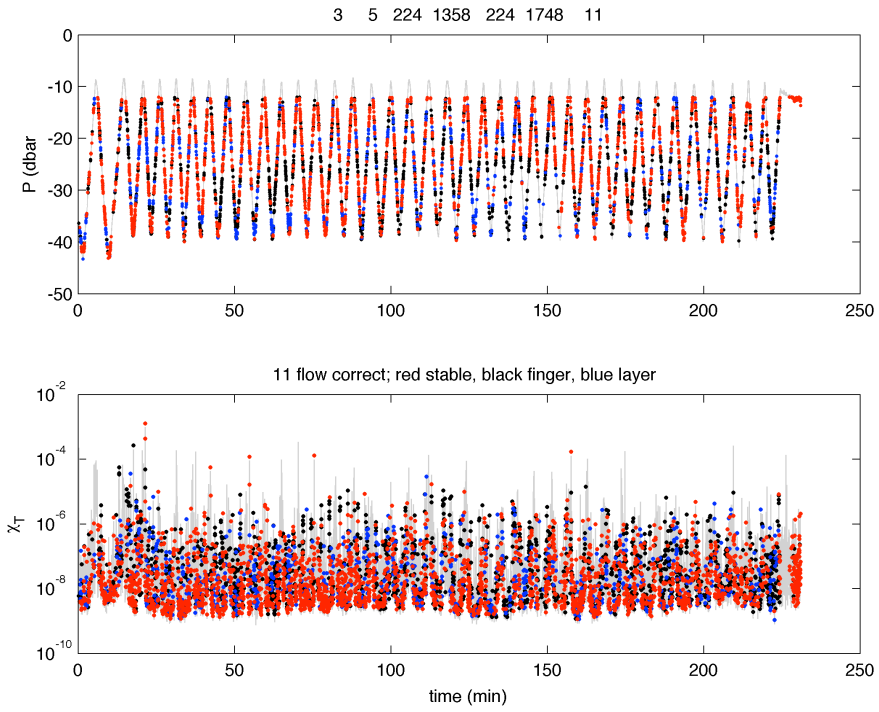


**Figure 5.3.5. T3-leg 5 (Transect 11).**

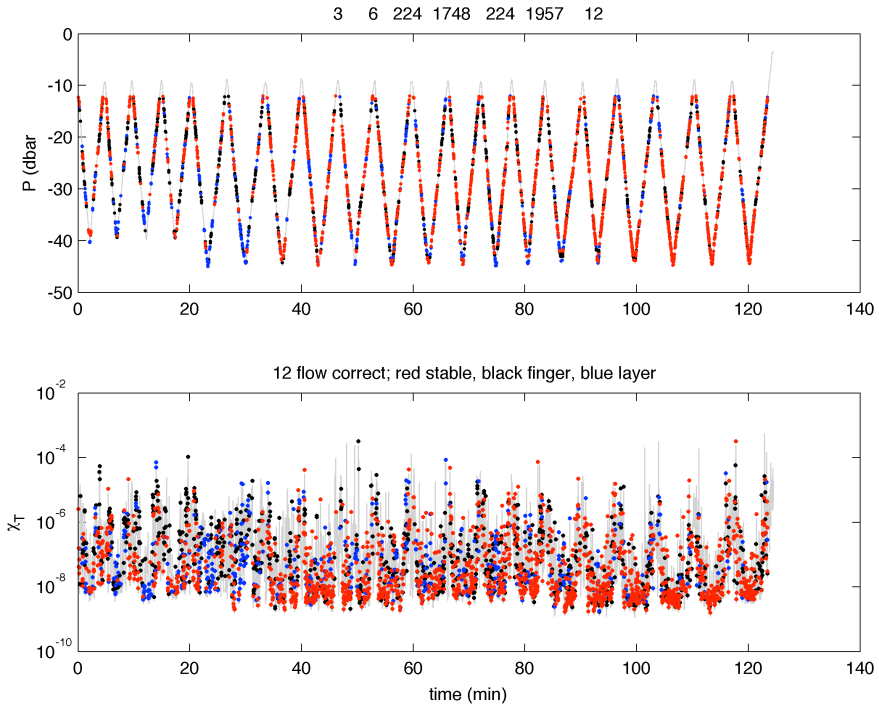


**Figure 5.3.6. T3-leg 6 (Transect 12).**

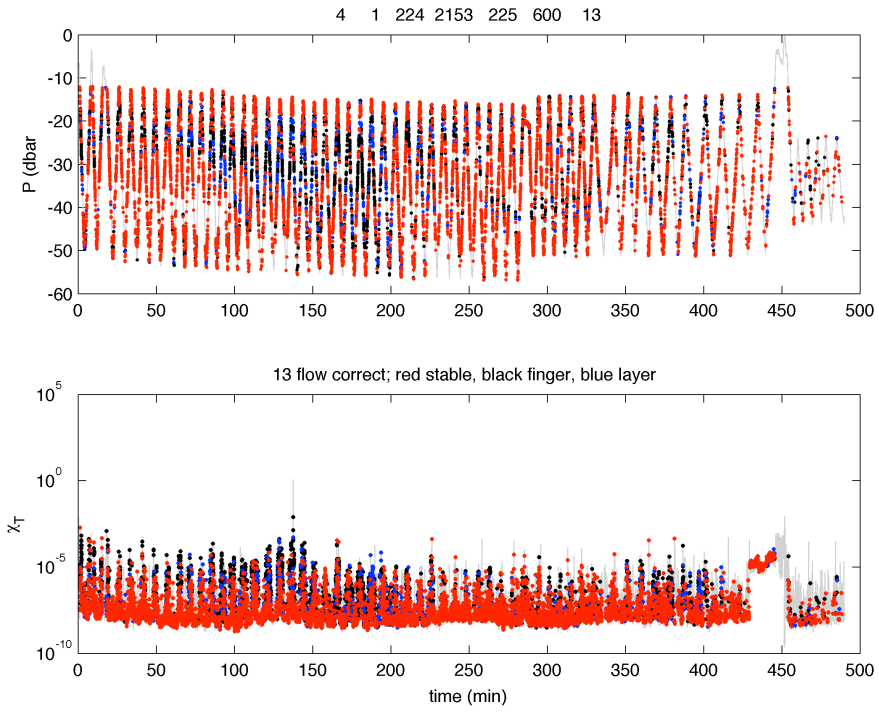


**Figure 5.4.1. T4-leg 1 (Transect 13).**

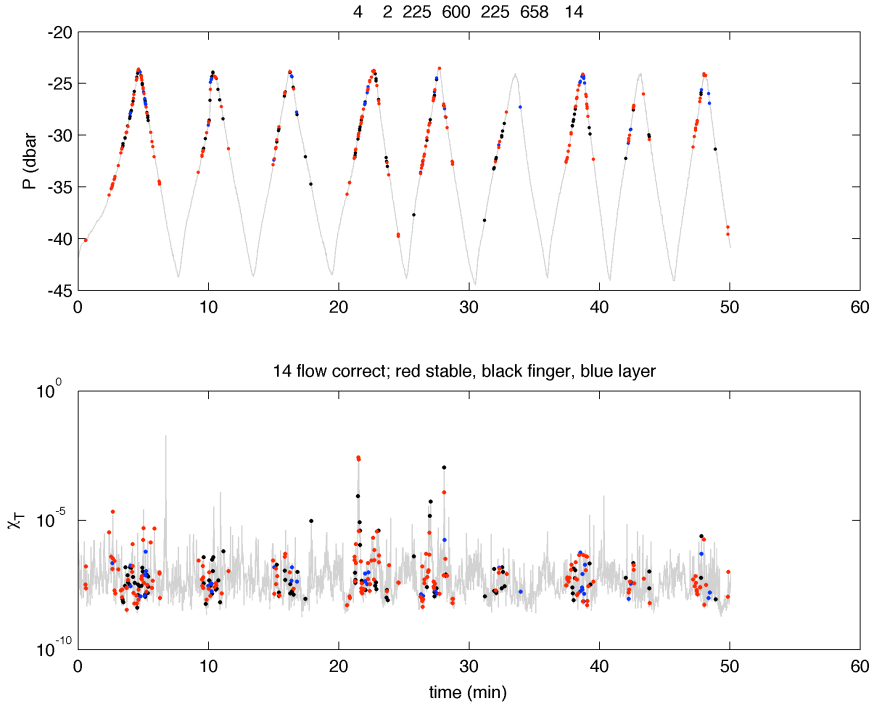


**Figure 5.4.2. T4-leg 2 (Transect 14).**

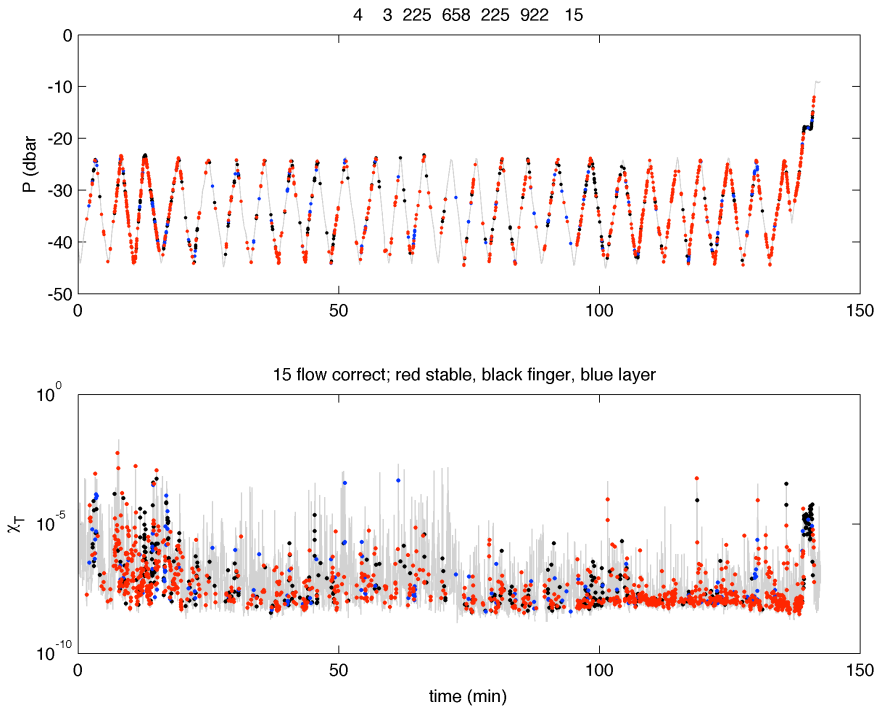


**Figure 5.4.3. T4-leg 3 (Transect 15).**

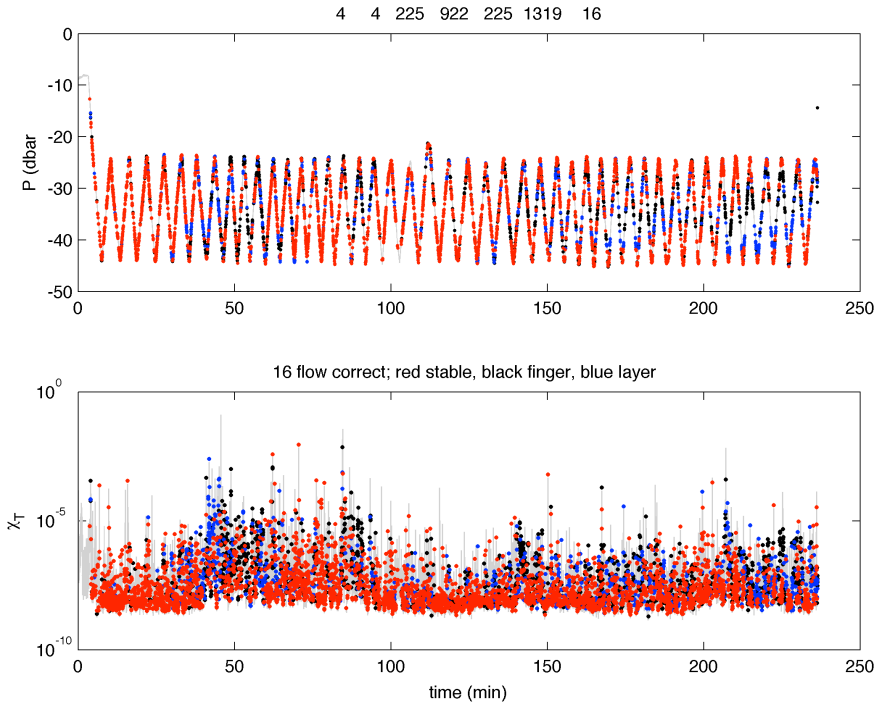


**Figure 5.4.4. T4-leg 4 (Transect 16).**

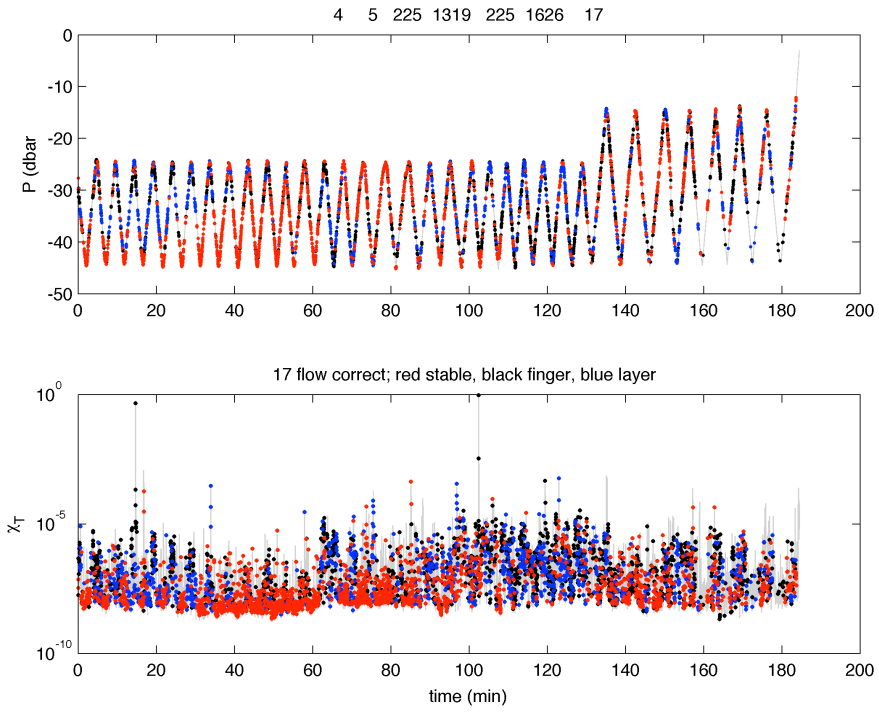


**Figure 5.4.5. T4-leg 5 (Transect 17).**

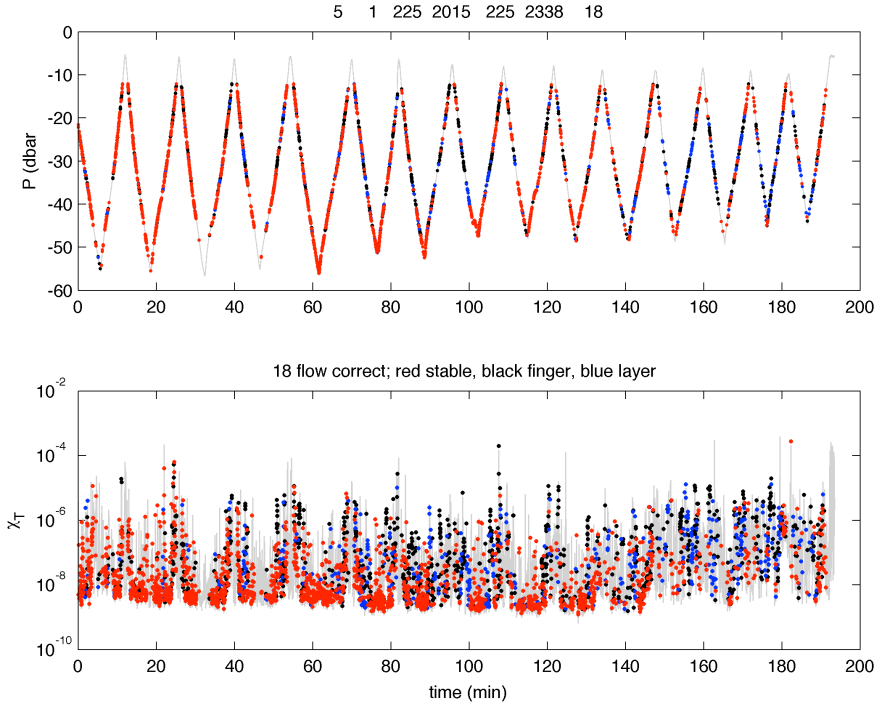


**Figure 5.5.1. T5-leg 1 (Transect 18).**

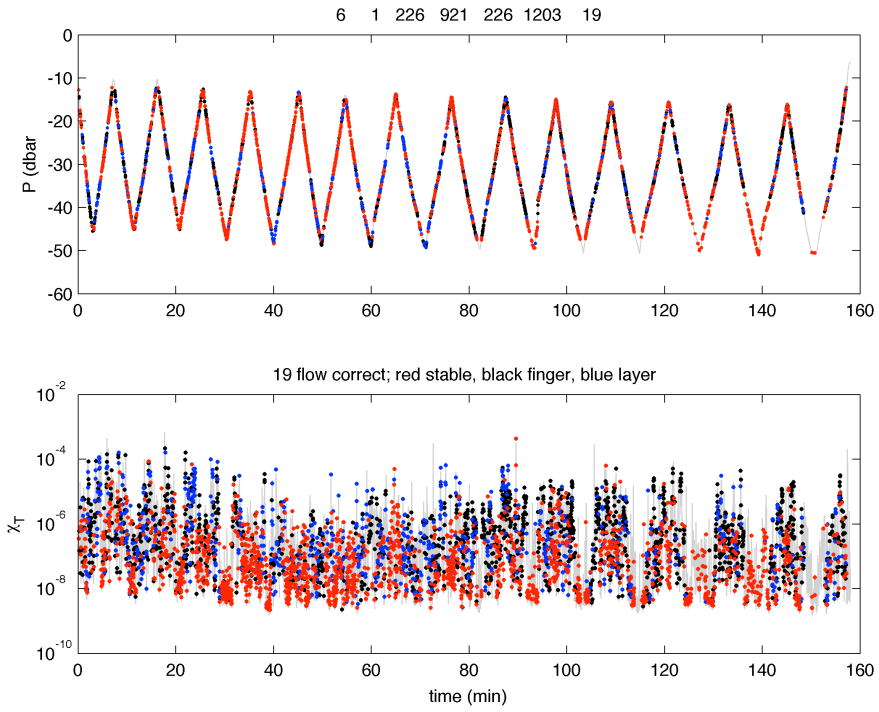


**Figure 5.6.1. T6-leg 1 (Transect 19).**

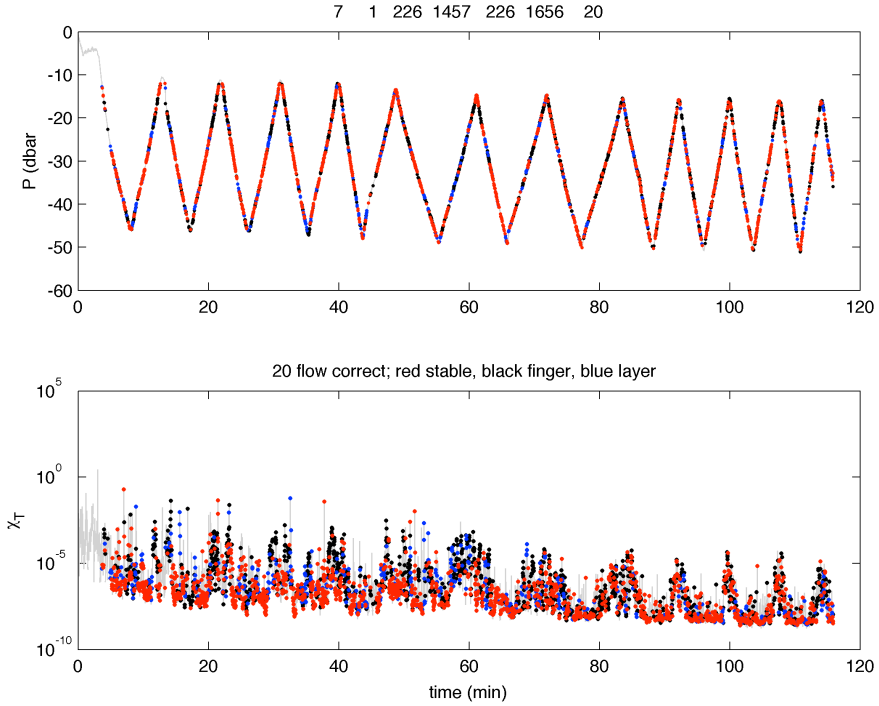


**Figure 5.7.1. T7-leg 1 (Transect 20).**

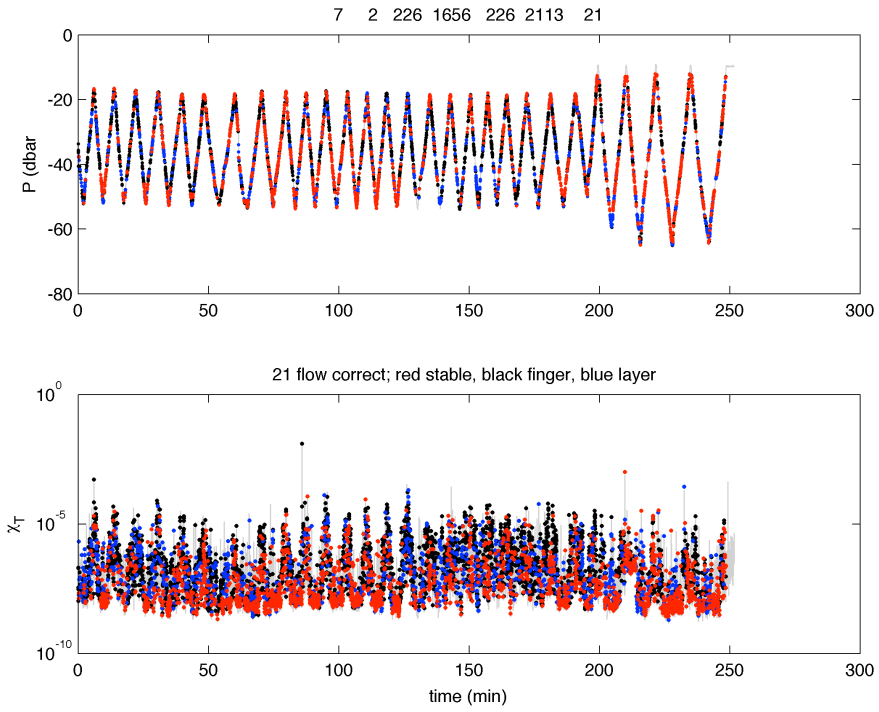


**Figure 5.7.2. T7-leg 2 (Transect 21).**

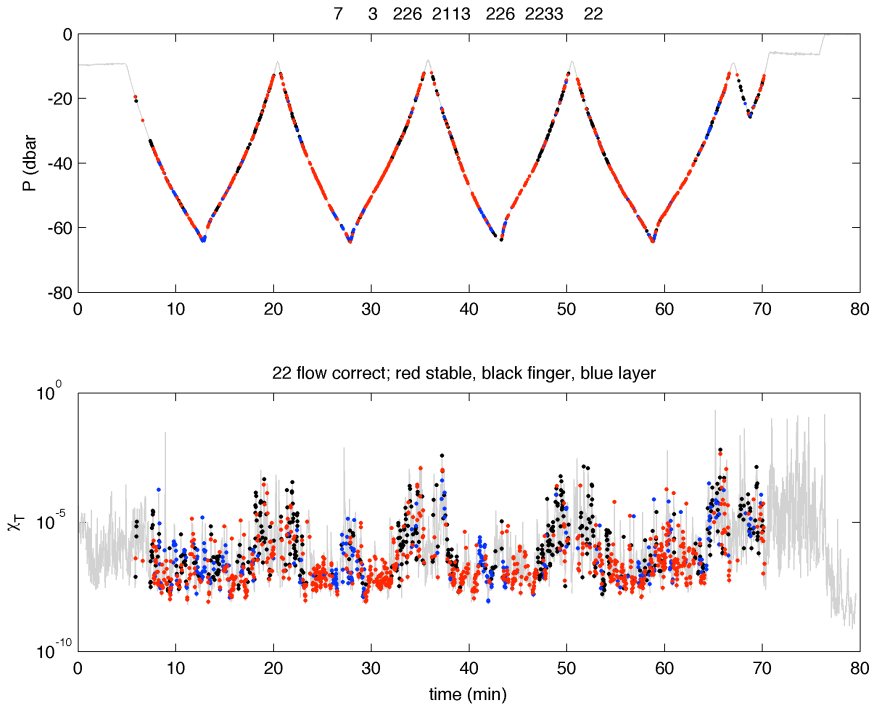


**Figure 5.7.3. T7-leg 3 (Transect 22).**

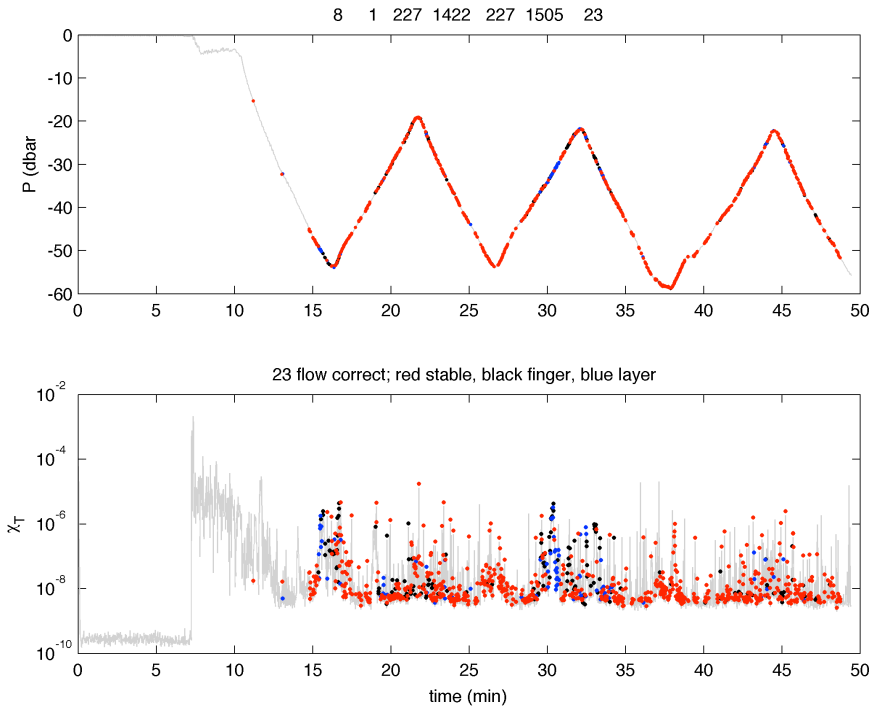


**Figure 5.8.1. T8-leg 1 (Transect 23).**

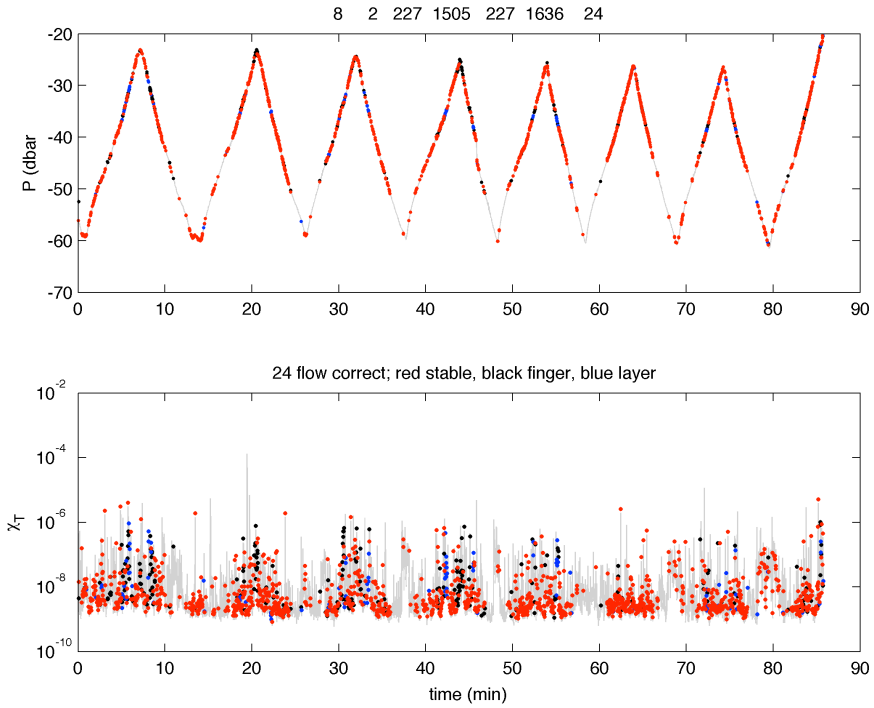


**Figure 5.8.2. T8-leg 1 (Transect 24).**

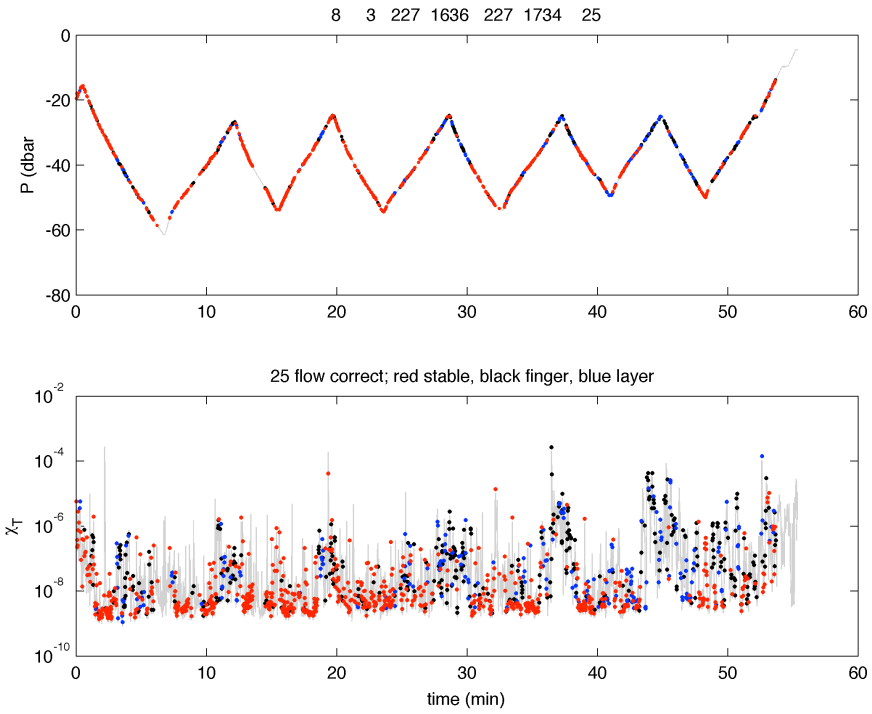


**Figure 5.8.3. T8-leg 3 (Transect 25).**

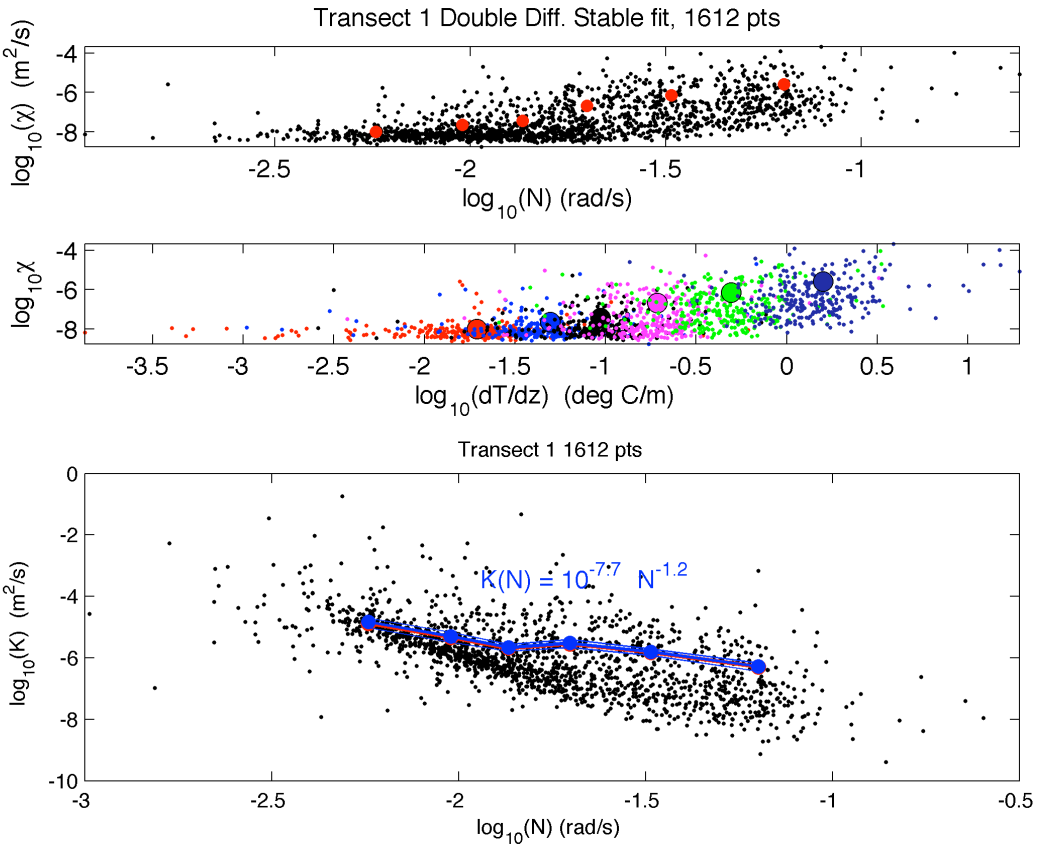


**Figure 6.A.1. T2-leg 1 (Transect 1). Top: χ and *N* are shown for 2-s data intervals, with means for six *N* bins shown. Middle: χ is plotted vs *dT*/*dz*, with data and means for each bin shown with different colors. Bottom: Diffusivity ($K_i$) estimates in 2-sec windows are plotted versus *N* as dots (for illustration, $K_i$ has no meaning). Diffusivity *K* for the six *N* bins with equal number of samples is plotted versus mean *N* for each bin (red dot), with connecting line segments. Means of 150 bootstrap estimates are also shown (blue dots), with +/ standard deviation. A power-law fit to the bootstrap means is written in the figure.**

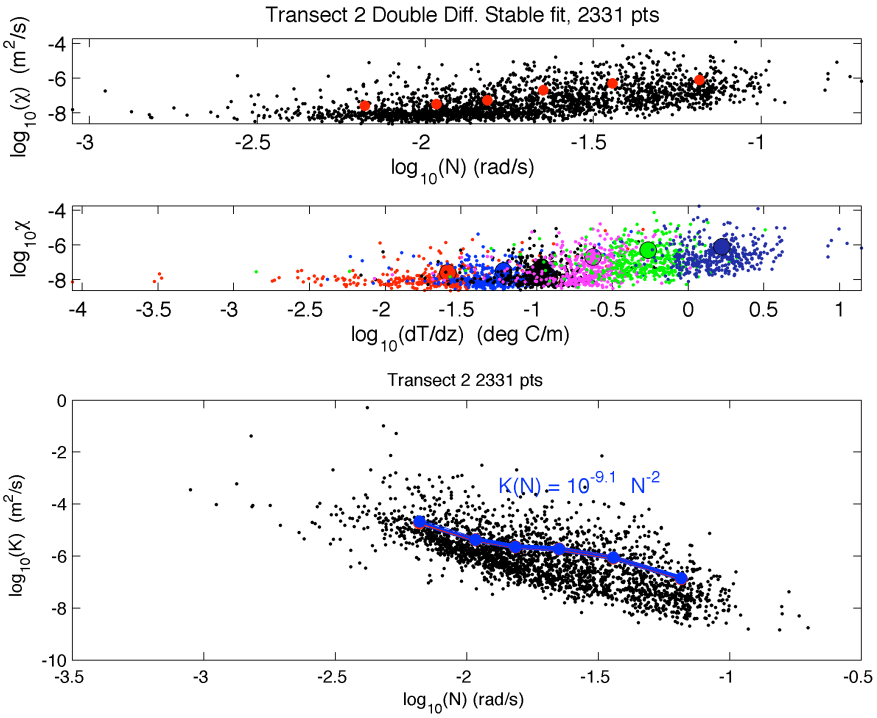


**Figure 6.A.2. T2-leg 2 (Transect 2).**

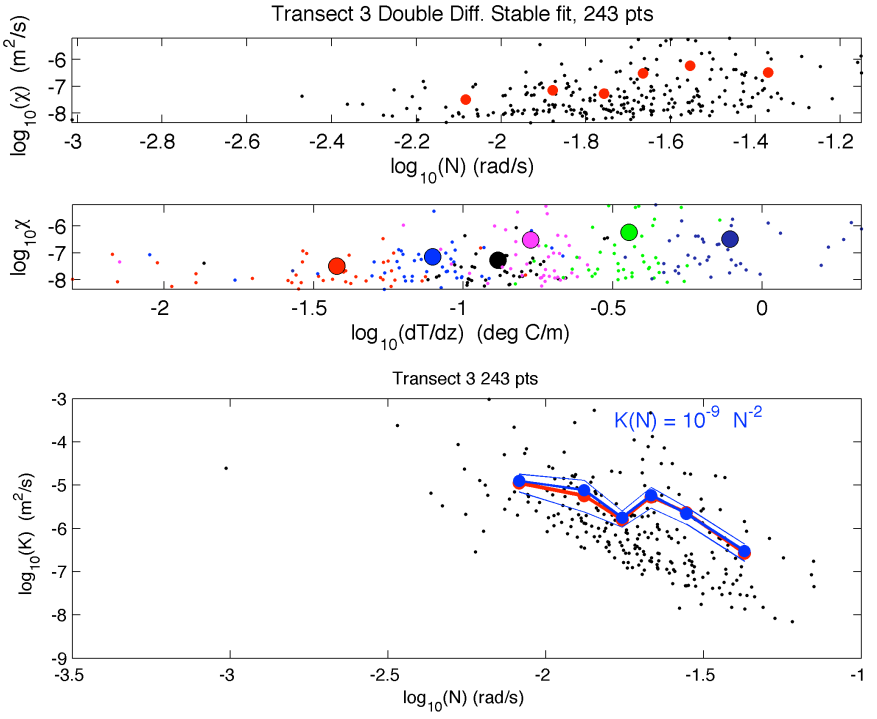


**Figure 6.A.3. T2-leg 3 (Transect 3).**

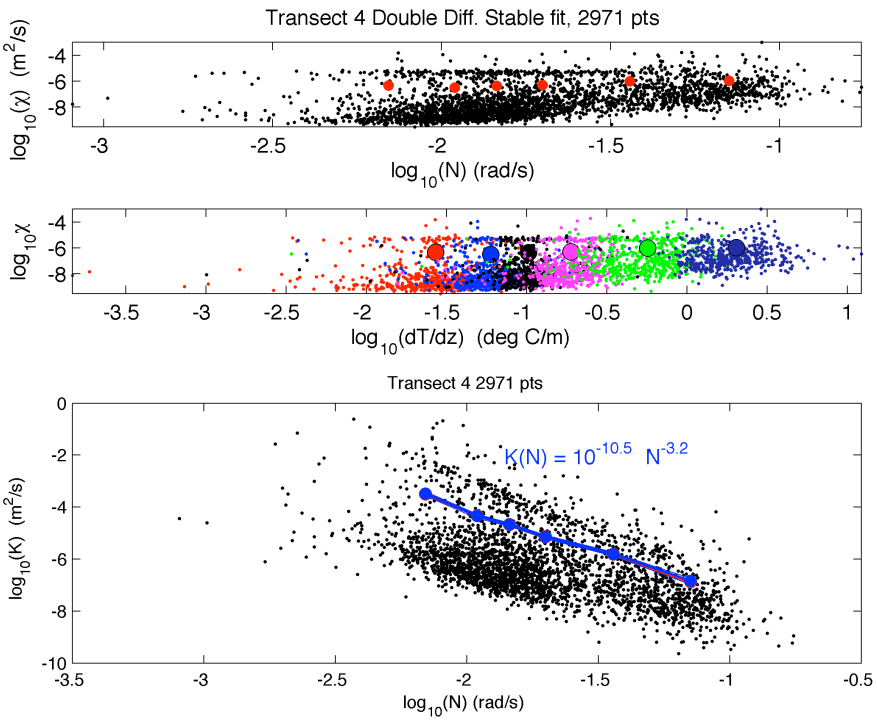


**Figure 6.A.4. T2-leg 4 (Transect 4).**

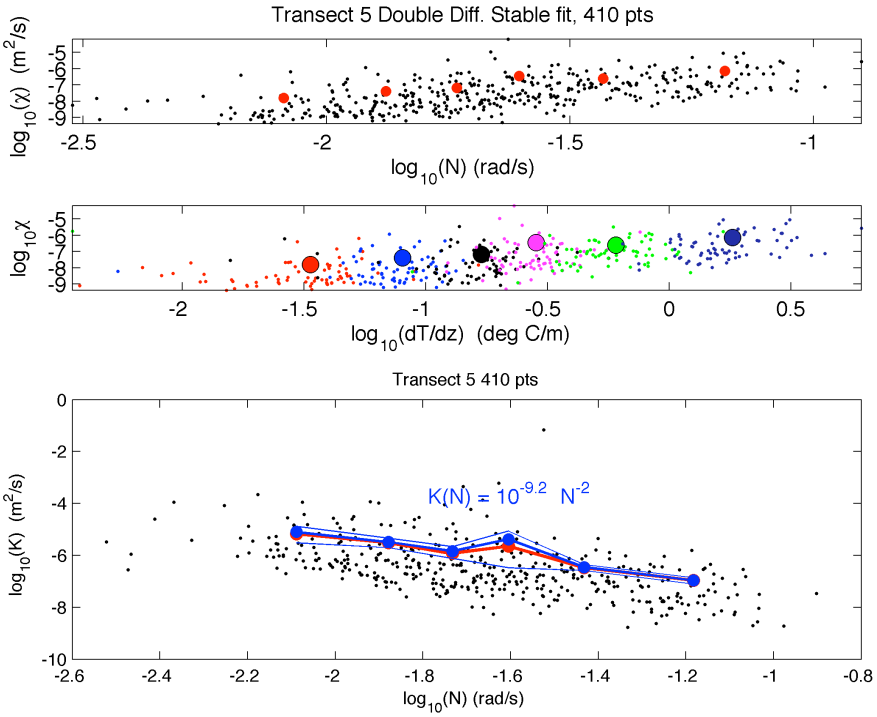


**Figure 6.A.5. T2-leg 5 (Transect 5).**

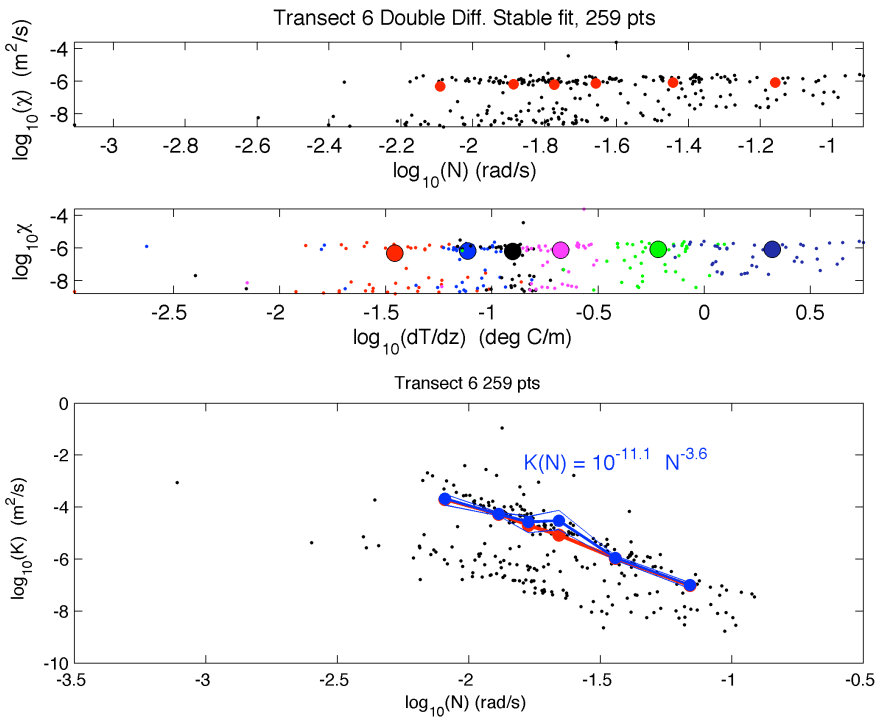


**Figure 6.A.6. T2-leg 6 (Transect 6).**

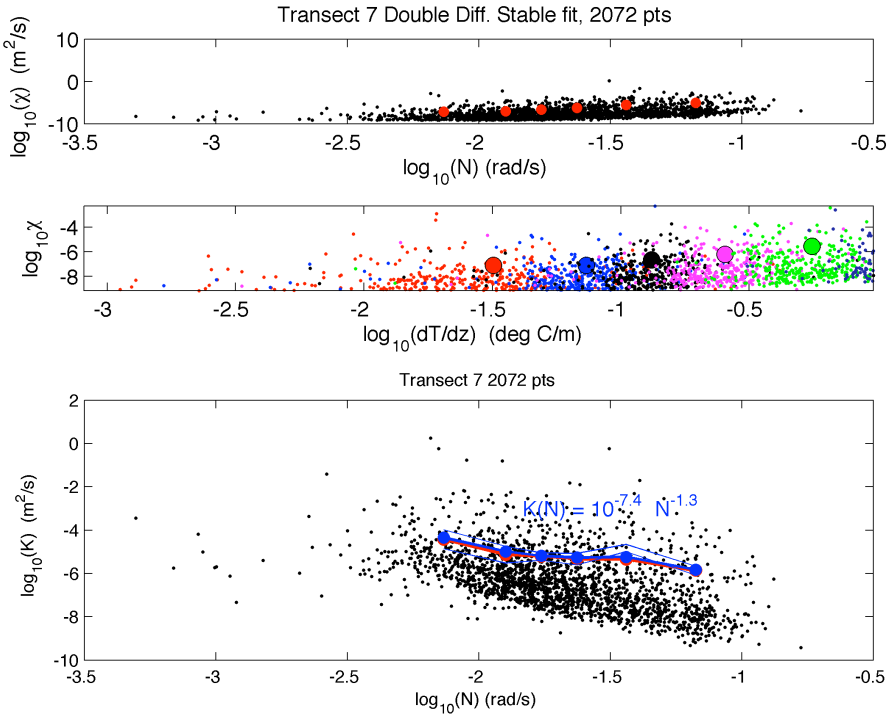


**Figure 6.B.1. T3-leg 1 (Transect 7).**

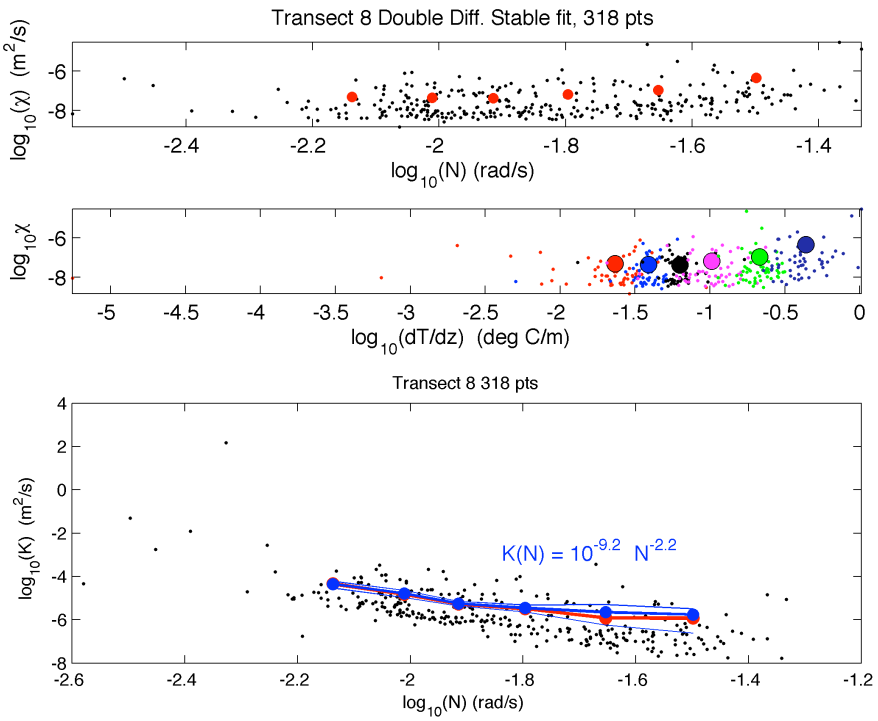


**Figure 6.B.2. T3-leg 2 (Transect 8).**

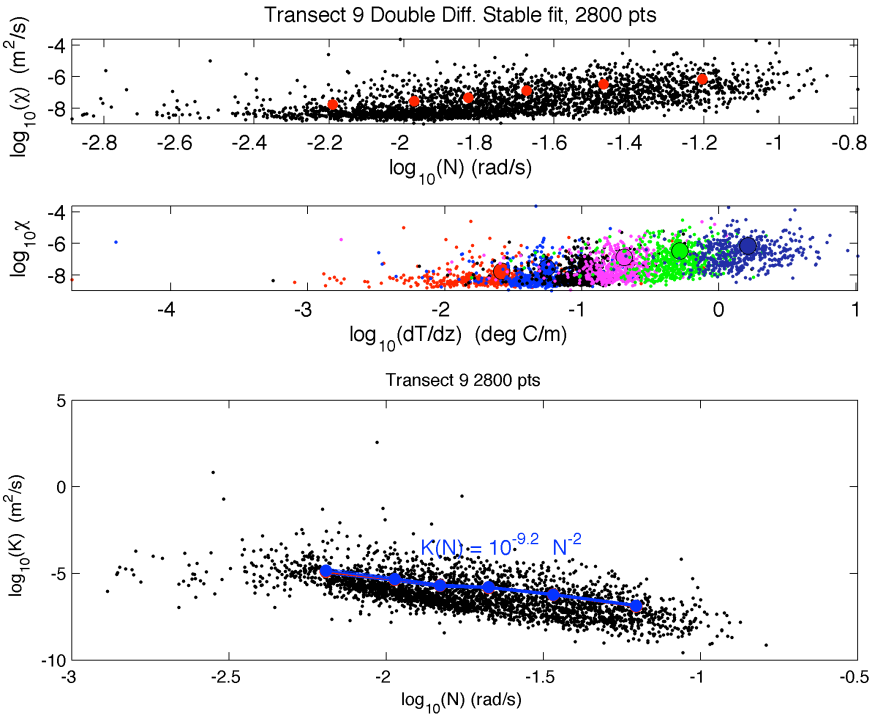


**Figure 6.B.3. T3-leg 3 (Transect 9).**

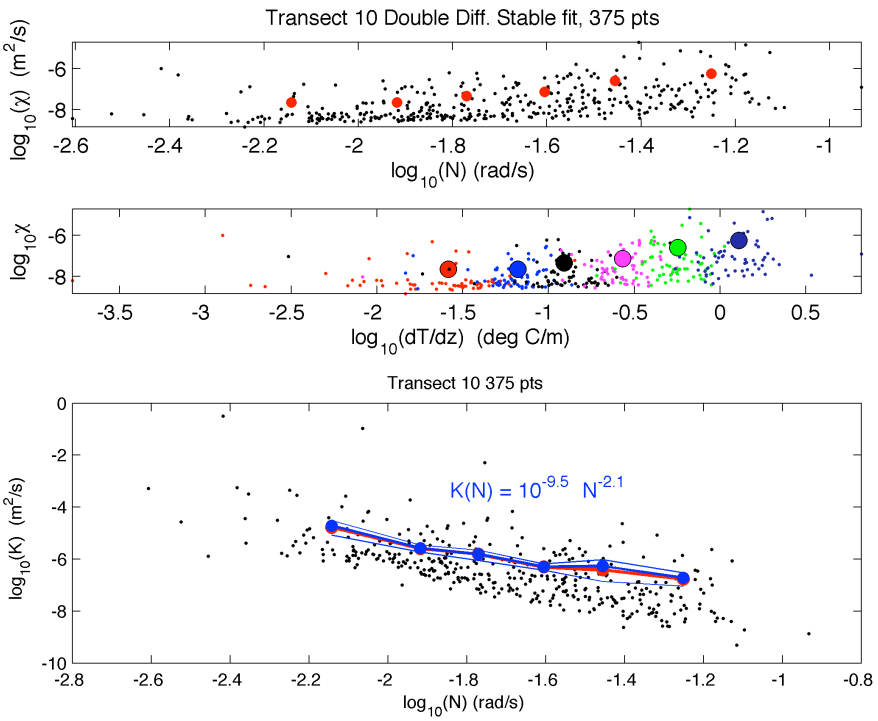


**Figure 6.B.4. T3-leg 4 (Transect 10).**

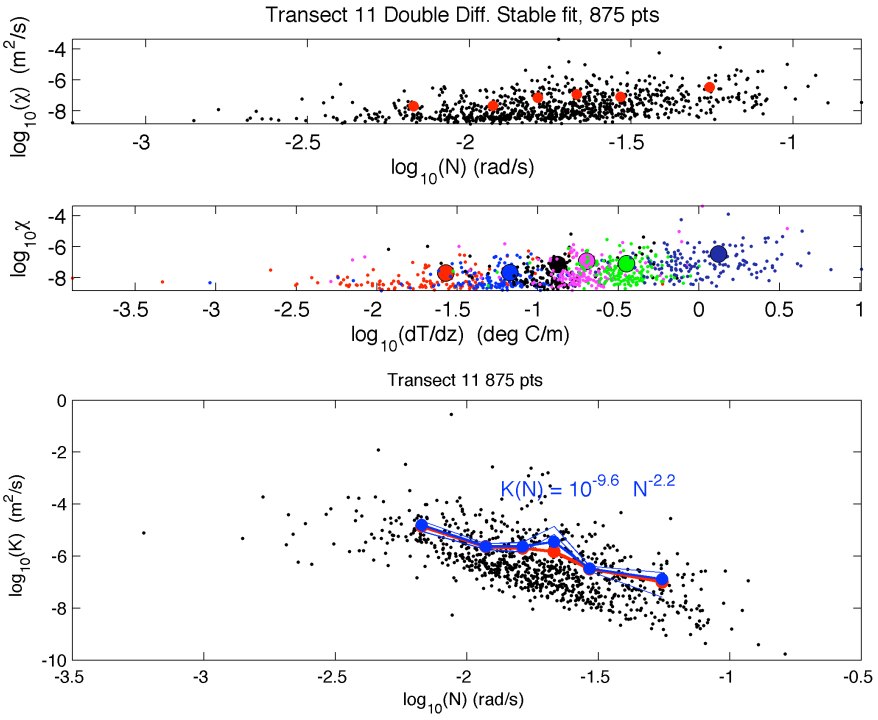


**Figure 6.B.5. T3-leg 5 (Transect 11).**

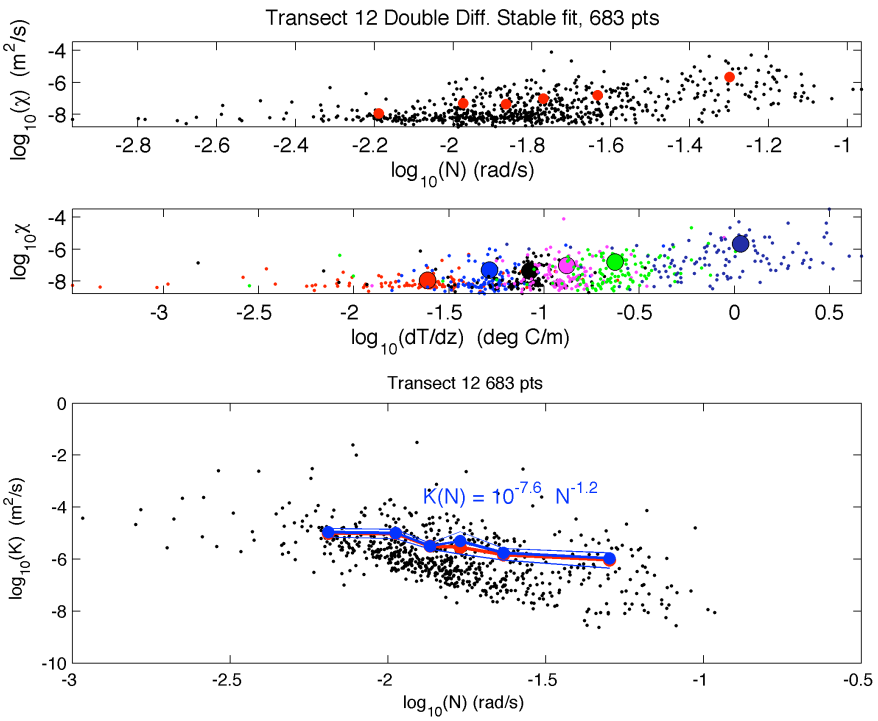


**Figure 6.B.6. T3-leg 6 (Transect 12).**

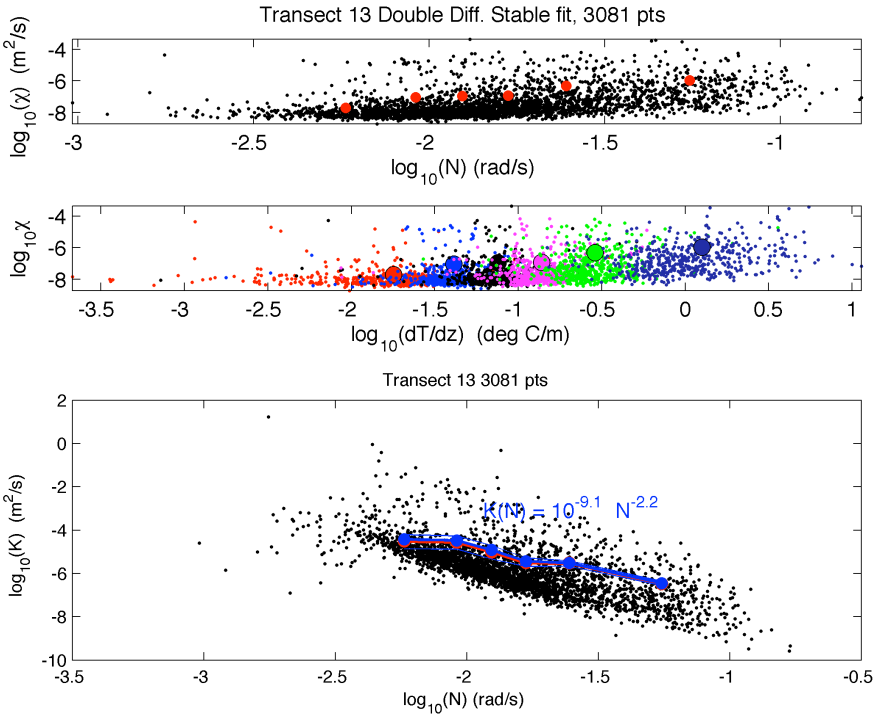


**Figure 6.C.1. T4-leg 1 (Transect 13).**

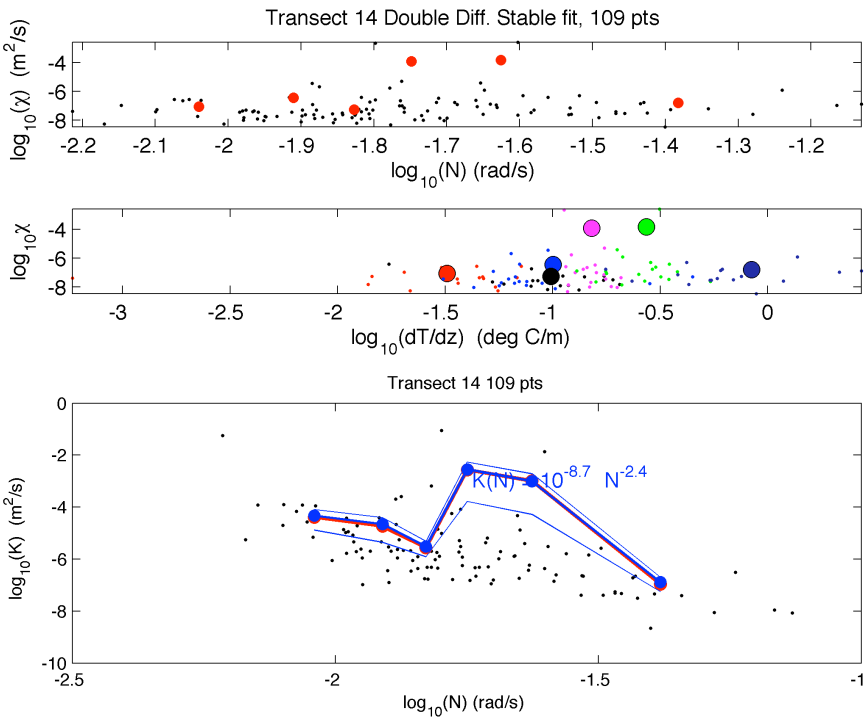


**Figure 6.C.2. T4-leg 2 (Transect 14).**

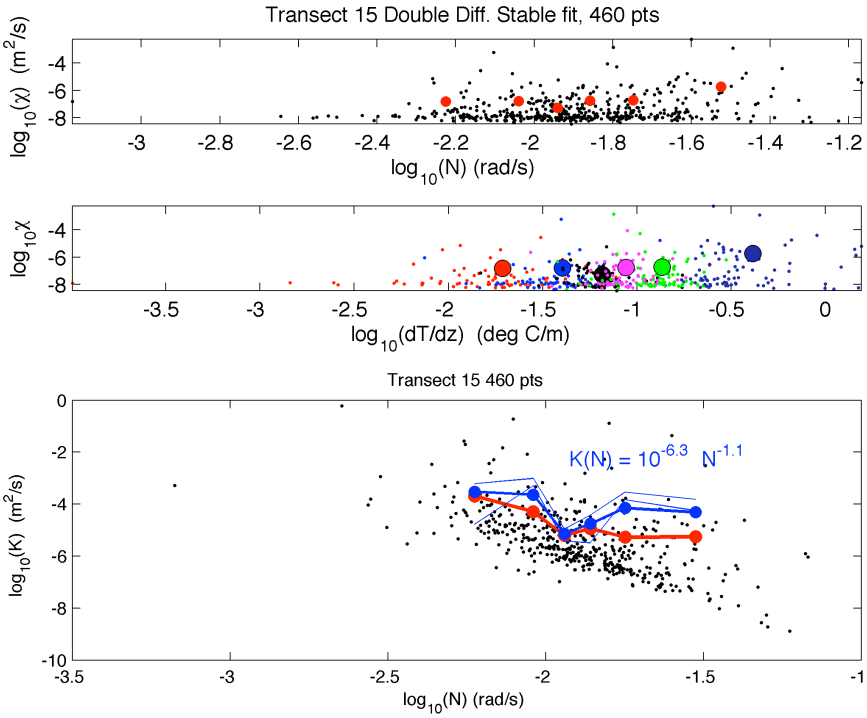


**Figure 6.C.3. T4-leg 3 (Transect 15).**

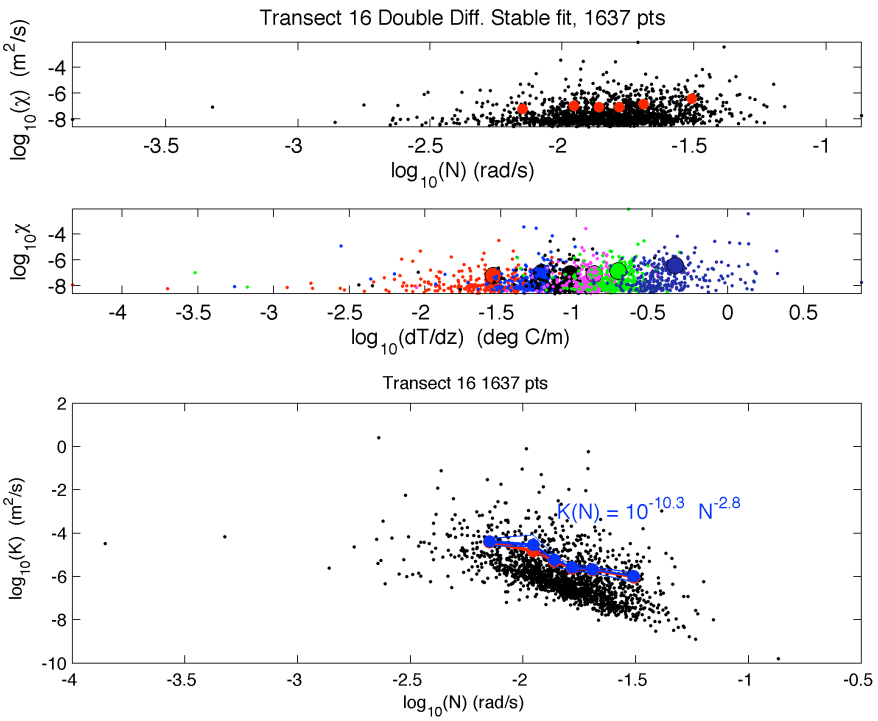


**Figure 6.C.4. T4-leg 4 (Transect 16).**

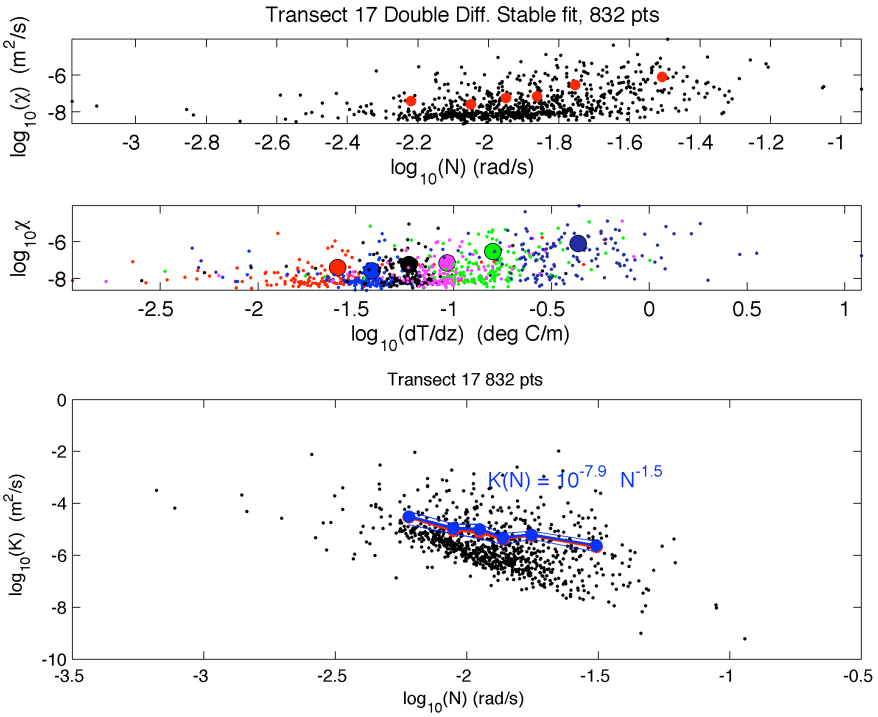


**Figure 6.C.5. T4-leg 5 (Transect 17).**

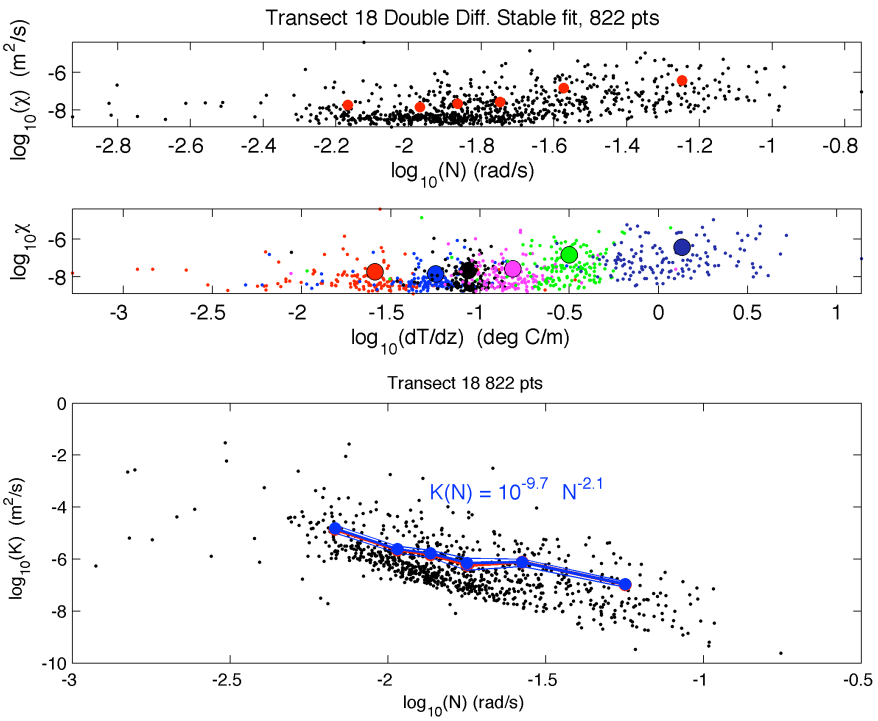


**Figure 6.D.1. T5-leg 1 (Transect 18).**

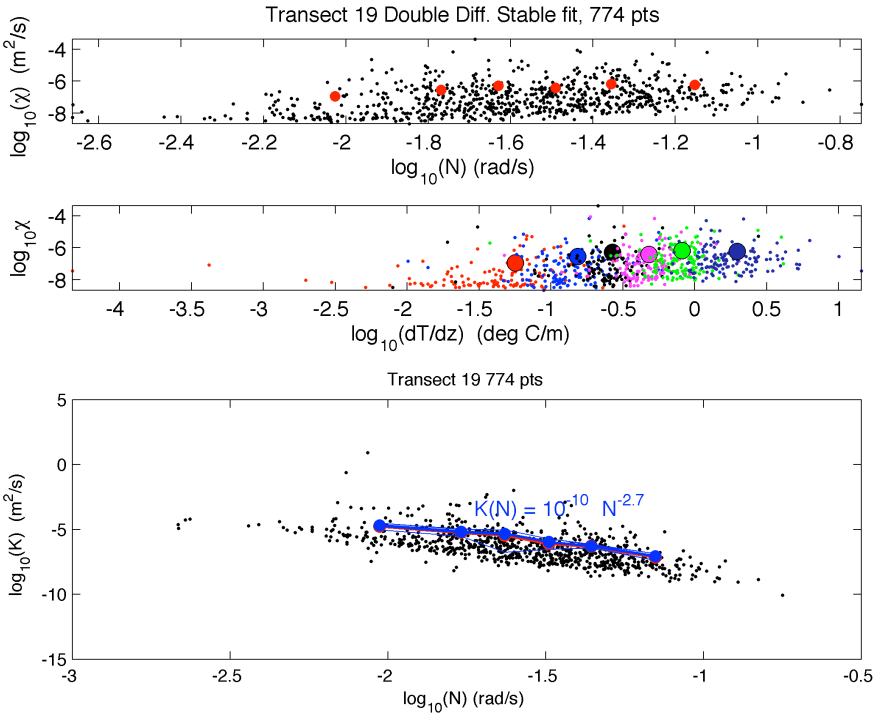


**Figure 6.E.1. T6-leg 1 (Transect 19).**

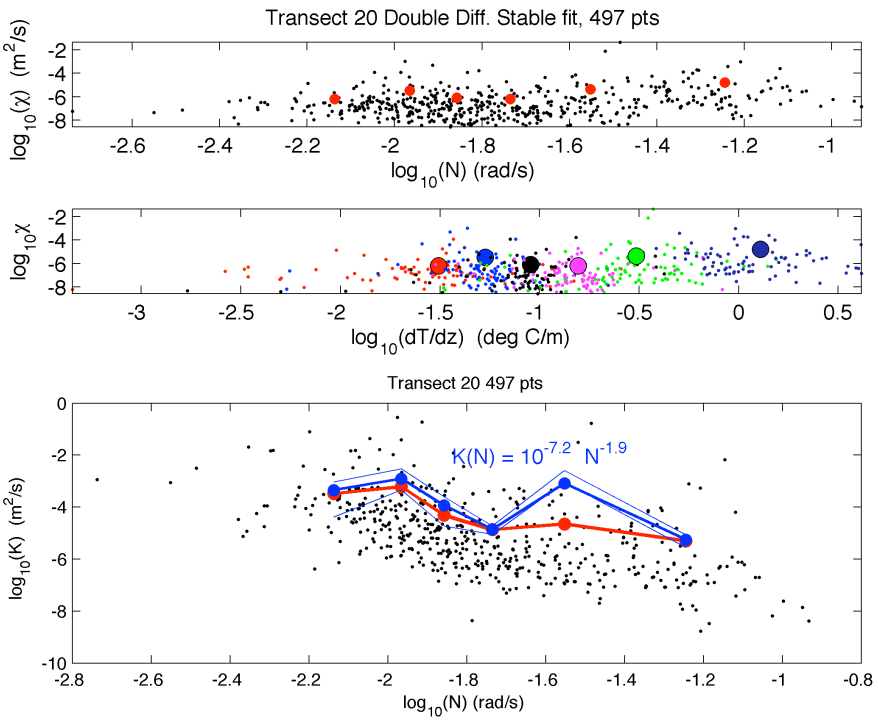


**Figure 6.F.1. T7-leg 1 (Transect 20).**

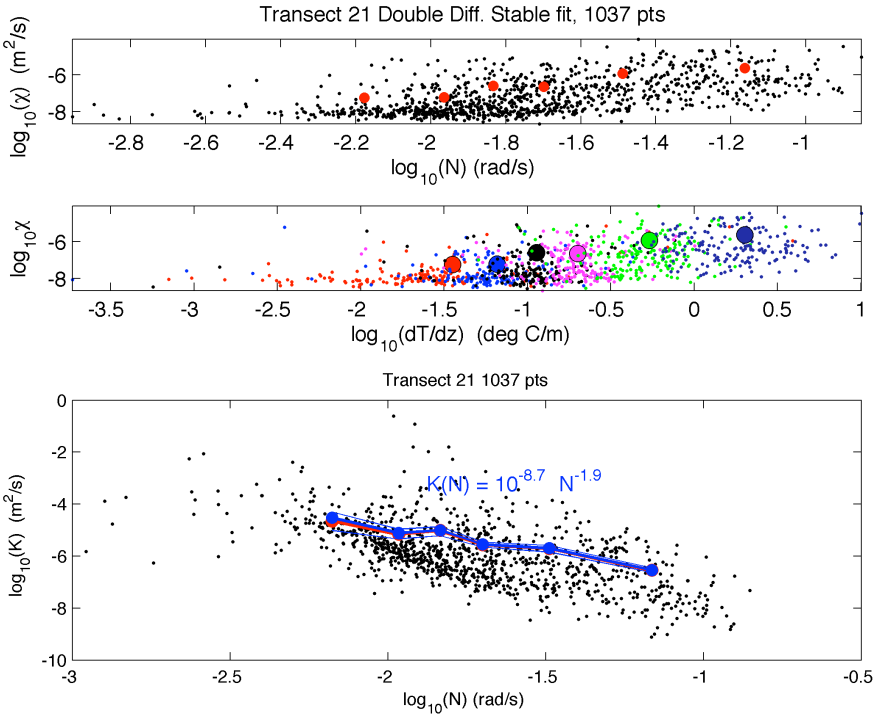


**Figure 6.F.2. T7-leg 2 (Transect 21).**

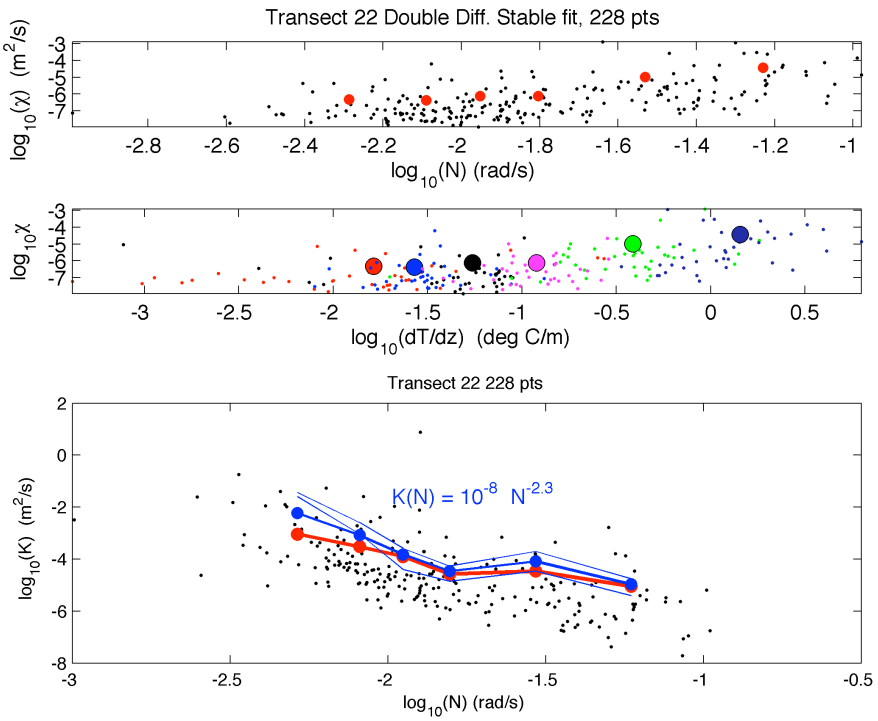


**Figure 6.F.3. T7-leg 3 (Transect 22).**

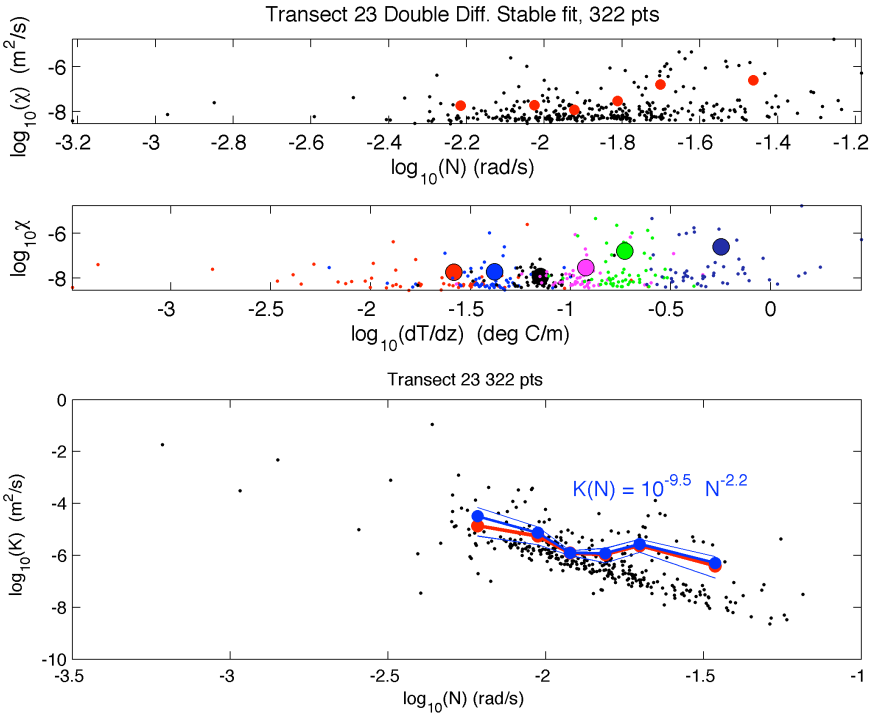


**Figure 6.G.1. T8-leg 1 (Transect 23).**

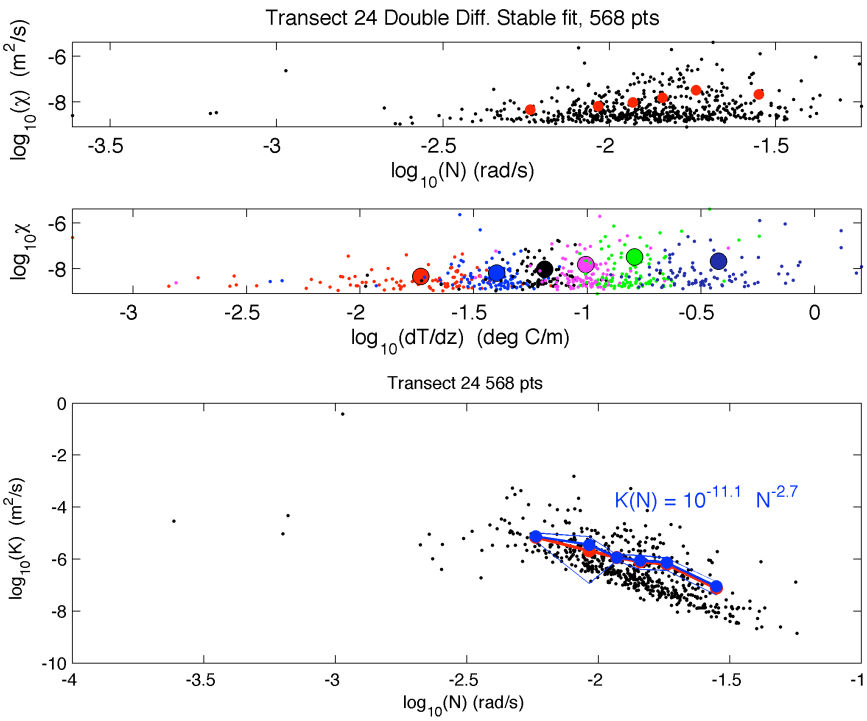


**Figure 6.G.2. T8-leg 2 (Transect 24).**

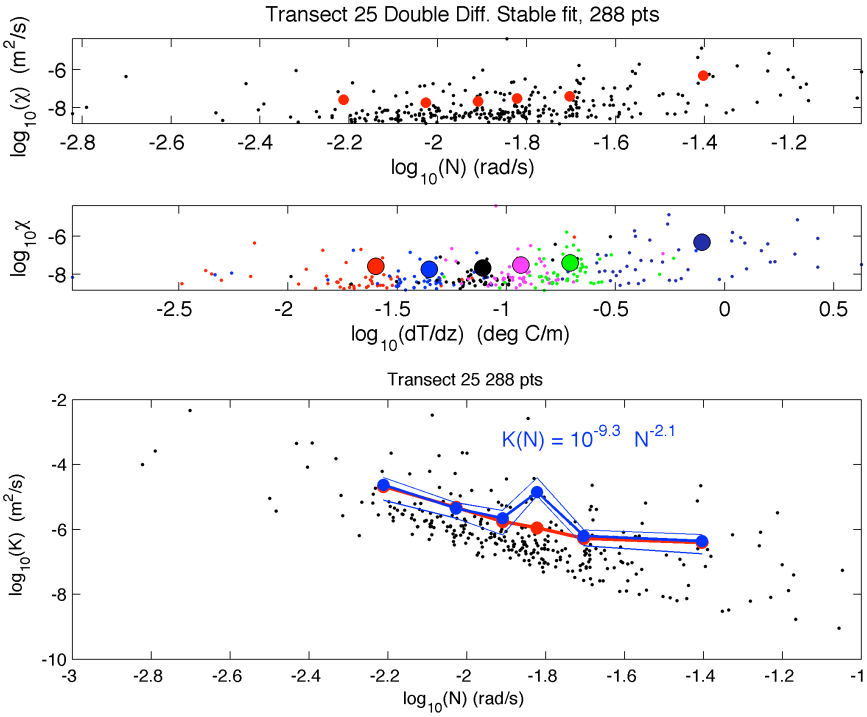


**Figure 6.G.3. T8-leg 3 (Transect 25).**

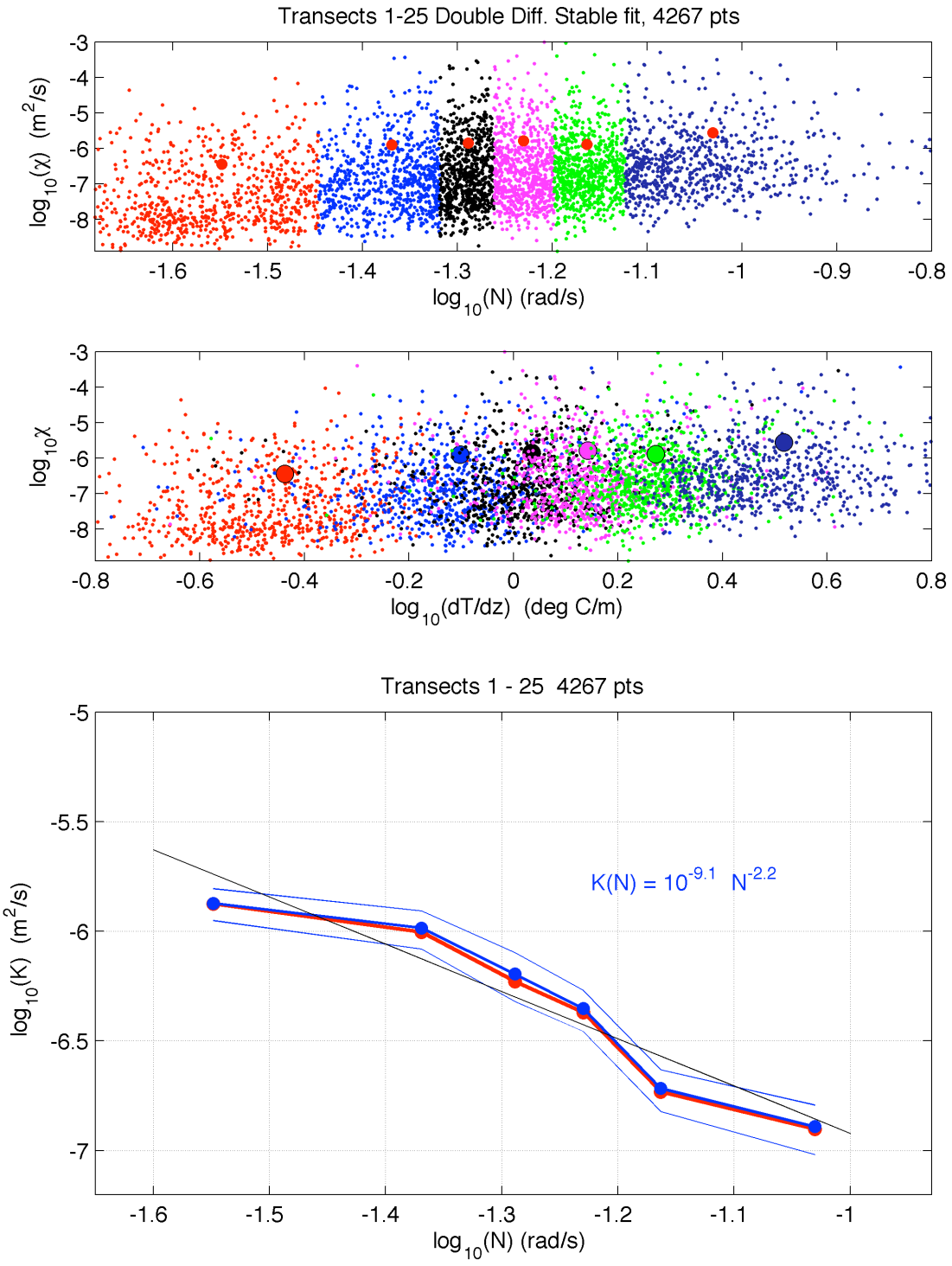


**Figure 7. The gradient and diffusivity quantities shown in Figures 6.m.n are given for the entire collection of points analyzed in those figures. The format is the same as in those figures, except the lowest panel shows the linear fit, the instantaneous $K_i$ values are not shown, and the top panel denotes $N$-bin members by color. The flux $F=KN^2$ is a decreasing function of $N$.**

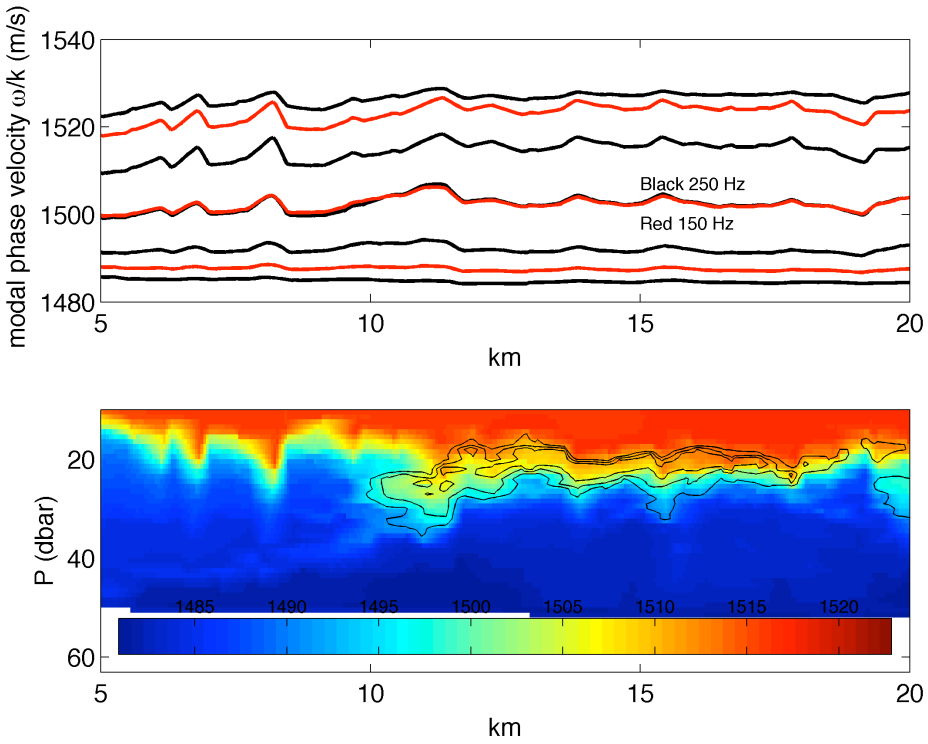


**Figure 8. The sound speed in transect 2 is shown below in color. Contours of high salinity are also shown (black). Above, phase speeds of modes 1:5 for 250 Hz sound are shown (black), with modes 1:3 for 150 Hz (red). The phase speed changes in the intrusion at km 10-20 are equal to those from the three internal waves at km 6-8.**

## Appendix: Post-Cruise Narrative Report (reprinted)

## Cruise EN396
## UNOLS Vessel *R/V Endeavor*
## August 8-15, 2004

**Prepared by**

Tim Duda (Chief Scientist)
Woods Hole Oceanographic Institution
Applied Ocean Physics and Engineering Department, MS 11
Woods Hole Oceanographic Institution
Woods Hole, MA 02543 USA

**Date**

13 September 2004

**Contents**

## Science Personnel

Chief Scientist: Tim Duda, Woods Hole Oceanographic Institution (WHOI)

| | |
|---|---|
| Tim Duda | WHOI AOPE Dept. |
| David Walsh | Naval Research Lab. |
| Nick Witzell | WHOI AOPE Dept. |
| Cynthia Sellers | WHOI AOPE Dept. |
| Heather Groundwater | URI GSO graduate student |
| Scott Hanchar | URI GSO graduate student |
| Tom Orvash | URI GSO Marine Tech. Services |
| Dave Nelson | URI GSO Marine Tech. Services |
| David Mangiante | URI GSO Marine Tech. Services guest |

The objective of this cruise was to obtain microscale conductivity data and density data from a towed measurement platform in order to investigate the relationship of diapycnal turbulent mixing to the density gradient.

## Log of Activities

### Sunday Aug 8

We departed the University of Rhode Island Bay Campus at approximately 1030 local time (EDT). The plan for this day was to collect a cross-shelf temperature/salinity/density ( $T/S/\sigma$ ) transect with the Scanfish system. This is to tell us the density profile conditions, and help us to locate the best location to make our measurements. The plan was to thereafter use microscale conductivity probes as thermometers, with approximate corrections required if salinity varies with temperature (with depth, essentially), but no corrections required if salinity is uniform. Thus, a low value of $\Delta S/\Delta T$ is helpful for reducing error bars in the interpretation of the microscale data.

After the safety meeting we were near the starting point of the Scanfish transect, near Block Island at 41-02.77 N, 71-24.71 W, at time 1929 UTC. (In this report position in degrees and minutes are written deg-min, with the dash separating degrees and minutes.) After instrument preparations were complete, the system was launched and the transect was run at approx 7.5 knots. The transect was completed at 40-9.70 N, 71-02.57 W, time 0255 Aug 9 UTC. Good conditions for our work were found near 40-36 N.

### Monday Aug 9

The WHOI MT (Micro Tow) system was deployed near 40-11.4 N, 71-3.3 W at 0413 UTC (0013 EDT). This was WHOI TM tow **segment T1**. This system has 400-Hz SBE 7 conductivity probes, SBE 9+ CTD, a 2-axis current meter, and attitude sensors. A cross-shelf transect back to the north was planned. A few hours into the tow problems with the winch level-wind developed, which were quickly remedied. Wave and wind conditions forced the speed

beyond what the MT could be towed smoothly at (4.5 knots) , and the platform encountered cable drag, roll, and yaw problems. It was helpful to know the behavior of the package when it was pushed beyond it's speed limit, in case encounters with other vessels forced evasive maneuvers.

Af ter about an hour the SBE 9+ primary conductivity sensor gave erratic readings. Eventually, it stabilized at a value of essentially zero conductivity. This turned off the T/C system pumps so that both primary and secondary T/C sensor pairs were inoperable. The MT was recovered at 40-15.7 N, 71-4.8 W, 0633 UTC. The sensor was replaced, and the system was redeployed at 40-16.9 N, 71-3.0 W, 0817 UTC, to begin **segment T2**.

Virtually all MT deployments were tow-yos, undulating under winch control, to provide *dT/dz* measurments to go along with microstructure. Tow-yoing with winch speeds of ±20 m/min was undertaken for the remaining hours of the day.

**Tuesday Aug 10**

Each of the micro probes was observed to give a steady standard deviation of 200 or more mV rms, with high mean voltage, indicating low conductivity. This steady behavior (as opposed to fluctuating standard deviation from ocean signal) could be brief, a few minutes, or last an hour or longer. We elected to continue if one probe was operational. This always remained the case, so towing continued until the package was recovered for inspection at about 1000 local time, 1355 UTC, 40-48.0 N 70-54.8 W. Flow angle of attack fluctuations were larger than expected and desired. At about 0200 local time the speed was increased to avoid another vessel, and MT yawed and rolled quite a bit when the speed exceeded the upper measurement limit of 3 m/s.

Upon recovery, it was noted that the sea cable armor was nearly severed by chafing with the shackle on the safety wire. The interior conductor core was visible. The wire was reterminated and tested. The non-functioning altimeter was removed, as was the safety wire. The micro probes were tested on deck in salt water, and each functioned well. It was determined that gummy plankton objects stuck between the probe stalks were the cause of the high-voltage, high variance failure mode.

The package was redeployed for tow **segment T3** near 40-48.0 N, 70-54.5 W at 1923 UTC, on the second eastbound leg of the survey pattern (Figure 1), north of the previous two zonal segments. On this course the MT vertical attack angle was very well behaved. This was with wind on the starboard beam. After a turn to the north (wind from astern), attack angle fluctuations increased, but they were not as bad as during the first deployment. At about this time the winch speed was changed to +/- 15 m/min. Various other speeds were tried, and package attitude and speed fluctuations were noted, with this settled upon.

During the towing up to this time, some areas of uniform *S(z)* were encountered, as were some areas that were less uniform and contained signatures of intrusive flow. The tow pattern of east-west tracklines south of Martha's Vineyard and west of Nantucket shoals that was established on Monday was continued.

**Wednesday Aug 11**

The pattern of approximately 35 nm long east-west tracklines between 70 and 50-m depth inshore of the shelf/slope-water front was continued. The data were examined for dS/dT and density step properties. The southern lines were found to alternate between areas desirable for conductivity probe measurements of mixing, and areas of variable salinity caused by intrusive flow. The wind has picked up to 16 knots from the south, so that the ship pitches and the A-frame moves around a bit more, causing pitching of MT and attack angle excursions above +/- 10 degrees, but extreme bad behavior was not seen.

The problem with one micro-conductivity probe arose again, but with one sensor still functioning the MT was left in throughout the day. At 1600 local time it was recovered for inspection, location 40-48.5 N, 70-44.2 W, 1957 UTC, and to move to the south to repeat measurements along the southern zonal trackline. The connection to the wire looked fine. The noisy micro sensor (SN 124) was observed to have cavities in the probe tips, not filled with platinum as with SN 114. This may be the cause of the pervasive noise and low conductivity readings. The Sea-Bird company was phoned to inquire about the probe noise, and a 1 to 10 percent Triton X-100 bath was recommended, swishing the probes around. This was done for both probes.

At 1800 local time the MT package was deployed again for **segment T4**, near 40-40.1 N, 71-4.0 W, 2153 UTC. Everything functioned as before, all well, with the exception of micro sensor 124 which began intermittently fouling soon after deployment. For the next few hours, the sensors often tracked together in the upper 10 meters of the tow-yo (10-25 db), but on the trips down SN 124 went into failure mode until the next time it came near the surface. This behavior is not yet fully understood.

**Thursday August 12**

In the early morning, the second two micro sensors, SN 114, showed low conductivity and high noise, the failure mode seen often in the other sensor, SN124. The attack angle and system speed through the water was also erratic. The system was brought to 5 m depth and left there for a few minutes, then the front of the system brought slightly out of the water for inspection. Nothing was seen to be blocking the micro sensors or the current meter. When dropped back in, both probes performed better. At this time we were in the southeast corner of out work area, in 50-m water and a very sharp thermocline, and there was a strong current shear pulling the instrument to port at ship course 90. We tried courses 45, 135 and 0, and finally settled on 210, no longer attempting to stay in the isosalinity conditions at that site because of the buffeting of the system and poor flow conditions at the sensors. A new plan was drafted to tow to the southwest, then the northwest, then northward across the prior east-west lines, in an area with some intrusions in the upper water column and good conditions below.

The next task was to make some comparison tows with the Scanfish and the MT at this site, towing systems alternately along the same track so as to sample similar conditions. The MT was towed to the north as the first step. After lunch the system was brought aboard, 40-56.8 N, 70-47.9 W, 1626 UTC. The Scanfish was launched nearby at 1640 UTC and towed to the south. It was recovered at 40-39.7 N, 70-48.0 W, 2008 UTC. MT was then launched at 40-39.3 N, 70-

48.0 W, 2018 UTC and towed to the north again, tow **segment T5**. Recovery was at 40-54.7 N, 70-47.9 W, 2338 UTC. Finally, the Scanfish was launched at 0017 UTC nearby and towed to the south.

At the completion of the comparison test, the Scanfish was left in the water and an intrusion survey was initiated. The trackline to the south was continued, as it passed across an area observed to have intrusions in initial east-west passes. After this, a turn to the southwest was planned, to remain in water of about 65-m depth and to remain parallel to the typical position of the shelf/slope-water front.

**Friday August 13, 2004**

Early in the morning at about 0650 UTC the Scanfish micro probes were smashed at approx 10-m depth, location 40-41.4 N, 71-01.9 W. Additional problems with the altimeter and with the Scanfish balance were encountered and Scanfish undulations were terminated for the time being.

Just after 0500L the MT was launched for tow **segment T6** at 40-41.3 N, 71-1.9 W, 0921 UTC to continue the intrusion study line to the southwest. At ~0800L it was removed at 40-38.7 N, 71-17 W, 1203 UTC in order to 'go fast' and clean out obstructions in the main engine exhaust system. It was redeployed for **segment T7** at approximately the same location at ~1100L (1457 UTC). This area did not have strong intrusions, or steps in the density profile, so abandoning the line and reversing back to the intrusion area was considered. Thus, the MT was recovered at approx. 1830 local (40-29.1 N, 71-21.1 W, 2233 UTC). The Scanfish was deployed with the intention of doing some higher-speed surveying about 45 minutes later at 40-29.7 N, 71-20.71 W.

**Saturday August 14, 2004**

The Scanfish survey of conditions to the west of our original work area was continued. Mid-morning it was determined that a site very suitable for sampling with MT was encountered during the night. Also, it became clear the tropical storm Charley was headed directly toward us and toward Rhode Island, to arrive Sunday AM, so it became clear that we would need to either return to port Saturday evening or Sunday evening. We would not be able to work Sunday morning, so the only logical choice was to return home Saturday evening.

To sample the discovered site with MT, Scanfish was recovered at 40-34.1 N, 70-38.6 W, 1325 UTC (0925 EDT), and MT redeployed nearby for final tow **segment T8** at 40-40.4 N, 70-44.9 W, 1434 UTC. The site to be sampled was roughly along the track to port. Thus the final MT data collection took place along a path having a slight zig-zag. Final MT recovery was at 1745 UTC (1345 EDT), 40-46.44 N, 70-57.92 W. We then headed to port, with mooring complete at 1912 EDT local time.

| Towing Operations, WHOI MT Instrument | | | | | | | | | |
|---|---|---|---|---|---|---|---|---|---|
| Tow Name | Start Day | Start Time UTC | Start Time EDT | End Day | End Time UTC | End Time EDT | Notes | | |
| T1 | 9 Aug UTC | 0413 UTC | 0013 L | 9 | 0633 UTC | 0233 L | CTD primary C-cell failure | | |
| T2 | 9 | 0817 UTC | 0417 L | 10 | 1355 UTC | 0955 L | Recover to check gear | | |
| T3 | 10 | 1932 UTC | 1523 L | 11 | 1957 UTC | 1557 L | Check noisy probe; move to south | | |
| T4 | 11 | 2153 UTC | 1753 L | 12 | 1626 UTC | 1226 L | Change to Scanfish for comparison | | |
| T5 | 12 | 2008 UTC | 1608 L | 12 | 2338 UTC | 1938 L | Finished 2nd comparison line | | |
| T6 | 13 | 0921 UTC | 0521 L | 13 | 1203 UTC | 0803 L | | | |
| T7 | 13 | 1457 UTC | 1057 L | 13 | 2233 UTC | 1833 L | | | |
| T8 | 14 | 1422 UTC | 1022 L | 14 | 1734 UTC | 1334 L | Terminating, Charley appoaching | | |

## Additional Comments

The Seawave Inc. email system did not accept the new users, the science party. This was a disappointment and helped some business back at WHOI to slip through the cracks. Also, we needed to break off our surveying in order to go fast for a few hours and clean soot out of the main engine exhaust system between the combustion chambers and the turbocharger. Originally it was thought that this would be required once in the middle of the trip, but the problem was worse than anticipated and the procedure was done three times.

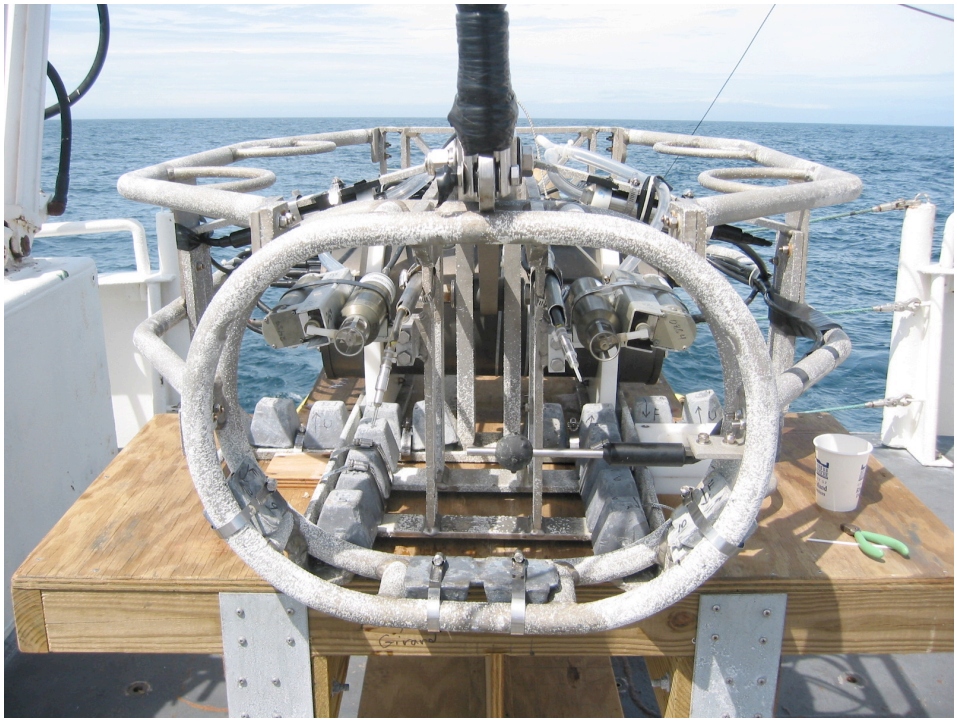

Photo 1. Photo of the front of the MT unit showing probes across the top, and black electromagnetic current meter below. From left at top: CTD probe pair, two 400-Hz conductivity probes taken apart for cleaning, and another CTD probe pair.

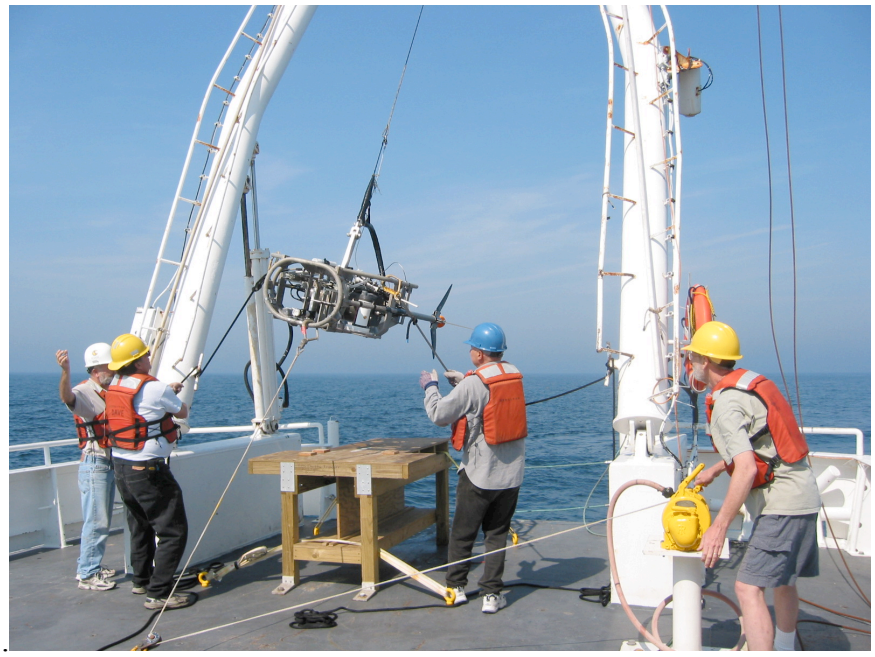

Photo 2: Micro-Tow recovery operation.

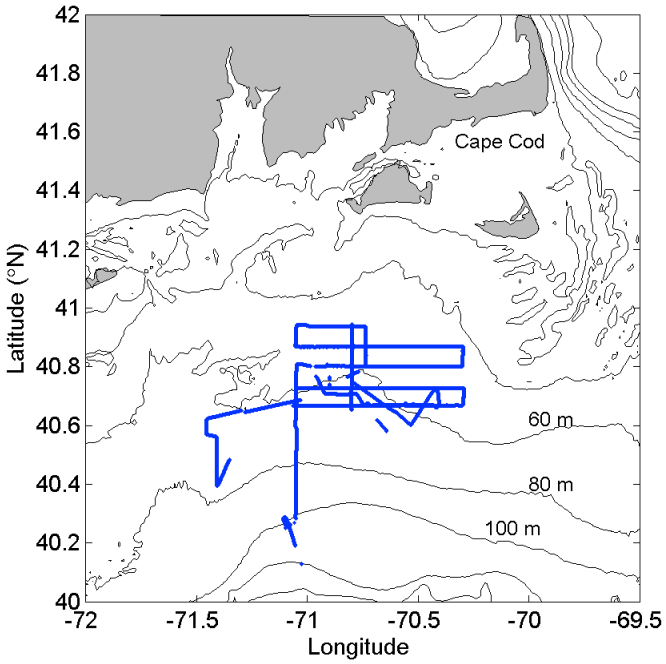


Chart 1: The area of operations is shown. Ship tracks for the MT surveys T1 to T8 are shown

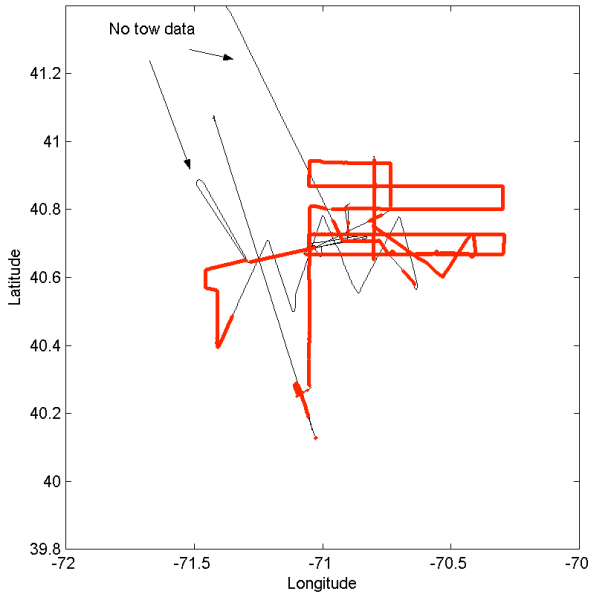


Chart 2: The complete ship track is shown. The MT surveys are shown in red. The Scanfish was in the water for most of the other times, with the exception that no data were collected along the indicated lines (indicated western loop is a speed run called by the engineer, northern line is heading to port).

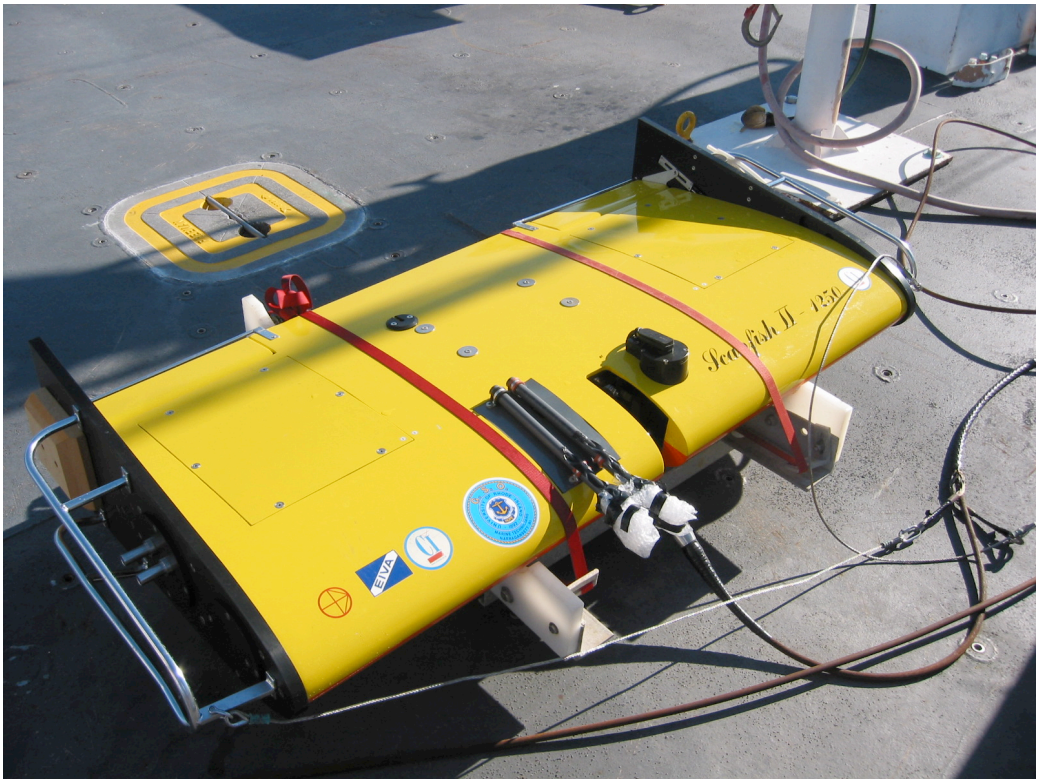

Photo 3: URI Scanfish with two microstructure probes.
The probes are covered with bubble wrap.

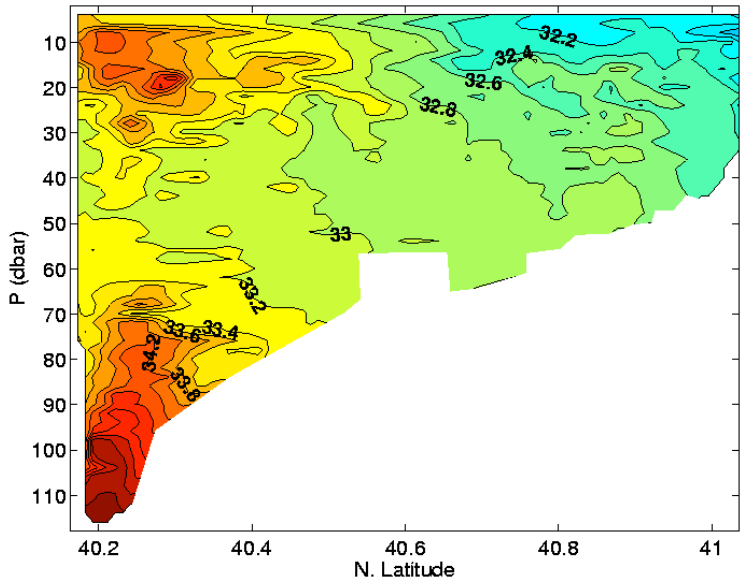


Figure 1. Salinity measured during the Scanfish cross-shelf transect of August 8.

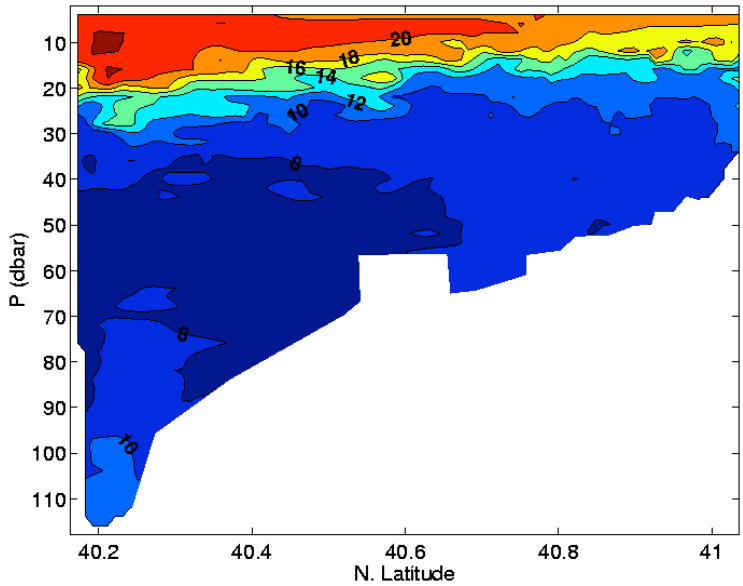


Figure 2. Temperature measured during the Scanfish cross-shelf transect of August 8.

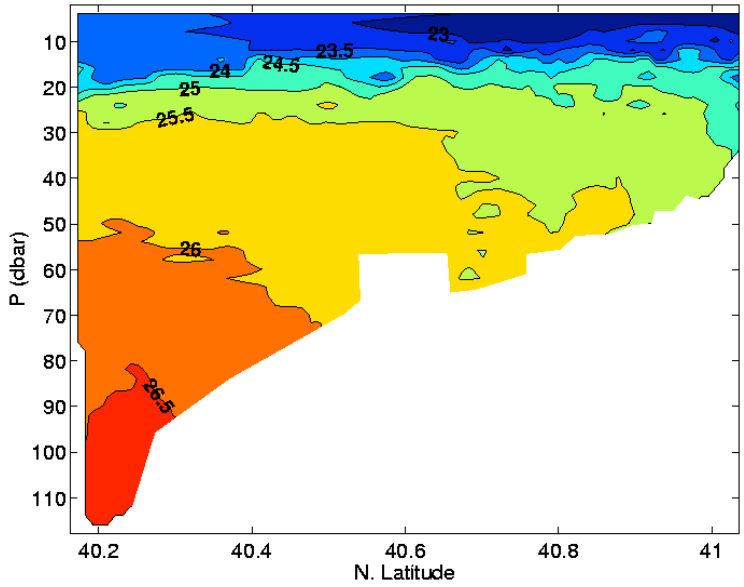


Figure 3. Density measured during the Scanfish cross-shelf transect of August 8.

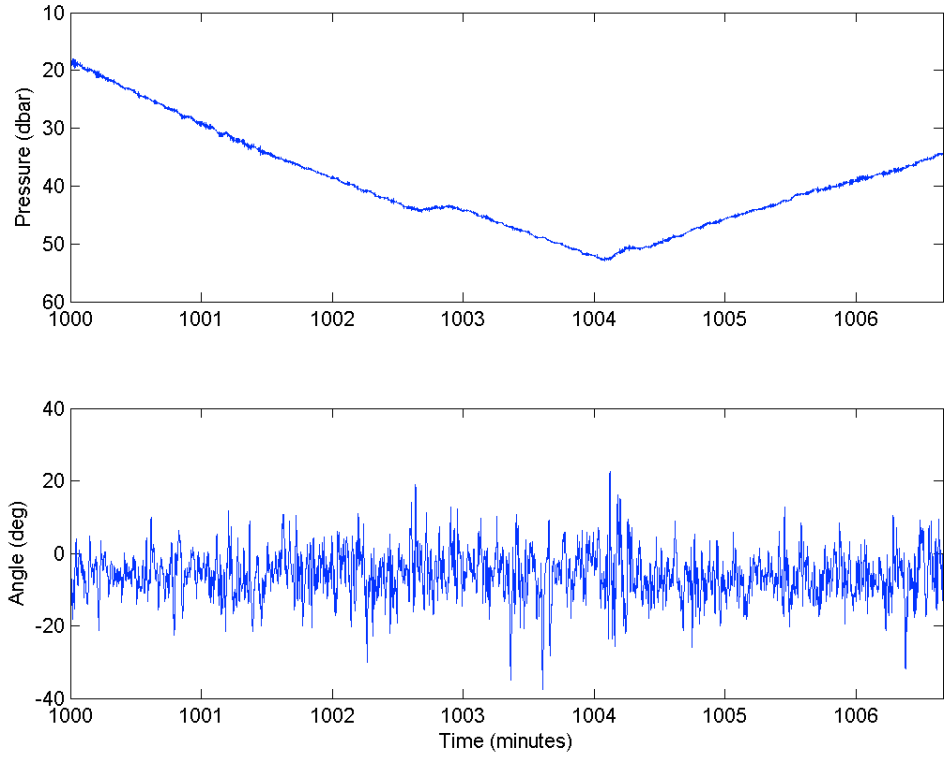


Figure 4. (lower panel) The angle of attack of flow at the front of the platform near the sensors, measured at 12 Hz. (upper panel) The pressure (depth) of the platform during the same time interval.

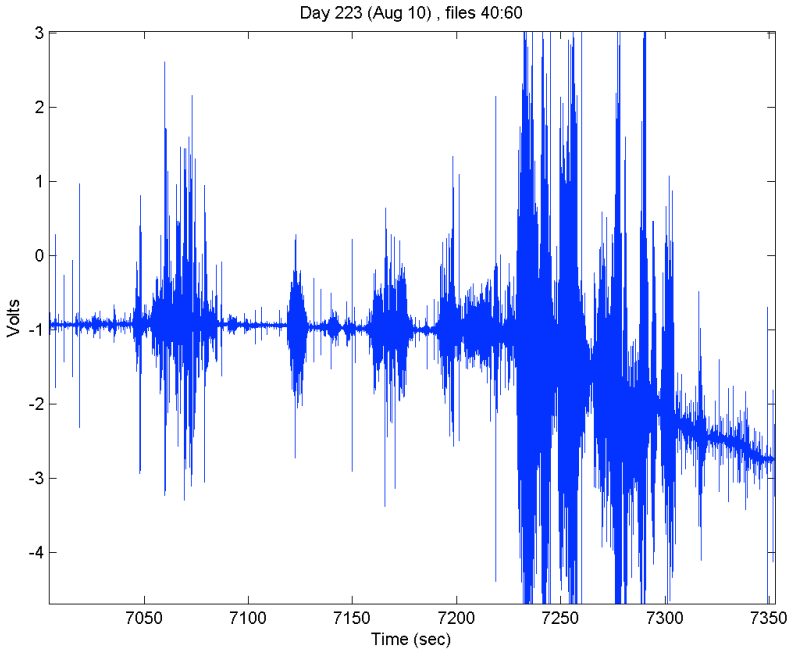


Figure 5. Pre-emphasized output one Sea-Bird Electronics SBE 7 microscale conductivity probe during a short time interval. This is essentially the mean conductivity plus its time derivative. The pulses of high oscillating output are areas of high gradients lasting from 5 to 40 seconds, which are of 10 to 80 m in size. The platform is moving downward at the beginning quarter of this plot and upward during the remainder of the time.

.

50272-101

| REPORT DOCUMENTATION PAGE | 1. REPORT NO. WHOI-2016-02 | 2. | 3. Recipient's Accession No. |
|---|---|---|---|

**4. Title and Subtitle**
Microscale, Finescale, and Mesoscale Measurements Made During the 2004 Structured Mixing Project (Micro-Tow 04) Cruise

**5. Report Date**
April 2016

**6.**

**7. Author(s)** Timothy F. Duda and Cynthia J. Sellers

**8. Performing Organization Rept. No.**

**9. Performing Organization Name and Address**

Woods Hole Oceanographic Institution
Woods Hole, Massachusetts 02543

**10. Project/Task/Work Unit No.**

**11. Contract(C) or Grant(G) No.**
(C) N00014-03-1-0335
(G) N00014-14-1-0223

**12. Sponsoring Organization Name and Address**
Office of Naval Research

**13. Type of Report & Period Covered**
Technical Report

**14.**

**15. Supplementary Notes**
This report should be cited as: Woods Hole Oceanographic Institution Technical Report, WHOI-2016-02.

**16. Abstract (Limit: 200 words)**
A physical oceanographic sampling voyage was made with RV Endeavor during August 2004 to evaluate diapycnal mixing processes on the continental shelf south of Massachusetts and Rhode Island, USA. The goal of the project was to look for a relationship between intensity of microstructure (thermal variance dissipation rate) and finestructure (background temperature gradient), in so-called doubly-stable water, which would be indicative of a density gradient-dependent diapycnal heat flux. To satisfy the requirement that a large amount of data be collected to constrain the statistically estimated result, a microstructure sensor was towed on a platform behind the ship, providing continuous sampling at the depths of interest. To obtain the necessary finestructure quantities the platform measured temperature, conductivity and depth with a standard pumped Seabird 9plus CTD. Attitude and speed of the platform were recorded to assure proper data quality. This report shows temperature, salinity, density, and sound speed in twenty-five tow-yo transects obtained using the towed unit. Only statistics and results from microscale data are shown. In waters with stable salt stratification and stable temperature stratification, a previously obtained empirical result of reduced flux at increased density gradient is supported by the data. The 2004 Cruise Report is included (Appendix).

**17. Document Analysis** **a. Descriptors**

Diapycnal mixing
Turbulent heat flux
Frontal intrusions

**b. Identifiers/Open-Ended Terms**

**c. COSATI Field/Group**

**18. Availability Statement**
Approved for public release; distribution unlimited.

**19. Security Class (This Report)**
UNCLASSIFIED

**20. Security Class (This Page)**

**21. No. of Pages**
81

**22. Price**

(See ANSI-Z39.18) *See Instructions on Reverse*

OPTIONAL FORM 272 (4-77)
(Formerly NTIS-35)
Department of Commerce